

# The Institute of Paper Chemistry

Appleton, Wisconsin

## Doctor's Dissertation

A Study of the Phenomenon of Rheological  
Dilatancy in an Aqueous Pigment Suspension

Robert J. Morgan

June, 1967

A STUDY OF THE PHENOMENON OF RHEOLOGICAL DILATANCY  
IN AN AQUEOUS PIGMENT SUSPENSION

A thesis submitted by

Robert J. Morgan

B.S. 1962, Oregon State University  
M.S. 1964, Lawrence University

in partial fulfillment of the requirements  
of The Institute of Paper Chemistry  
for the degree of Doctor of Philosophy  
from Lawrence University,  
Appleton, Wisconsin

Publication Rights Reserved by  
The Institute of Paper Chemistry

June, 1967

# TABLE OF CONTENTS

	Page
SUMMARY	1
INTRODUCTION	3
Rheological Properties of Pigment Suspensions	3
Historical Review	6
STATEMENT OF THE PROBLEM AND OBJECTIVES OF THE THESIS	13
Formulation of Hypotheses	13
First Hypothesis	13
Second Hypothesis	13
Colloidal Considerations	14
Interpretation Based on First Hypothesis	14
Interpretation Based on Second Hypothesis	14
Objectives of the Thesis	16
EXPERIMENTAL	17
Summary of Experimental Program	17
Selection and Characterization of the Pigment	18
Selection	18
Size and Shape	18
Removal of Soluble Salts	20
The Nature of the Surface of Iron Oxide	21
Selection and Characterization of Dispersing Agent	23
Information Furnished by Supplier	23
Elemental Analysis of Tamol 850	24
Infrared Analysis of Tamol 850	25
Sulfate Analysis	25
Procedure Used to Disperse the Pigment	26
Rheological Measurement	27
Measurement of Shear Stress and Shear Rate	27

Low Shear Viscosity Measurements	29
Acid-Base Titrations of Tamol 850	29
Adsorption Measurements	31
Dispersing Agent Adsorption	31
Hydrogen Ion Adsorption and Desorption	32
Sulfate and Chloride Adsorption	33
Calculation of Adsorbed Surface Charge	33
Variation of Pigment Volume Concentration at Constant Adsorbed Charge	34
PRESENTATION OF EXPERIMENTAL RESULTS	35
Results of the Adsorbed Measurements	35
Polyelectrolyte Adsorption	35
Hydrogen Ion Adsorption and Desorption	38
Desorption of Sulfate and Chloride	38
Sulfate Desorption	38
Chloride Desorption	42
Total Adsorbed Charge	42
The Relationship Between Rheological Behavior and Adsorbed Charge	44
Low Shear Viscosity Data	44
Extent of Rheological Dilatancy as a Function of Adsorbed Charge	46
Representation of Data	46
Presentation of Data	48
The Relationship Between Rheological Behavior and Pigment Volume Concentration	48
Extent of Dilatancy as a Function of Pigment Volume Concentration	48
Newtonian Viscosity as a Function of Pigment Volume Concentration	50
Seizure and Fracture of Dilatant Suspensions	54
DISCUSSION	58
Mechanisms of Colloidal Stability	58

Steric Hindrance or Entropic Stabilization	58
Hydration of the Pigment Surface	59
Relationship Between Charge and Colloidal Stability	60
The Mechanism of Rheological Dilatancy	61
Qualitative Considerations	61
Dilatancy and Pseudoplasticity Considered as Competitive Rate Processes	62
The Effect of Pigment Volume Concentration	67
The Effect of Particle Size on Dilatancy	68
CONCLUSIONS	71
SUGGESTIONS FOR FUTURE WORK	73
NOMENCLATURE	75
ACKNOWLEDGMENTS	77
LITERATURE CITED	78
APPENDIX I	81
Experimental Procedures and Apparatus	81
Preparation of Electron Micrographs	81
Removal of Soluble Salts	81
Evaluation of Dispersing Agent	82
Acid-Base Titration of Tamol 850	83
Experimental Method	83
Calculations	83
Analysis of Titration Data to Obtain the Intrinsic Dissociation Constant	84
Oxidation of Polymer in Suspending Fluids Prior to Chloride and Sulfate Analyses	85
APPENDIX II	87
Determination of Shear Stress and Shear Rate with The Hercules Viscometer	87
Cup and Bob Geometry	87

Measurement of Bob Speed and Torque	87
Rigorous Calculation of the Rate of Shear at the Bob	88
APPENDIX III	89
Experimental Data	89
Titration Data	89
Adsorption Data	89
Brookfield Viscosity Data	92
Shear Stress-Shear Rate Data	92

## SUMMARY

The primary objective of this study was to gain a better understanding of the mechanisms responsible for rheological dilatancy in concentrated pigment suspensions. Previous studies suggested that the phenomenon could be due to one of two mechanisms: (1) shear-induced flocculation or association of the particles, or (2) disturbance of streamline flow by virtue of the Brownian motion of the particles. It was felt that a study of the relationship between the extent of dilatancy and colloidal stability would furnish evidence in support of one of these two mechanisms.

Red iron oxide was used as the pigment in this study. Aqueous suspensions of the pigment were prepared using a carboxylated polyelectrolyte as a dispersant. Experiments were made to characterize more completely both the pigment and the dispersing agent.

The degree of colloidal stability of the suspensions was varied by changing the degree of dissociation of the carboxyl groups on the polymer. Experiments were made to determine the extent of adsorption of the polyelectrolyte and the other anions in the system. The adsorbed charge was found to correlate very well with the colloidal stability as measured with a Brookfield viscometer.

Rheological measurements were obtained using a Hercules Hi-Shear cup and bob viscometer. These measurements were obtained over a range of shear between zero and  $5000 \text{ sec.}^{-1}$ . It was found that the extent of dilatancy increased with decreasing colloidal stability. This result was taken as evidence in support of the shear-induced flocculation mechanism for dilatancy. The rate at which flocs are formed due to shear is believed to increase with a decrease in the repulsive colloidal forces between the particles.

At very low shear rates (less than  $50 \text{ sec.}^{-1}$ ) the suspensions were slightly pseudoplastic, whereas at high rates of shear the suspensions were dilatant.

That is, the viscosity first decreased with shear and then increased. This reversal in flow behavior was explained by considering the manner in which the rate constants for both the collision and disruption processes vary with shear rate.

In the region of low shear, the rate constant for floc disruption is believed to increase more rapidly with shear than does the rate constant for the collision process. This causes the aggregate size, and hence the viscosity, to decrease. At higher rates of shear, the rate constant for the collision process is thought to increase more rapidly than the rate constant for disruption. Therefore, the aggregate size increases with shear and the flow is dilatant.

The effect of pigment volume concentration was determined over the range of 40 to 47% in such a way that the adsorbed charge remained essentially constant. When the particle concentration was increased, the suspensions became more dilatant. This effect is thought to be consistent with the concept of shear-induced flocculation since an increase in particle concentration would be expected to increase the average floc size. When the particle concentration increases, a given level of flocculation can be reached at progressively lower rates of shear.

The conclusions reached in this study suggest that rheological dilatancy is restricted to suspensions containing particles which are of colloidal size. Work reported in the literature supports this contention. It was hypothesized that, within the colloidal size range, the extent of rheological dilatancy will increase with decreasing particle size, providing the degree of colloidal stability remains constant.

## INTRODUCTION

### RHEOLOGICAL PROPERTIES OF PIGMENT SUSPENSIONS

Rheology can be defined as the science of the deformation and flow of matter. With regard to pigment suspensions, the term rheological behavior is used in reference to the relationship which exists between the rate of shear and the imposed shear stress. The rheological phenomenon of dilatancy, which is often observed in highly concentrated suspensions, has been recognized for at least 35 years. Despite the fact that this unusual type of rheological behavior is of considerable importance in many technological applications, the phenomenon has received relatively little scientific investigation. The purpose of this study is to obtain a better understanding of the hydrodynamic and colloidal mechanisms involved in this type of flow.

A generalized shear stress-shear rate relationship is shown in Fig. 1 which illustrates the different types of rheological behavior which can be observed in some pigment suspensions. A single curve is used to indicate the relative levels of shear rate at which these flow phenomena are usually observed. Depending upon the specific nature of a suspension, all three of these different types of flow may or may not be observable.

In the region of low shear, the flow curve is concave toward the shear rate axis. This progressive decrease in viscosity with shear is referred to as pseudoplasticity. For suspensions containing highly asymmetric particles, the reduction in viscosity can result from a progressive alignment of the particles in the flow field. More generally, however, pseudoplasticity is caused by a progressive disruption of flocculated structure within a suspension. In this regard, the extent of pseudoplasticity is often used as an index of the extent of

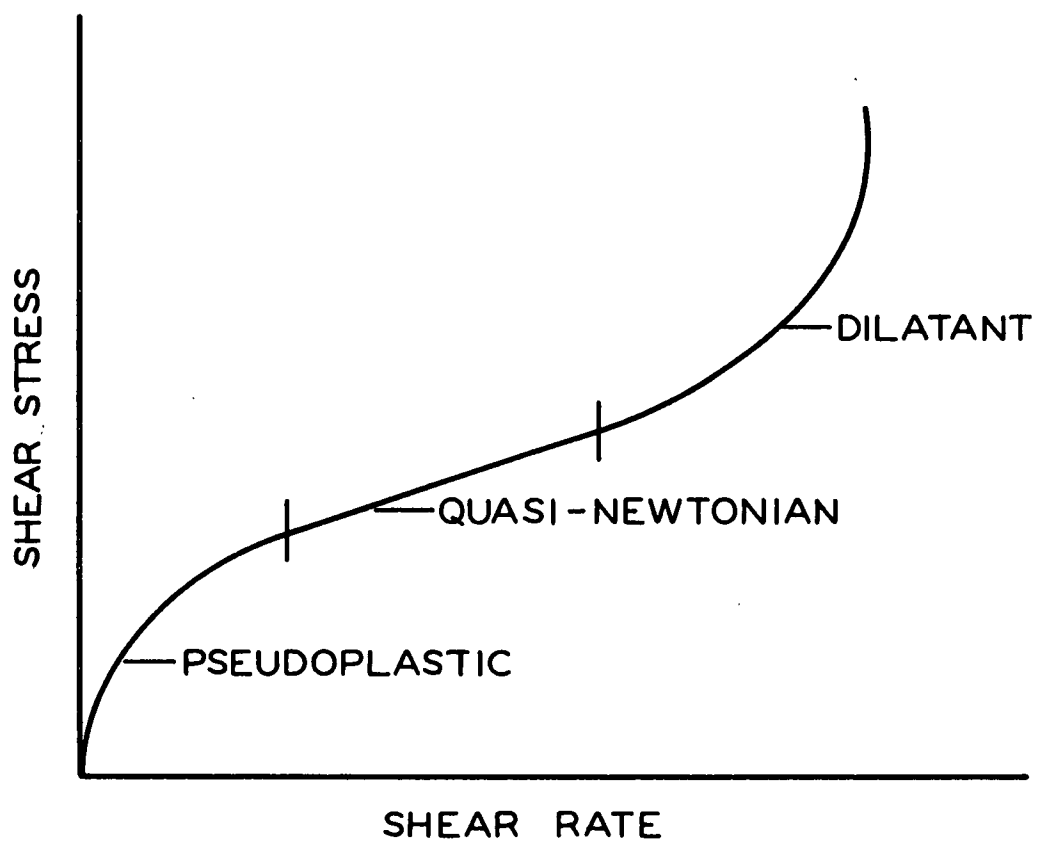


Figure 1. General Flow Behavior of Concentrated Pigment Suspensions

flocculation, and hence the degree of colloidal stability, of the system. More thorough discussions of this phenomenon are given by Kruyt (1), Fischer (2), and Thomas (3). Structural models for pseudoplastic flow have been proposed by Michaels and Bolger (4), Casson (5), and Krieger and Dougherty (6).

At this point, a distinction should be made between the terms pseudoplasticity and thixotropy. The term trixotropy is used to describe a decrease in viscosity with time under conditions of steady shear. Pseudoplasticity refers to a relationship between shear rate and shear stress which is independent of the duration of the shear. Both phenomena are explained on the basis of a breakdown in structure. Since the breakdown of a flocculated network usually requires a finite length of time, flocculated systems are usually thixotropic. A pseudoplastic flow curve is obtained provided sufficient time is allowed for structural equilibrium to be obtained at any shear rate. If structural equilibrium is not obtained, then the flow curve will exhibit a hysteresis loop which is characteristic of thixotropy.

After the shear stresses have reduced the particle aggregates to their minimum size, a linear relationship between shear stress and shear rate is observed. This type of relationship is frequently referred to as Newtonian. Strictly speaking, however, the flow cannot be considered Newtonian since the linear portion of the curve does not extend through the origin. For this reason the designation of "quasi-Newtonian" was used in Fig. 1. For suspensions in which the relationship between shear stress and shear rate is linear, the viscosity is primarily controlled by the particle volume concentration and the viscosity of the suspending fluid. A large amount of theoretical and experimental work has been published in this area and the reader is referred to Chong (7) and Rutgers (8) for excellent summaries.

At still higher levels of shear rate, the flow curve becomes concave toward the shear stress axis. That is, the viscosity of the suspension increases with

increasing shear rate. This type of non-Newtonian flow is referred to as dilatancy. Whereas orientation and flocculation effects account satisfactorily for pseudo-plasticity and thixotropy, a well-established explanation for dilatancy does not exist. It is the purpose of this thesis to obtain a better understanding of the fundamental mechanisms responsible for this type of flow behavior.

## HISTORICAL REVIEW

In 1885 Reynolds (9) introduced the term dilatancy to describe the increase in void volume within a closely packed assemblage of particles which occurs when the system is subjected to shear. This phenomenon was demonstrated by filling a flexible rubber bag with shot and a sufficient amount of water to just fill the void spaces. The mouth of the bag was then connected to a glass tube filled with water. When the bag was squeezed, the water level in the tube decreased. Reynolds concluded that distortion of the bag must have produced a volumetric expansion or dilation of the packing arrangement. The reason for this phenomenon is visualized in Fig. 2.

When the system is at rest, the spheres are in a closest packed rhombohedral arrangement. This corresponds to a volume fraction of the solid phase of 0.7405. As seen in Fig. 2, in order for the particles to flow past one another, the system must expand. The geometry in this situation will approach that of simple cubic packing which corresponds to a volume fraction of spheres of 0.5233.

Williamson (10) was one of the first investigators to report the occurrence of dilatancy in a colloidal suspension. When stirred gently, a concentrated suspension of cornstarch and water was found to be quite fluid. However, when the suspension was stirred more rapidly, a marked increase in viscosity was observed. Williamson referred to this phenomenon as inverted plasticity. It was also observed that the rapid increase in viscosity was accompanied by a very

noticeable amount of surface drying. That is, when the suspension was sheared, the liquid receded into the suspension and the surface became dry and rough in appearance. On the basis of this observation, Williamson concluded that the phenomenon was essentially the same as that described by Reynolds. The increased resistance to shear was attributed to the fact that, after volumetric dilation occurred, insufficient water was present in some regions to permit relative motion between the particles.

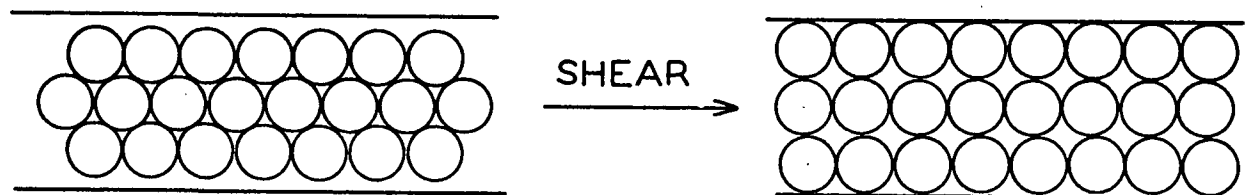


Figure 2. The Effect of Shear on the Packing of an Assemblage of Spheres

Dilatancy of the type discussed by Williamson has been reported in a variety of other pigment-vehicle systems (11-16). In each of these studies, the explanation of the phenomenon was essentially the same as that given by Williamson. Since the increase in viscosity was believed to be the result of volumetric dilation, the entire phenomenon was referred to as dilatancy. Thus, the meaning of the term was extended to describe a condition in which the viscosity increases with increasing shear. In each of these studies, the importance of a very high level of dispersion was emphasized. At low levels of dispersion, the flow was reported to be thixotropic rather than dilatant.

In a later study, Williamson and Heckert (17) made semiquantitative rheological measurements on aqueous suspension of cornstarch. Their measurements were made with a Stormer viscometer equipped with a paddle-type rotor. Dilatant flow was observed over a particle concentration range of 35 to 44% by volume. The extent of swelling of the starch grains was negligible and surface drying of the suspensions was not reported. In this range of particle volume concentration, Williamson and Heckert calculated that the void volume was greater than that corresponding to a cubic-packing arrangement. Since this ruled out the possibility of volumetric expansion during shear, they concluded that the phenomenon was not the same as that described by Reynolds. This was the first instance in the literature that a distinction was made between rheological dilatancy as defined by the relationship between shear stress and shear rate and volumetric dilatancy. Williamson and Heckert also found that good wetting of the particles by the suspending fluid was necessary for this type of flow behavior.

Williamson and Heckert proposed the following explanation for rheological dilatancy. At low levels of shear, the particles are thought of as being arranged into discrete cylinders or shells. As the rate of shear increases, the shear stresses between the shells increase until they reach a level such that the particles are pulled out from adjoining shells or layers. At this point, the discrete shells start to lose their identity and the viscosity of the suspension begins to increase.

The occurrence of rheological dilatancy in suspensions with particle concentrations less than that required for cubic packing (approximately 52% by volume) has also been reported by Freundlich and Roder (18). In this study, dilatancy was detected by measuring the force required to pull a sphere through the suspension as a function of velocity. Both starch and silica suspensions were found to be dilatant at volume concentrations between 42 and 45%. The phenomenon was explained by assuming

that the particles piled up in front of the sphere to such an extent that a closed packed condition was effected and therefore part of the suspension behaved as a solid. These workers also concluded that dilatancy is observable only if the particles are completely deflocculated. Gallay and Puddington (19) studied dilatancy in a potato starch-water system and arrived at essentially the same conclusions as did Freundlich and Roder.

The relationship between deflocculation and dilatancy was markedly demonstrated by Verwey and de Boer (20). At a volume concentration of 46%, a suspension of carboxyl iron powder (3  $\mu\text{m}$ .-particle diameter) in carbon tetrachloride, was a thick, stiff paste. However, when a trace of oleic acid was added, the suspension became quite fluid and was highly dilatant.

Verwey and de Boer advanced the following mechanism to explain the dilatant phenomenon. At low rates of shear, the particles are able to slide past one another due to the protective coating action of the oleic acid. Higher shear rates result in local forces which are large enough to push aside the polar layers surrounding the particles so that the particles can adhere and form a flocculated network. This mechanism increases the potential energy barrier for flow and therefore an increase in viscosity is observed. Verwey and de Boer expressed the view that the same mechanism is applicable in the case of aqueous suspensions in which the particles are stabilized by an electrical double layer. That is, dilatancy is observed when the shear stresses are large enough to overcome the electrical repulsive barriers between particles and thereby promote flocculation.

In a study of the structural viscosity of coating-clay slurries, Sheets (21) found that both thixotropy and dilatancy could be observed in the same slip. Sheets observed that clays of large particle size exhibited a weakly dilatant behavior over a wide range of concentration, whereas clays of smaller particle

size showed a strongly dilatant behavior over a narrow range of clay concentration. In each instance, sufficient dispersing agent was added to give a minimum initial viscosity.

Another interesting study of dilatancy was made by Fischer (22). Using a cup and bob viscometer, he obtained rheological data on a variety of pigment-vehicle systems. Most of the suspensions became dilatant at volume concentrations of 30% or higher. However, Fischer found that an aqueous suspension of red iron oxide became dilatant at a volume fraction of 12%. This result was later confirmed by Roberts (23) using a high-shear, capillary viscometer. The iron oxide particles used in these studies had the shape of parallelepipeds. Fischer inferred that because of their asymmetric shape the particles were able to sweep out larger spheres of action as their orientation was disturbed by shear and this mechanism was thought to increase the effective pigment volume concentration. Fischer's explanation for dilatancy is similar to that proposed by Freundlich and Roder (18) and Galloway and Puddington (19). That is, the application of shear was thought to cause a localized piling up of the particles with the result that the system as a whole began to behave more as a solid.

The most recent study of dilatant flow was reported by Metzner and Whitlock (24). Their experiments were made over wide ranges of pigment concentration and shear rate using both a cup and bob and capillary viscometer. They observed no rheological dilatancy whatsoever in suspensions containing glass beads of 28  $\mu\text{m}$ . or larger diameter. This was true even at volume concentrations as high as 64%. Therefore, Metzner and Whitlock concluded that rheological dilatancy is restricted to suspensions in which the particles are of colloidal size. Aqueous suspensions of  $\text{TiO}_2$ , having particle diameters between 0.2 and 1.0  $\mu\text{m}$ ., were found to be dilatant in the concentration range between 27 and 47% by volume. Dilatancy was

also observed when the  $\text{TiO}_2$  was suspended in sucrose solutions having viscosities as high as 42 cp. However, in these suspensions, the onset of dilatancy did not occur until much higher levels of shear stress were reached.

Metzner and Whitlock report that surface drying of the dilatant suspensions occurred during shear. This observation was made by visual inspection of the top of the suspension in the annulus of the cup and bob viscometer. This was interpreted as evidence for volumetric expansion. However, it was found that the surface drying always occurred at a level of shear well below that at which rheological dilatancy was observed. Metzner and Whitlock expressed the view that a careful distinction should be made between volumetric and rheological dilatancy.

Based on their experimental results, Metzner and Whitlock proposed the following qualitative theory to explain the mechanism of dilatancy. After the shear stresses have reduced the aggregates to their minimum size, pseudoplasticity is no longer observed. As the shear rate is further increased, the suspension undergoes volumetric dilation. At this point, entire layers of particles begin to slide past adjacent layers; that is, a streamlining effect is produced. Prior to the onset of volumetric dilation and streamlining, the momentum transfer occurs between localized particles or groups of particles. But once the particles have become arranged into streamlines, the movement of just one particle from one layer to another, by virtue of its Brownian motion, necessarily brings about a change in momentum of all the particles following behind in the streamline. Thus, as the rate of shear is increased, there is a progressive increase in the mass of the particles which undergo lateral movement and momentum transfer.

According to Metzner and Whitlock, the mechanism discussed above becomes operative as soon as some volumetric dilation occurs. However, at this point, the flow may still be pseudoplastic since not all of the flocs are yet reduced

to their minimum size. It is for this reason that rheological dilatancy is not observed until after volumetric dilation occurs. Thus, the onset of dilatancy is, in Metzner and Whitlock's theory, determined by a balance between two mechanisms. This balance is between progressively increased rates of alignment due to the velocity gradient and disalignment due to Brownian motion.

It is felt that Metzner and Whitlock's observations regarding volumetric dilation are subject to question. The volume concentrations of their suspensions were in all cases less than that required for simple cubic packing. It is possible that a very small amount of volumetric dilation could result from elastic collisions between particles and that this would cause the surface to become dry. The apparent dryness of the surface may also have been caused by evaporation.

The preceding literature review has shown that a well-established explanation for dilatancy has not yet evolved. Nevertheless, some facts do seem to have been well substantiated and these are summarized as follows:

1. At very high volume concentrations, the packing arrangement within a suspension can be such that volumetric dilation occurs during deformation. In this instance, the suspension is likely to be extremely dilatant in the rheological sense.
2. Rheological dilatancy can also occur at volume concentrations less than that required for volumetric dilation.
3. Rheological dilatancy is most prevalent in suspensions containing particles of colloidal size.
4. The extent of rheological dilatancy increases with increasing pigment volume concentration.
5. A very high level of particle independence (good dispersion) is a necessary condition for rheological dilatancy.
6. There is evidence that suspensions of asymmetric particles are more dilatant than those of isotropic particles.

STATEMENT OF THE PROBLEM AND  
OBJECTIVES OF THE THESIS

FORMULATION OF HYPOTHESES

The explanations which have been advanced to account for the phenomenon of rheological dilatancy can be roughly divided into two categories. These are presented below as the underlying hypotheses of this study.

FIRST HYPOTHESIS

The basic concept expressed in this hypothesis is that rheological dilatancy occurs when the shear stresses are large enough to promote localized increases in particle concentration within a suspension. According to Freundlich and Roder (18), Gallay and Puddington (19), and Fischer (22), when the shear stresses are sufficiently large, the particles pile up and the suspension begins to behave as a solid. Verwey and de Boer (20) extended this idea to take into consideration the colloidal nature of the particles. According to their view, when the shear stresses are large enough to overcome the repulsive forces between particles, a flocculated network is formed which increases the viscosity of the suspension. The first hypothesis therefore embraces the concept of shear-induced particle association or flocculation.

SECOND HYPOTHESIS

According to Metzner and Whitlock (24), rheological dilatancy results from the exchange of momentum due to the movement of particles from one streamline to another by virtue of their Brownian motion. The essential feature of this hypothesis, therefore, is that the extent of dilatancy is controlled by the extent of Brownian motion of the particles.

## COLLOIDAL CONSIDERATIONS

It is of interest now to consider more carefully the relationship between colloidal stability and dilatancy. To begin with, a relatively high level of colloidal stability is required in order to disperse a pigment to the relatively high concentrations required for dilatancy. Assuming this condition is fulfilled, the question arises as to how the extent of dilatancy varies with colloidal stability at a constant pigment volume concentration.

### INTERPRETATION BASED ON FIRST HYPOTHESIS

According to the first hypothesis, dilatancy results when the shear stresses are large enough to promote particle flocculation or association. If this is true, then it follows that a decrease in the repulsive forces between particles should increase the extent of dilatancy. However, a decrease in colloidal stability should also increase the extent of pseudoplasticity. Presumably, the increase in pseudoplasticity would be most noticeable at low rates of shear while the increase in the extent of dilatancy would be manifest at much higher rates of shear. At very low levels of colloidal stability, it might be expected that the initial level of flocculation would be so great that the suspension would be pseudoplastic over a very wide range of shear, and therefore, within this range dilatancy would not occur. This progressive change in flow behavior with decreasing stability is illustrated in Fig. 3.

### INTERPRETATION BASED ON SECOND HYPOTHESIS

The important consequence of the second hypothesis is that the extent of rheological dilatancy should increase with increasing degree of Brownian motion. In a concentrated suspension, the distance of separation between particles is such that the energy of interaction due to colloidal forces is significant. If the

state of dispersion of a concentrated suspension were such that the particles were completely flocculated, then an increase in the repulsive forces between the particles would tend to decrease the extent of Brownian motion. However, if the initial degree of flocculation is appreciable, the level of Brownian motion should increase with increasing stability since the average aggregate size would be reduced. As will be demonstrated later in this study, even at high levels of dispersion, concentrated suspensions are usually partially flocculated. Based on these considerations, it is concluded that the extent of Brownian motion will increase with increasing colloidal stability. Therefore, if the second hypothesis is correct, the extent of dilatancy should increase with increasing colloidal stability. This would result in the type of flow behavior shown in Fig. 4.

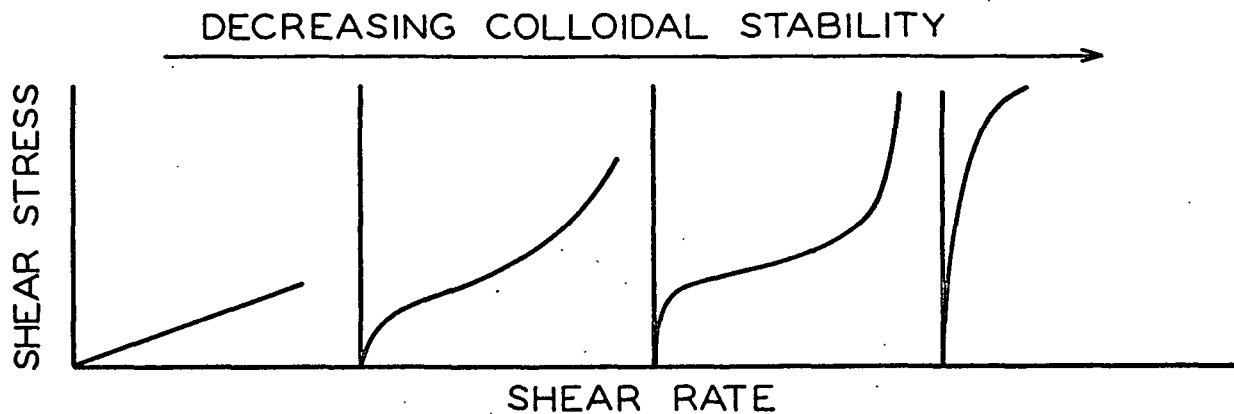


Figure 3. The Relationship Between Flow Behavior and Colloidal Stability as Predicted by the First Hypothesis

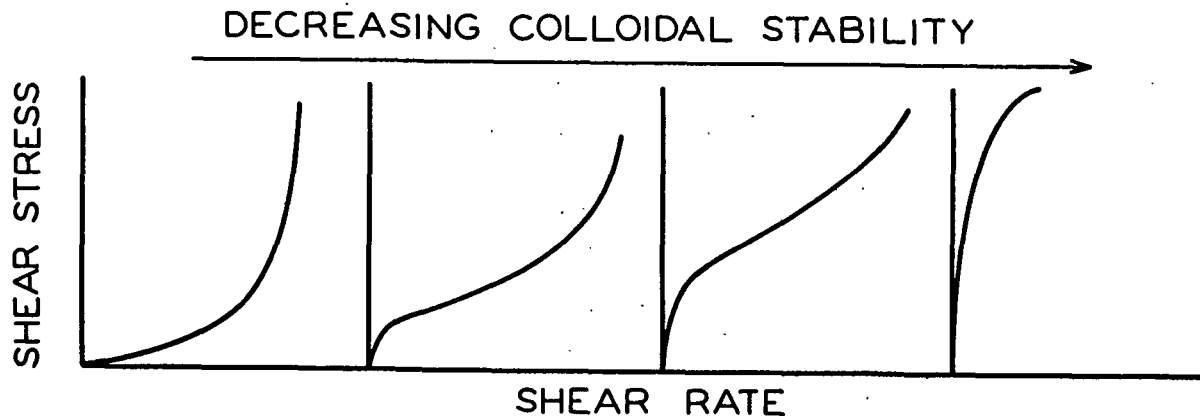


Figure 4. The Relationship Between Flow Behavior and Colloidal Stability as Predicted by the Second Hypothesis

## OBJECTIVES OF THE THESIS

The primary objective of this thesis was to experimentally investigate the relationship between colloidal stability and rheological dilatancy. It was felt that a thorough study of this relationship would furnish evidence in support of one of the two hypotheses discussed above. In the event that evidence was obtained in support of the Brownian motion hypothesis, additional experimental work was planned in order to elucidate the variables involved. This included a study of the effect of particle size and viscosity of the suspending phase.

A second objective of this research was to obtain meaningful data concerning the relationship between pigment volume concentration and dilatancy. The studies reported in the literature concerning this variable are subject to criticism since in most instances the colloidal variables were not carefully controlled. It was felt that a quantitative understanding of the effect of pigment volume concentration would be of value in analyzing the flow mechanism responsible for dilatancy.

## EXPERIMENTAL

### SUMMARY OF EXPERIMENTAL PROGRAM

This study of dilatancy was made using aqueous suspensions of a red iron oxide pigment. A carboxylated polyelectrolyte was used as the dispersing agent. Experiments were made to characterize the size and shape of the pigment and to establish the physical and chemical nature of the dispersant.

Preliminary experiments indicated that the colloidal stability of the suspensions was a function of the pH of the dispersing agent solution. A study was made to determine the mechanisms responsible for colloidal stabilization in the system. Acid-base titrations of the dispersant were made in order to determine the relationship between pH and the degree of dissociation of the carboxyl groups on the polymer. Next, the extent of adsorption of the polyelectrolyte onto the pigment was measured as a function of degree of dissociation. The techniques used for these measurements also provided information regarding the extent of hydrogen ion desorption from the pigment surface. Since the pH of the dispersant solution was adjusted with HCl, it was also necessary to account for chloride ion adsorption. These adsorption measurements were then used to determine quantitatively the variation in total adsorbed surface charge as a function of pH. Thus, the adsorbed surface charge was used as an index for the degree of colloidal stability.

The rheological measurements were made using a cup and bob rotational viscometer. Measurements were made as a function of adsorbed surface charge at a constant pigment volume concentration (PVC). Finally, rheological measurements were obtained as a function of PVC in such a manner that the surface charge was maintained constant.

## SELECTION AND CHARACTERIZATION OF THE PIGMENT

### SELECTION

The pigment used in this study was a high purity, red iron oxide ( $\text{Fe}_2\text{O}_3$ ) produced by the Chas. F. Pfizer Co. (code number R8098). This pigment was selected for two reasons: (1) The particles were reported to be essentially spheroidal in shape, and (2) iron oxides of this type are commercially available in several different sizes. It was felt that the use of spherical rather than asymmetric particles would simplify the analysis and interpretation of the flow data. The availability of different sizes was also thought to be advantageous since the relationship between particle size and dilatancy has not been definitely established.

### SIZE AND SHAPE

Both the size and shape of the pigment were determined from electron micrographs. The experimental details of this method are discussed in Appendix I.

A representative electron micrograph of the pigment is shown in Fig. 5. It is seen that most of the particles, while not perfectly spherical, tend toward a spheroidal or isotropic shape. A small number of particles were found to have either dumbbell or kidney shapes.

Because the particles were not completely separated on the grids, the measurement of particle size was somewhat subjective. In many instances, only part of a particle could be completely discerned and it was necessary to estimate the rest of the shape. The diameters of the particles were found to vary between 0.01 and 1.0  $\mu\text{m}$ . The average diameter, obtained from a count of 433 particles, was 0.20  $\mu\text{m}$ . The maximum error of the measurement was estimated to be less than 0.1  $\mu\text{m}$ , so that the average diameter is believed to be between 0.1 and 0.3  $\mu\text{m}$ .

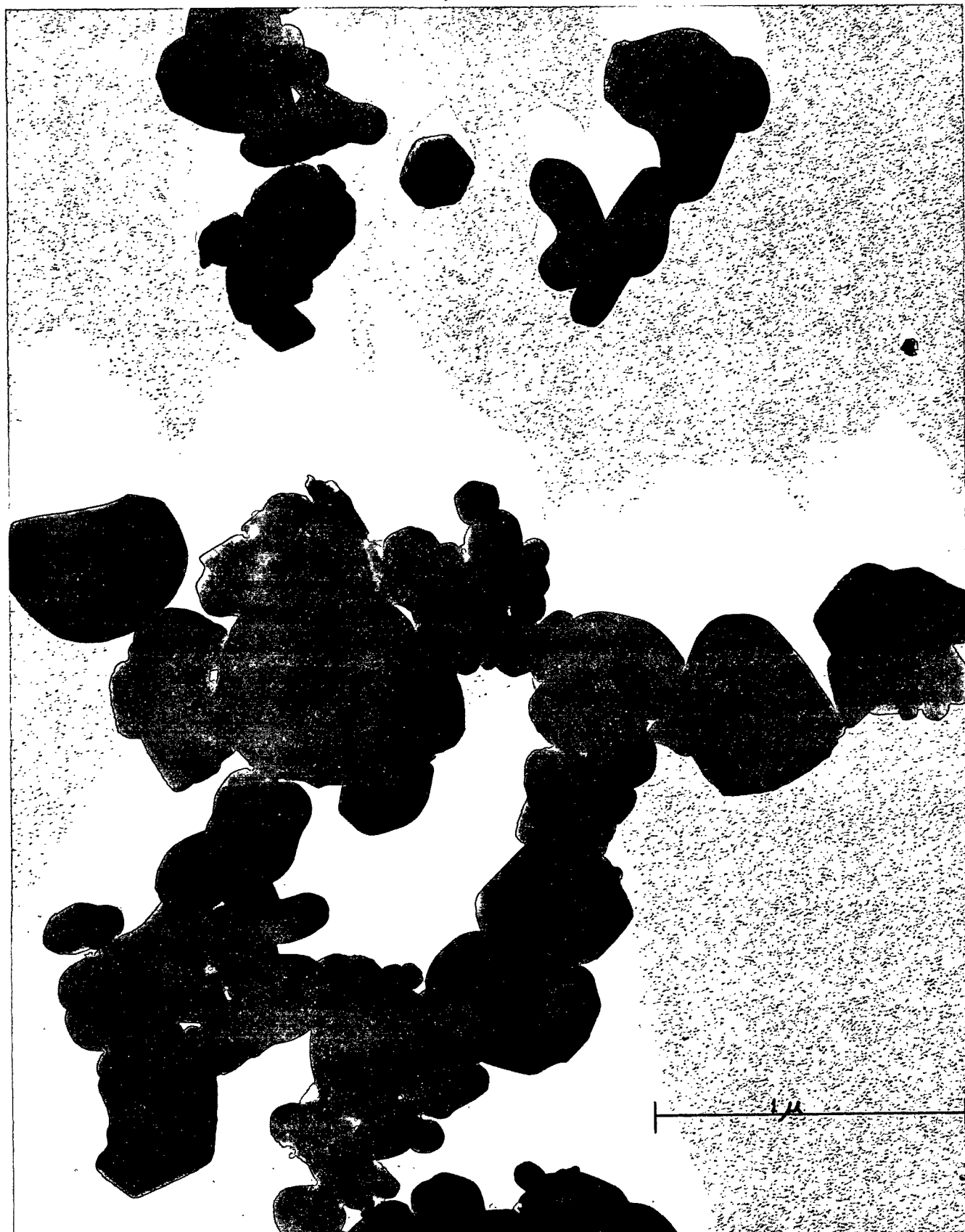


Figure 5. Electron Micrograph of Iron Oxide Pigment  
Chas. Pfizer Co.-R8098

## REMOVAL OF SOLUBLE SALTS

Data furnished by the supplier indicated that the pigment contained approximately 0.1% soluble salt. This value was experimentally confirmed in this study. According to the supplier, most of this material was either sodium sulfate or calcium sulfate. It was felt that removal of these salts would simplify the colloidal aspects of the study. Most of the salts were removed by repeatedly washing the pigment with distilled water. The details of this procedure are given in Appendix I.

The effectiveness of the leaching procedure was determined by measuring the specific conductivity of a 10% pigment slurry both before and after washing. In addition, the concentrations of sodium, potassium, and calcium in the supernatants of these slurries were determined using a flame photometer. The results of these tests are shown in Table I.

TABLE I

### REMOVAL OF SOLUBLE SALTS FROM R8098 IRON OXIDE PIGMENT

Analysis of Supernatant - 10% Slurry	Unwashed Pigment	Washed Pigment
Specific conductivity, ohms <sup>-1</sup> cm. <sup>-1</sup>	11.09 x 10 <sup>-4</sup>	1.83 x 10 <sup>-5</sup>
Sodium ion concentration <sup>a</sup>	0.0048%	0.0005%
Potassium ion concentration <sup>a</sup>	negligible	negligible
Calcium ion concentration <sup>a</sup>	0.0068%	0.0006%

<sup>a</sup>Concentrations based on the weight of pigment present in slurry.

The results shown in Table I indicate that approximately 90% of the soluble salts were removed during the leaching process.

#### THE NATURE OF THE SURFACE OF IRON OXIDE

It is well established in the literature that the potential determining ions in the  $\text{Fe}_2\text{O}_3 - \text{H}_2\text{O}$  system are  $\text{H}^+$  and  $\text{OH}^-$ . In this respect, the surface chemical properties of iron oxide are similar to those of most other metallic oxide pigments. That is, the surface consists primarily of oxygen and hydroxyl ions which behave as proton acceptors and donors.

Several investigators have measured the isoelectric pH (point of zero surface charge) of  $\text{Fe}_2\text{O}_3$  and the results of these studies are shown in Table II.

The data in Table II show that the isoelectric pH, and hence the physical and chemical nature of the surface, is dependent upon the chemical procedure used to prepare the oxide. In addition, the conditions used for washing and drying the sample are also important.

Atkinson, et al. (26) measured the adsorption of  $\text{H}^+$  and  $\text{OH}^-$  ions onto the surface in the presence of indifferent electrolytes. He found that potassium, chloride, and nitrate ions were not adsorbed at the point of zero surface charge.

According to Atkinson, the iron oxide surface consists of coordinated water molecules as well as oxygen and hydroxyl groups. This conclusion is supported by the results of Healey, et al. (29) and Jurinak (30). These workers found that, in the region of relative pressures where monolayer coverage is normally encountered, two-thirds of the water on the surface was physically adsorbed. On the remainder of the surface, the water was chemisorbed and could be released only by heating above  $450^\circ\text{C}$ .

TABLE II

## ISOELECTRIC pH VALUES REPORTED FOR FERRIC OXIDE

Material	Method of Preparation	Observation Technique	Isoelectric pH	Investigators
Precipitate ( $\alpha$ -Fe <sub>2</sub> O <sub>3</sub> )	Hydrolysis of Fe(NO <sub>3</sub> ) <sub>3</sub> at boiling point	Potentiometric titration	8.5	Parks and de Bruyn ( <u>25</u> )
Precipitate ( $\alpha$ -Fe <sub>2</sub> O <sub>3</sub> )	Same as above. Different methods to purify the sol.	Potentiometric titration	8.6 to 9.27	Atkinson ( <u>26</u> )
Precipitate	Reaction of FeNH <sub>4</sub> (SO <sub>4</sub> ) <sub>2</sub> with ammonia	Microelectrophoresis	8.0	Johansen and Buchanan ( <u>27</u> )
Precipitate	Same as above except precipitate was ignited at 850°C. for 2 hr.	Microelectrophoresis	6.5	Johansen and Buchanan ( <u>27</u> )
Natural hematite	Ground in an iron mortar, washed with dilute HCl, dried at 120°C.	Microelectrophoresis	6.7	Johansen and Buchanan ( <u>27</u> )
Precipitate	Industrial pigment produced by the calcination of ferrous-sulfate	Potentiometric titration	6.9	Princen ( <u>28</u> )

The literature indicates that the ferric oxide surface has a high affinity for anionic dispersing agents. Shimoizaka, et al. (31) found that addition of various phosphate ions caused the zeta potential of  $\text{Fe}_2\text{O}_3$  particles to become more negative. Kling and Lange (32) observed a similar effect upon addition of Na-dodecyl sulfate, K-laurate, and Na-alkyl benzene sulfonate. The effect of additions of potassium salts of n-fatty acids to  $\text{Fe}_2\text{O}_3$  suspensions was studied by Strange and Hazel (33). Addition of these surface-active agents resulted in a change of zeta potential from positive to negative.

#### SELECTION AND CHARACTERIZATION OF DISPERSING AGENT

Appendix I contains a listing and discussion of the various dispersants which were evaluated during the course of this study. The most suitable product was found to be Tamol 850. Using this dispersant, a high level of fluidity could be achieved at pigment volume concentrations as high as 47%. Furthermore, the suspensions were stable with respect to aging.

#### INFORMATION FURNISHED BY SUPPLIER

Tamol 850 is a sodium salt of a carboxylated polyelectrolyte which is produced by the Rohm and Haas Co. Although the company could not disclose the exact chemical composition of the polymer, a representative of their research department (34) provided the following helpful information: (1) The number average molecular weight of a representative sample of the neutralized polymer, as measured with a Mechrolab Vapor Pressure Osmometer, was approximately 4000. (2) The polyelectrolyte is most effective as a dispersant at a pH of 9.0 to 10.5. This corresponds to complete saponification of the carboxyl groups. (3) The polyelectrolyte is believed to adsorb onto the iron oxide surface as a negatively charged anion and thus increase the colloidal stability of the particles.

Because of the importance of the colloidal variables in this study, it was felt that a better understanding was required concerning the chemical composition and ionization behavior of Tamol 850. A preliminary acid-base titration indicated that the only ionizable groups present were carboxyl. Furthermore, the dissociation constant obtained from the titration was very close to that reported by Tanford (35) for polymethacrylic acid.

#### ELEMENTAL ANALYSIS OF TAMOL 850

A freeze-dried sample of Tamol 850 was submitted to Geller Laboratories for analysis of carbon, hydrogen, oxygen, nitrogen, and sodium. The results of this analysis are summarized in Table III. For comparison, the calculated elemental compositions of sodium-polyacrylate and sodium polymethacrylate have also been included.

TABLE III  
ELEMENTAL ANALYSIS OF TAMOL 850,  
SODIUM POLYMETHACRYLATE,  
AND SODIUM POLYACRYLATE

Polymer	C, %	H, %	O, %	Na, %	N, %	Total
Tamol 850	41.58	5.17	33.32	19.66	0	99.73
Na polymethacrylate	44.4	4.63	29.6	21.3	0	100
Na polyacrylate	38.3	3.19	34.05	24.5	0	100

As seen in Table III, Tamol 850 contains no nitrogen and the remainder of the elements, carbon, hydrogen, oxygen, and sodium, account for essentially all of the weight of the polymer.

The Tamol 850 polymer was noticeably hygroscopic and it is possible that the samples used for the elemental analysis may not have been completely free of

moisture. Therefore, the elemental analyses for carbon and sodium might be somewhat low while the analyses for hydrogen and oxygen might be somewhat high. On this basis, it was possible to rule out the possibility that Tamol 850 is sodium polyacrylate. However, the data in Table III indicated that the dispersant might be sodium polymethacrylate.

#### INFRARED ANALYSIS OF TAMOL 850

Samples of both Tamol 850 and pure sodium polymethacrylate were submitted to the Analytical Department of The Institute of Paper Chemistry for infrared spectroscopy analysis. The infrared spectra of these two polymers were virtually identical. However, the spectrum of Tamol 850 showed one small adsorption peak at  $8.9 \mu\text{m}$ . which was not present in the spectrum of sodium polymethacrylate. Since the spectra were the same in all other respects, it seemed likely that the adsorption peak was due to the presence of a small amount of inorganic material. The position of the peak suggested that this material might be sulfate.

#### SULFATE ANALYSIS

The procedure used to analyze for sulfate in the polymer solution will be discussed in a subsequent section. It was found that the polymer solution contained approximately 2.3% sulfate based on the weight of oven-dry solids in the solution. More precisely, the solution contained 0.0552 meq. sulfate per meq. carboxyl. This amount of sulfate is sufficient to account for the previously mentioned adsorption peak at  $8.9 \mu\text{m}$ . Note that the summative elemental analysis reported in Table III for Tamol 850 is too high to also include 2.3% sulfate. This is a further indication that the sample used for carbon, hydrogen, oxygen, and sodium analysis must have contained some bound water. Thus, the values reported in Table III are slightly in error.

## PROCEDURE USED TO DISPERSE THE PIGMENT

The first step in the dispersion procedure was to prepare a dispersant solution having the desired polymer concentration and pH. A predetermined volume of this solution was transferred with a pipet into a beaker and the pigment was added directly. The required weight of pigment was calculated based upon the desired PVC, the volume of suspending fluid, and the density of the pigment particles (5.15 g./ml.).

Mechanical shearing of the suspensions was necessary in order to effect adequate dispersion. This was accomplished using an Eppenbach Homo-Mixer (Laboratory Model 1L). In this device, the suspension is sheared between a motor-driven rotor and stationary bars. The shearing mechanism is contained in a homogenizing head which is immersed directly into the suspension and the design of the instrument is such that the suspension is continuously pumped from the bottom of the container through the shearing mechanism. In order to eliminate the effect of mechanical dispersion as a variable, the suspensions were sheared at a constant rheostat setting for a length of time which was proportional to the total weight of pigment present.

After mechanical dispersion, an appreciable quantity of small air bubbles was present in the suspensions. This was removed by subjecting the suspensions to the vacuum from a water aspirator for approximately five minutes. No air bubbles could be observed in the suspension after this treatment. The suspensions were then filtered through a nylon mesh and stored in polyethylene bottles. To ensure equilibrium conditions and to prevent sedimentation of the pigment, the bottles were slowly rotated for at least twelve hours before rheological and adsorption measurements were made.

## RHEOLOGICAL MEASUREMENTS

### MEASUREMENT OF SHEAR STRESS AND SHEAR RATE

Measurements of the extent of dilatancy of the suspensions were obtained using a Hercules Hi-Shear Viscometer which was produced by the Martinson Machine Co. For a detailed description of this instrument, the reader is referred to the literature (63). In this viscometer, the suspension is sheared in the annular space between a rotating, cylindrical bob and a somewhat larger cup. A variable speed transmission is used to regulate the angular velocity of the bob. A string attached at both ends to calibrated springs is wrapped around the cup and the extension of the springs provides a measure of the torque transmitted through the fluid to the cup. The design of the instrument is such that the torque on the cup is continuously plotted as a function of bob speed directly onto a sheet of graph paper. The dimensions of the cup and bob are given in Appendix II.

The shear stress at the bob was calculated from the torque as follows:

$$\begin{aligned}\tau_b &= \text{Force/Area} = (T/R_b)/2\pi R_b h \\ \tau_b &= T/2\pi R_b^2 h\end{aligned}\tag{1}$$

where

$$\begin{aligned}\tau_b &= \text{shear stress at bob;} \\ T &= \text{torque;} \\ R_b &= \text{radius of the bob;} \\ h &= \text{calculated bob length.}\end{aligned}$$

The calculated bob length was determined by calibration of the viscometer with oils of accurately known viscosity. In this way, the effect of viscous drag on the bottom of the bob was automatically taken into consideration.

The rate of shear at the bob was calculated using the following approximation:

$$G = \text{peripheral speed of bob / thickness of annular gap} \quad (2)$$
$$G = \omega R_b / (R_c - R_b)$$

where

$$\begin{aligned} \underline{G} &= \text{shear rate at bob;} \\ \underline{\omega} &= \text{angular velocity of the bob;} \\ \underline{R_c} &= \text{radius of the cup.} \end{aligned}$$

The assumption implicit in this equation is that the velocity gradient across the annular gap is linear. Providing the gap thickness is very small, this approximation can be used without serious error.

A rigorous calculation of the shear rate at the bob must take into account the non-Newtonian behavior of the fluid. An analytical solution to this problem was obtained by Krieger and Elron (36) and is presented in Appendix II. Krieger and Elron's analysis was used to determine the applicability of Equation (2). The maximum error introduced by use of Equation (2) was found to be less than 2% which was considered acceptable for the purposes of this thesis.

When the flow curves were obtained in such a manner that the rate of rotation of the bob was continuously changing, a hysteresis effect was noticed. That is, the flow curve obtained on the decreasing cycle of shear was not the same as that obtained on the increasing cycle. This problem was eliminated by maintaining the bob speed constant until an equilibrium level of torque was obtained. In this way, the hysteresis loop was eliminated. When the bob speed was increased to a higher level, a finite length of time was required for the torque to increase to its equilibrium level. For weakly dilatant suspensions, the time required was of the order of one or two seconds. However, for strongly dilatant suspensions, the time required to reach a condition of equilibrium was often as great as five to ten seconds.

## LOW SHEAR VISCOSITY MEASUREMENTS

At shear rates less than  $200 \text{ sec.}^{-1}$ , most of the suspensions were slightly pseudoplastic and the extent of this shear thinning behavior was a function of the colloidal stability. The Hercules Viscometer was designed primarily for high shear rate measurements and it is not sufficiently sensitive at low rates of shear to provide a good comparison between the extent of pseudoplasticity of different suspensions. In order to obtain a more sensitive comparison, low shear viscosity measurements were obtained using a model LVF, Brookfield Viscometer. These measurements did not determine the extent of pseudoplasticity since the shear rate was not varied. However, they did provide a sensitive comparison of the viscosities of different suspensions in the range of pseudoplastic flow.

## ACID-BASE TITRATIONS OF TAMOL 850

Aqueous solutions of Tamol 850 were titrated with NaOH and HCl in order to determine the relationship between pH and degree of dissociation. Discussions concerning the experimental techniques and calculations are given in Appendix I, and the experimental data are tabulated in Appendix III. In general, the procedures used were similar to those recommended by Kenchington (37) and Tanford (38).

Two titration curves were obtained for use in conjunction with the adsorption experiments. These were obtained at different polymer concentrations and are shown in Fig. 6. It is seen that the ionization behavior is slightly dependent upon the polymer concentration (expressed in terms of carboxyl groups in Fig. 6). This effect is thought to be due to either a change in the activity coefficient of the solution or to a change in the configuration of the polymer with dilution.

Titration number one (upper curve in Fig. 6) was made using a starting carboxyl concentration of 165 meq./liter, which in the adsorption study, corresponded

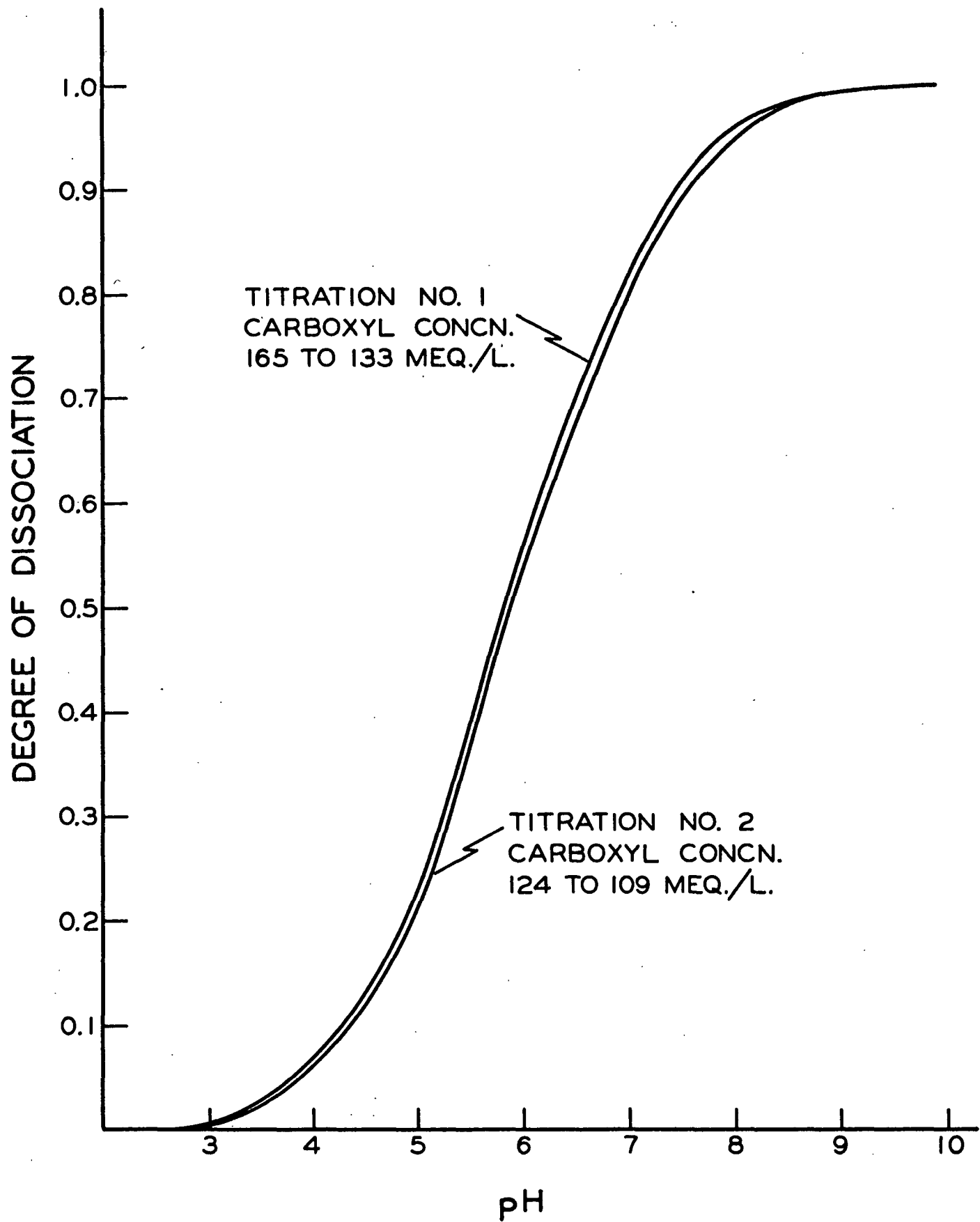


Figure 6. Ionization Curve for Tamol 850

to the concentration of the dispersant prior to pigment addition. Titration number two was made at a starting carboxyl concentration of 124 meq./liter. This concentration corresponds approximately to the amount of polymer which remained in the interparticle solution after adsorption.

The intrinsic dissociation constant for the carboxyl groups was calculated according to a method given by Tanford (35) and discussed in Appendix I. The value obtained was approximately 4.9 which is in good agreement with the value of 4.85 obtained by Tanford using polymethacrylic acid.

## ADSORPTION MEASUREMENTS

### DISPERSING AGENT ADSORPTION

The adsorption of the Tamol 850 polymer was measured as a function of degree of dissociation at a constant PVC of 45%. To further simplify the experiments, the total level of polymer addition was maintained constant at 0.0391 meq. carboxyl/gram of pigment. This corresponds to a polyanion addition of 0.27% based on the weight of the pigment. With these variables held constant, the pH of the suspending fluid was varied by addition of HCl or NaOH.

After dispersion of the pigment, a two-stage centrifugation procedure was used to obtain pigment-free samples of the interparticle solution. Most of the pigment was removed in the first stage by centrifugation for 45 minutes at approximately 900 x g using an International Centrifuge. The remaining pigment was removed by centrifugation for two hours at 75,000 x g using a Beckman Model L-2 Ultracentrifuge. A simple calculation showed that the extent of polymer sedimentation under these conditions was negligible.

A conductometric titration technique was used to determine the extent of adsorption of the polyelectrolyte. After removal of the pigment by centrifugation,

50 ml. of the suspending fluid were diluted to 300 ml. and a sufficient amount of NaOH was added to ensure that all of the carboxyl groups were in the salt form. The sample was then titrated conductometrically with standardized HCl to determine the total number of carboxyl groups present. The end points on both the acid and base sides were very sharp and the accuracy of the determinations is believed to be better than 2%. By knowing the total amount of carboxyl originally present, the extent of carboxyl adsorption was calculated by difference.

In the method discussed above, the extent of adsorption was measured in terms of carboxyl groups rather than the weight of polymer. Initially, attempts were made to measure the extent of adsorption using a gravimetric method of analysis. However, because of the hygroscopic nature of the Tamol 850 polymer, this method was far less accurate than the conductometric titration technique. In addition, the measurement of carboxyl adsorption provides a more direct measure of the level of colloidal stability since presumably it is the adsorbed, ionized carboxyl groups which impart the charge to the pigment surface. The weight of adsorbed polymer can be estimated by assuming that the Tamol 850 polymer is sodium polymethacrylate.

#### HYDROGEN ION ADSORPTION AND DESORPTION

During the adsorption experiments, it was found that the pH of the inter-particle solution was usually different from that of the initial dispersant solution. This meant that, upon addition of pigment, the polyelectrolyte underwent a change in degree of dissociation. At levels of pH above 6.7, the final pH was less than the initial pH while at levels of pH less than 6.7, the converse was true. It is believed that this shift in degree of dissociation results from the adsorption or desorption of hydrogen ions onto or away from the pigment surface. By referring to the data obtained for titration number two (see Appendix III), it

was possible to determine the amount of hydrogen ion adsorption or desorption required to cause the observed shift in pH.

#### SULFATE AND CHLORIDE ADSORPTION

Since both sulfate and chloride ions were present in the dispersing agent solutions, experiments were made to determine the extent of adsorption of these anions as a function of pH. Analysis for these anions was complicated by the presence of the polymer in the interparticle solutions. Accordingly, it was necessary to completely oxidize the organic material prior to analysis. The oxidation procedure is discussed in Appendix I.

After oxidation of the polymer, the concentrations of sulfate in the suspending fluids were determined by titrations with barium perchlorate according to the procedure of Fritz and Yamamura (39). Chloride ion concentrations were determined using the standard Volhard method (40). These analyses were made by the Analytical Department of The Institute of Paper Chemistry.

#### CALCULATION OF ADSORBED SURFACE CHARGE

The adsorption measurements were used in conjunction with the titration data to calculate the magnitude of the adsorbed charge as a function of pH. For this purpose, it was assumed that the degree of dissociation of the adsorbed polymer was the same as that of the unadsorbed polymer remaining in the suspending fluid. The extent of polymer adsorption,  $\Gamma_c$ , was expressed in terms of the total meq. of adsorbed carboxyl per gram of pigment. To convert to units of charge, it was necessary to multiply the values of  $\Gamma_c$  by the degree of dissociation of the carboxyl groups, Avogadro's number, and the charge on an electron. This relationship is expressed in the following equation:

$$\sigma_p = \Gamma_c \alpha_f N_a e \quad (3)$$

where

$$\begin{aligned}\sigma_p &= \text{adsorbed charge due to polymer adsorption, esu/g.}; \\ \Gamma_c &= \text{extent of carboxyl adsorption, meq. carboxyl/g.}; \\ \alpha_f &= \text{degree of dissociation of the carboxyl groups in} \\ &\quad \text{the interparticle solution}; \\ N_a &= \text{Avogadro's number, } 6.023 \times 10^{20} \text{ molecules/millimole}; \\ e &= \text{charge on an electron} = 4.8 \times 10^{-10} \text{ esu.}\end{aligned}$$

The values for  $\alpha_f$  used in Equation (3) were determined by measuring the pH of the interparticle solution and then referring to titration number two which was obtained at a carboxyl concentration close to that measured in the interparticle solution. In this way, the error due to the previously mentioned dilution effect was minimized.

The contributions to charge due to adsorption of hydroxyl, sulfate, and chloride ions were calculated simply by multiplying the meq. adsorbed per gram of pigment by  $N_a e$ .

#### VARIATION OF PIGMENT VOLUME CONCENTRATION AT CONSTANT ADSORBED CHARGE

In order to determine the effect of PVC on the extent of dilatancy, it was necessary to vary the PVC in such a manner that the pigment surface charge remained essentially constant. This was accomplished in the following manner:

- (1) A suspension was dispersed which had the highest PVC of interest (47%);
- (2) The interparticle solution was analyzed for carboxyl content and pH; (3) A Tamol 850 dilution solution was prepared having the same carboxyl content and pH; and (4) Suspensions of lower PVC were prepared by adding this dilution solution to a suspension dispersed at the maximum PVC. Adsorption measurements were made on a suspension diluted in this manner and the extent of adsorption and pH were almost exactly the same as those of the most highly concentrated suspension. Therefore, it was concluded that the charge on the pigment remained essentially constant during dilution.

## PRESENTATION OF EXPERIMENTAL RESULTS

### RESULTS OF THE ADSORPTION MEASUREMENTS

#### POLYELECTROLYTE ADSORPTION

A summary of the results of all of the adsorption measurements is given in Appendix III.

Both the extent of carboxyl adsorption,  $\Gamma_{\underline{c}}$ , and the degree of dissociation of the carboxyl groups are shown as a function of pH in Fig. 7. It is seen that the amount of adsorbed polymer decreases with increasing pH or degree of dissociation. A similar finding was reported by Michaels and Morelos (41) in a study of the adsorption of sodium polyacrylate onto kaolinite. This behavior is best explained on the basis that the adsorption of a carboxylated polymer occurs via hydrogen bonding between nonionized carboxyl groups on the polymer and oxygen atoms on the surface of the ferric oxide. As the pH increases, both the pigment surface and the polymer become more negatively charged and the adsorption decreases due to the increase in electrostatic repulsion.

As discussed in the experimental section, the charge due to polymer adsorption,  $\sigma_{\underline{p}}$ , is proportional to the product of  $\Gamma_{\underline{c}}$  and  $\alpha_{\underline{f}}$ . For these calculations, values of  $\Gamma_{\underline{c}}$  were taken from the smoothed curve in Fig. 7 rather than from the actual data points. The variation of  $\sigma_{\underline{p}}$  with pH is shown in Fig. 8. Since the polymer is adsorbed as an anion, the values for  $\sigma_{\underline{p}}$  are understood to be negative. Figure 8 shows that the charge due to polymer adsorption reaches a maximum at pH 7.0. At lower pH levels,  $\alpha_{\underline{f}}$  decreases more rapidly than  $\Gamma_{\underline{c}}$  increases and so the charge decreases. Above pH 7.0 the situation is reversed;  $\Gamma_{\underline{c}}$  decreases more rapidly than  $\alpha_{\underline{f}}$  increases and this also causes a decrease in surface charge.

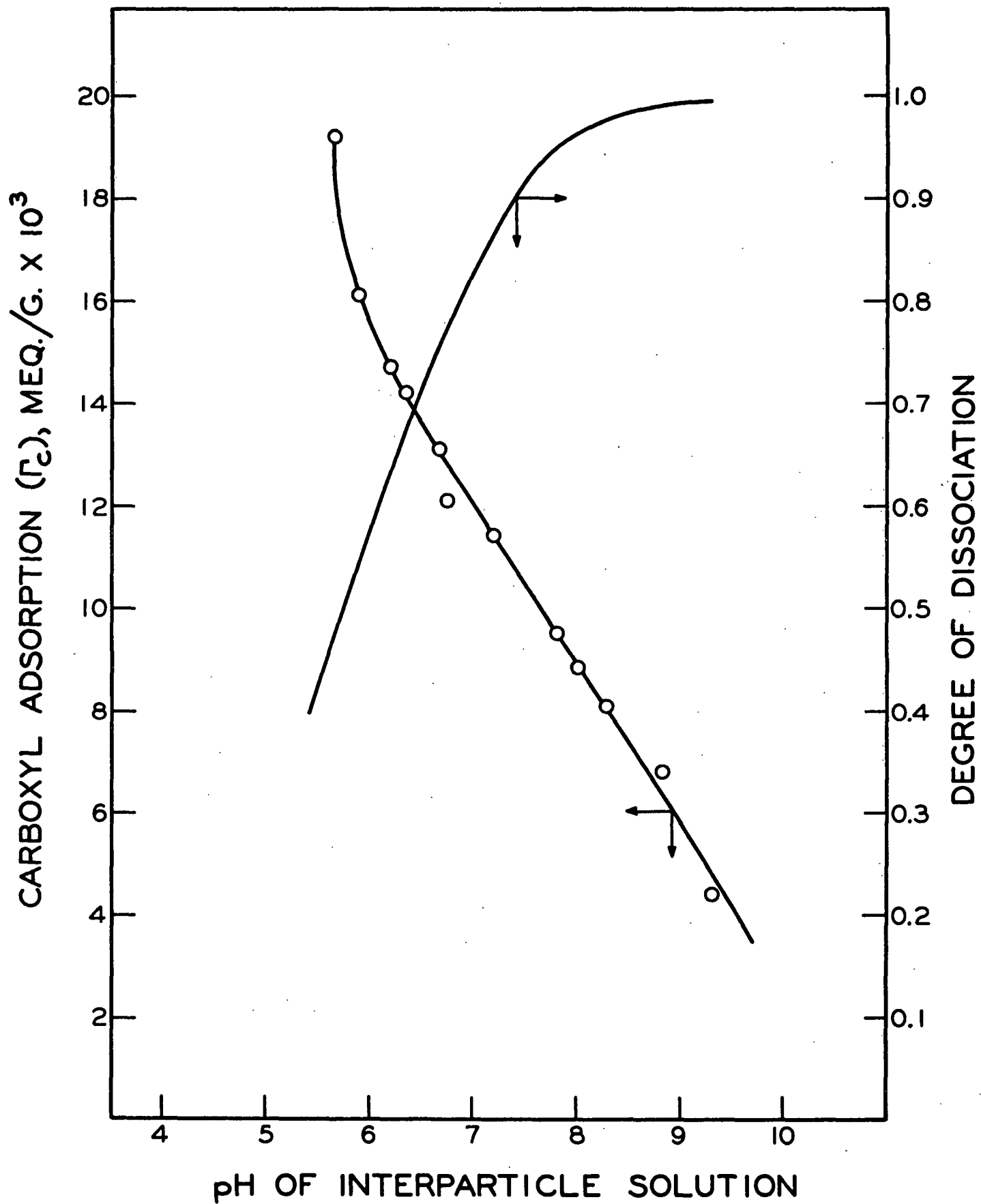


Figure 7. Total Carboxyl Adsorption and Degree of Dissociation as a Function of pH

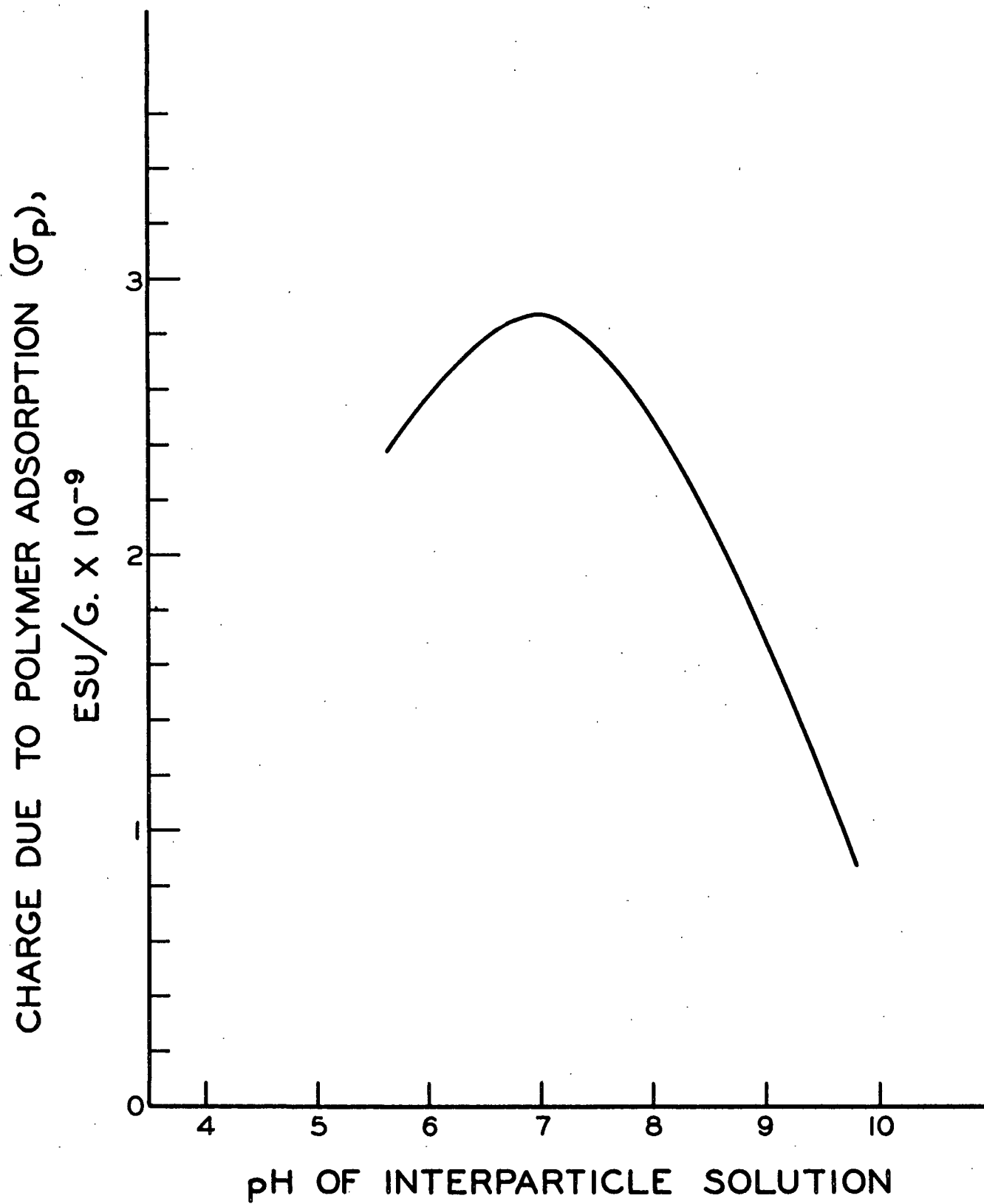


Figure 8. Charge Due to Polymer Adsorption as a Function of pH

## HYDROGEN ION ADSORPTION AND DESORPTION

Figure 9 shows the contribution to charge,  $\sigma_{\text{H}}$ , which results from the adsorption or desorption of protons. It is seen that a reversal of charge occurs at pH 6.7. At higher levels of pH, the negative charge increases due to the desorption of protons. At lower levels of pH, proton adsorption results in a positive contribution to the surface charge.

The pH at which there is neither adsorption nor desorption of protons should correspond to the isoelectric point of  $\text{Fe}_2\text{O}_3$ . Values reported in the literature for the isoelectric point of  $\text{Fe}_2\text{O}_3$  were summarized in Table II (see experimental section). Princen (28) obtained a value of 6.9 for the isoelectric pH of an industrial pigment similar to that used in this study. The value of 6.7 obtained from Fig. 9 appears to be reasonable compared with the results reported in the literature.

In order to be consistent, the data in Fig. 9 were reported in terms of hydrogen ion adsorption or desorption. Actually, it was not possible to experimentally differentiate between proton desorption and hydroxyl ion adsorption (or vice versa). However, the distinction is not critical since both processes are equivalent as far as the contribution to charge is concerned.

## DESORPTION OF SULFATE AND CHLORIDE

### Sulfate Desorption

It was expected that the extent of sulfate ion adsorption would be small in comparison to the extent of polyanion adsorption. This expectation was based upon the fact that the dispersant solution contained only 0.055 meq. of sulfate per meq. of carboxyl. Also, it was thought that the adsorption of sulfate would be appreciable only at the lower levels of pH since at high pH levels the sulfate would have to compete with hydroxyl ions for adsorption onto the pigment surface.

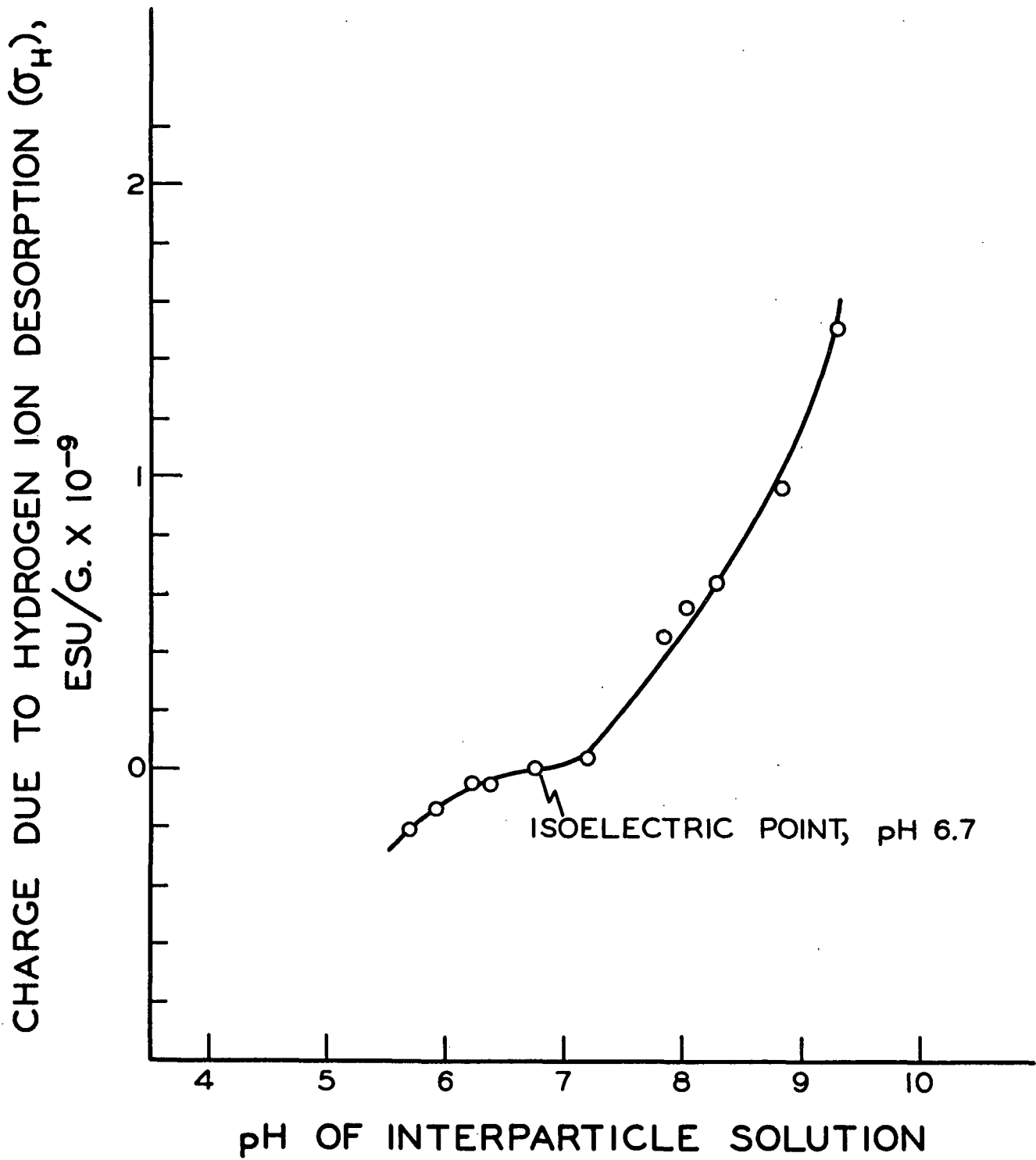


Figure 9. Charge Due to Hydrogen Ion Adsorption or Desorption as a Function of pH

The results of the adsorption experiments were surprising in that the concentration of sulfate in the suspending fluid increased upon addition of pigment. It is evident that the pigment contained an appreciable amount of sulfate which was not removed by leaching with distilled water. Figure 10 shows the extent of the sulfate desorption as a function of pH. The extent of desorption appears to increase somewhat with pH which is consistent with the concept that sulfate and hydroxyl adsorption are competitive processes.

According to the supplier, most of the sulfate associated with the pigment is present in the form of sodium and calcium salts. In this regard, the data reported in Table I (see experimental section, page 19) concerning the soluble salt content of the pigment are of interest. Based on the concentrations of sodium and calcium shown in Table I, the amount of sulfate desorbed in a 10% slurry of washed pigment was about 0.002% (based upon weight of pigment). However, based upon the data shown in Fig. 10, the amount of sulfate desorbed was approximately 0.015%. This indicates that addition of a carboxylated dispersing agent greatly facilitates the desorption of sulfate. One reason for this might be that, because of the deflocculating effect of the dispersant, a much greater amount of surface is accessible to the suspending fluid. Also, the adsorption of both polymer and hydroxyl ions might involve a displacement of sulfate ion at the pigment surface.

The question now arises as to how the desorption of sulfate ion influences the charge on the pigment surface. If just sulfate ions are desorbed, and not the corresponding cation, then the desorption will significantly reduce the negative charge on the surface. But if the corresponding cations are also desorbed, the charge will not be altered. The possibility of cation desorption seems likely because the interparticle solution contains unadsorbed, ionized carboxyl groups which have an affinity for cations. Unfortunately, time did not

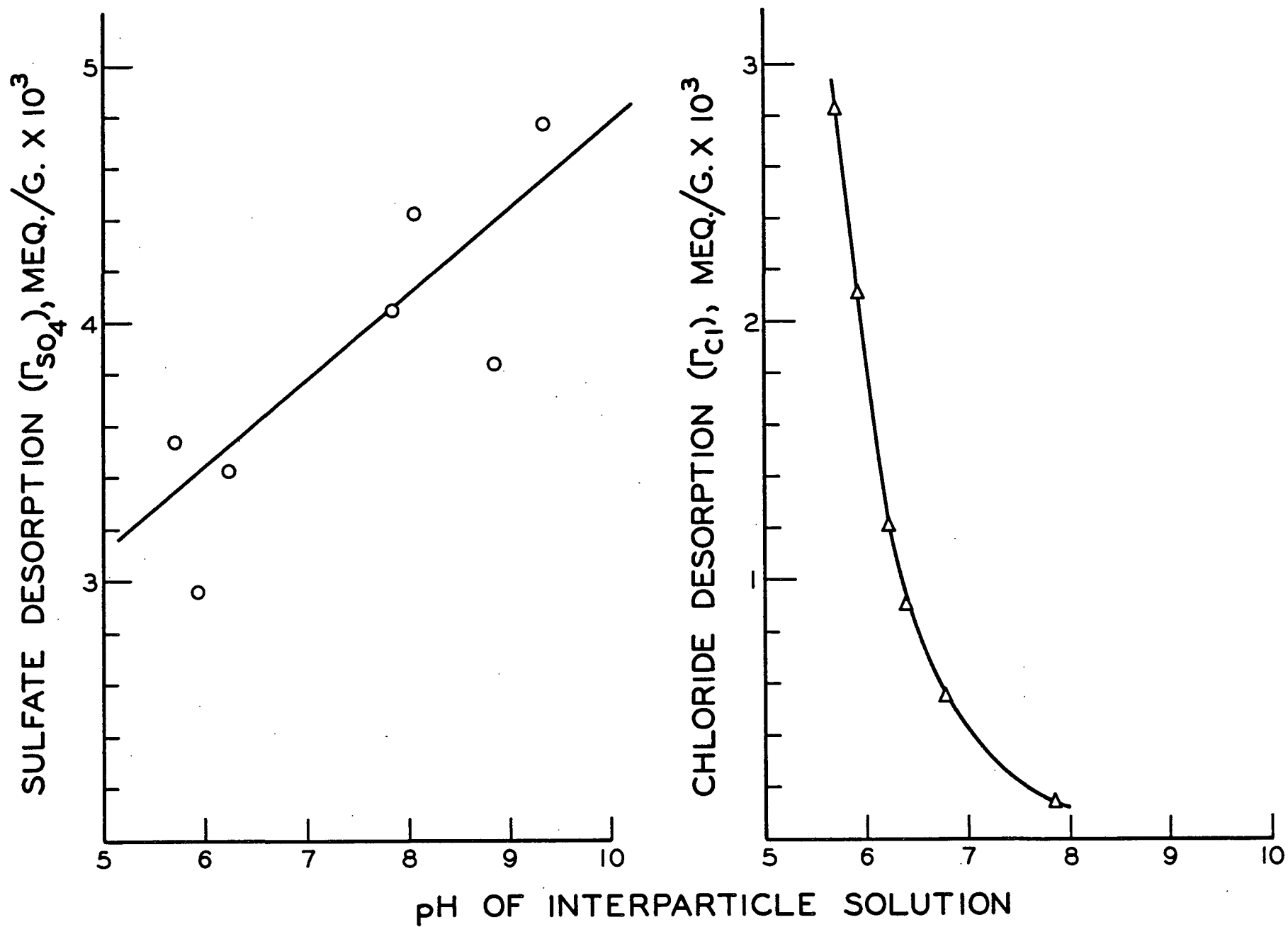


Figure 10. Desorption of Sulfate and Chloride as a Function of pH

permit a detailed cationic analysis of the interparticle solutions and therefore the relationship between sulfate desorption and surface charge is not fully understood.

### Chloride Desorption

The results of the chloride adsorption measurements were somewhat similar to those obtained for the adsorption of sulfate. That is, chloride ion was found to desorb rather than adsorb. The relationship between chloride desorption and pH is shown in Fig. 10. Unlike the sulfate desorption, it is seen that the extent of chloride desorption increases with decreasing pH. This result is somewhat surprising since the pH was adjusted by addition of HCl and therefore the concentration of chloride in the suspending fluid was greatest at low pH. It must be concluded therefore that the desorption of chloride is primarily determined by pH rather than by the amount of chloride present in the interparticle solution.

A possible explanation for this behavior is that the chloride is chemically bonded to iron atoms on the pigment surface and therefore is not readily displaced by other anions in the system. However, the excess of hydrogen ions at low pH may be sufficient to ionize the chloride and effect its removal from the interface.

### TOTAL ADSORBED CHARGE

From the preceding discussions, it is evident that the magnitude of the adsorbed charge,  $\sigma_t$ , depends upon whether or not the desorption of sulfate and chloride is accompanied by cation desorption. However, subsequent discussion will show that the conclusions reached in this thesis are based primarily upon the manner in which the surface charge varies with pH rather than upon the actual magnitude of the charge. The relationship between charge and pH was calculated both with and without the sulfate and chloride desorption data and the results of these calculations are shown in Fig. 11.

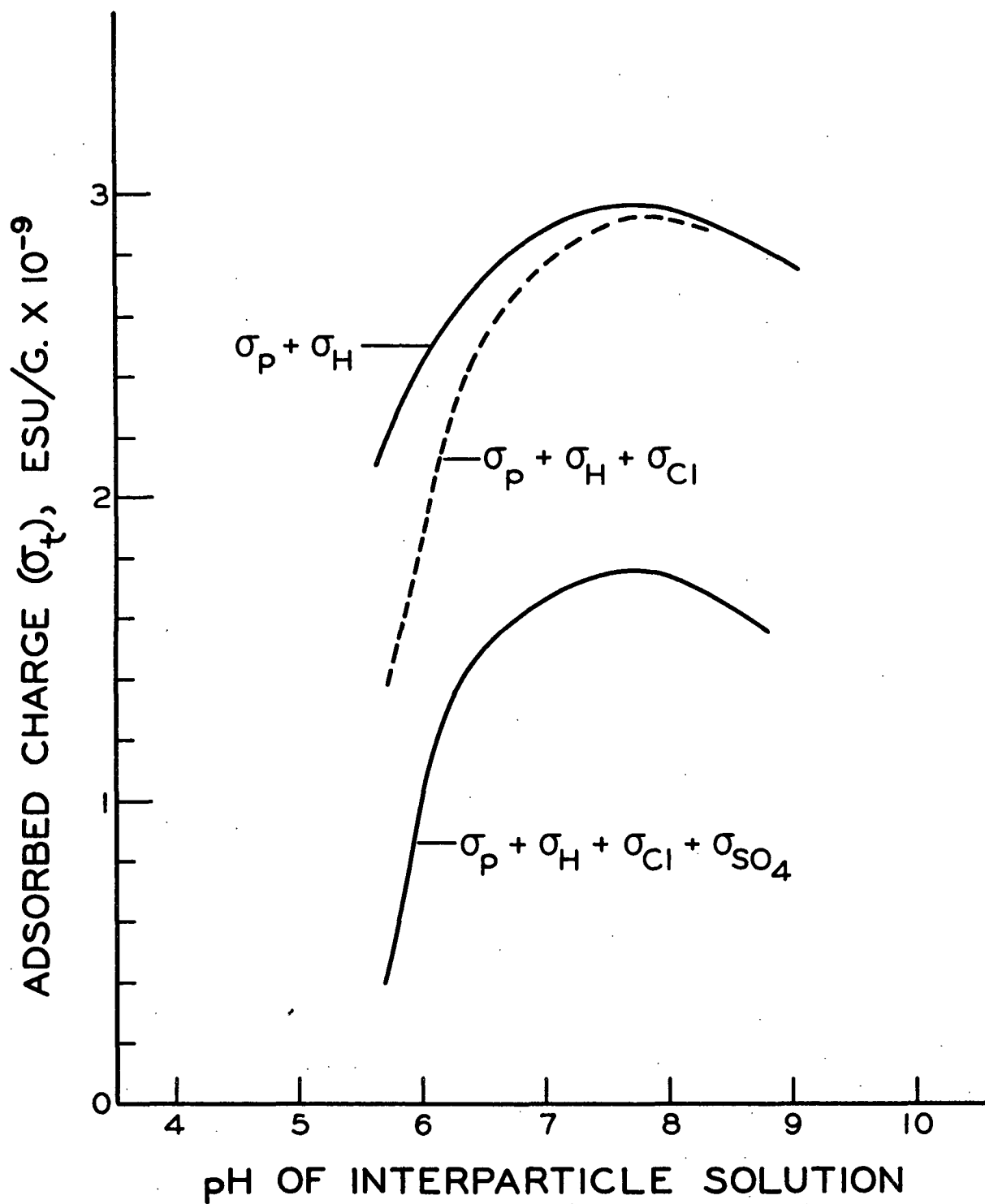


Figure 11. Adsorbed Charge as a Function of pH

The top curve in Fig. 11 was obtained by considering only the effects of polymer adsorption and hydrogen ion adsorption or desorption. It is seen that the charge reaches a maximum at a pH of about 7.8. The dashed curve in Fig. 11 represents the extent to which the surface charge is influenced by considering the extent of chloride desorption. While the negative charge decreases more rapidly at the lower levels of pH, the general shape of the curve and the position of the maximum remain the same. The lower curve in Fig. 11 was obtained by considering the effect of both chloride and sulfate desorption. Again, the position of the maximum and general shape of the curve remain unchanged but the actual magnitude of the adsorbed charge is significantly reduced.

It can be concluded from the curves shown in Fig. 11 that the variation in adsorbed charge with pH is primarily controlled by the extent of polymer adsorption and hydrogen ion adsorption or desorption. In order to simplify subsequent discussions, the top curve in Fig. 11 will be used to represent the variation in adsorbed charge with pH. The relationship between the magnitude of the charge and colloidal stability will be discussed in greater detail in a later section.

#### THE RELATIONSHIP BETWEEN RHEOLOGICAL BEHAVIOR AND ADSORBED CHARGE

##### LOW-SHEAR VISCOSITY DATA

Figure 12 shows the relationship between Brookfield viscosity and surface charge. The data show that the viscosity at low shear ( $\dot{\gamma} < 50 \text{ sec.}^{-1}$ ) is a minimum at the pH corresponding to the maximum surface charge. As previously discussed, this type of relationship is well substantiated in the literature. As the charge decreases, the particles are less stable and the extent of flocculation increases. This results in an increase in viscosity since additional energy is required to disrupt the flocs. The primary significance of the viscosity

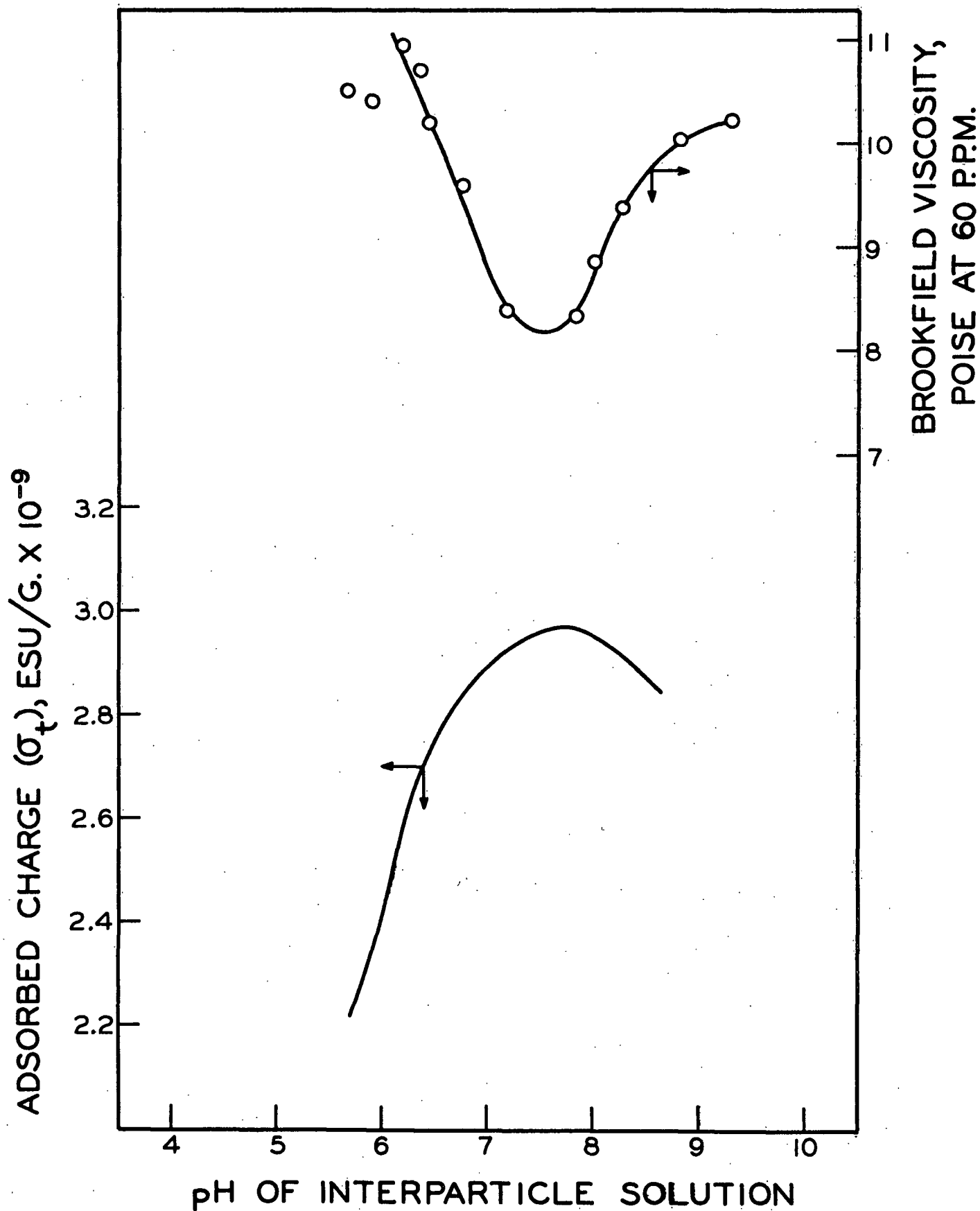


Figure 12. Adsorbed Charge and Brookfield Viscosity as a Function of pH

data shown in Fig. 12 is that they indicate that the adsorbed charge represents a valid measure of the extent of colloidal stability of the particles.

## EXTENT OF RHEOLOGICAL DILATANCY AS A FUNCTION OF ADSORBED CHARGE

### Representation of Data

In the absence of a theoretically based model for the description of dilatant flow, an empirical model was needed so that the extent of dilatancy could be expressed in terms of a numerical value. The approach used in this study was based upon an equation similar to that proposed by Goodeve (42) to describe thixotropy. Implicit in this equation is the assumption that the mechanisms responsible for non-Newtonian behavior are distinct from those involved in Newtonian flow and that the shear stress requirements for the two processes are additive;

$$\tau_b - \tau_o = \eta^*G + \theta(G) \quad (4).$$

The significance of the terms in Equation (4) is illustrated in Fig. 13. The quasi-Newtonian viscosity,  $\eta^*$ , corresponds to the slope of the flow curve in a region of shear intermediate between pseudoplasticity and dilatancy and therefore represents the minimum viscosity of the suspension. The quantity  $\theta$  represents the additional amount of shear stress required above that needed for quasi-Newtonian flow. In the context of this study,  $\theta$  can be considered as the dilatant component of shear stress. The magnitude of  $\theta$  is a function of the shear rate as well as the other variables influencing the extent of dilatancy. Since the suspensions were slightly pseudoplastic at low shear, the linear portion of the flow curve (having a slope of  $\eta^*$ ) does not pass through the origin. Therefore, it was necessary to introduce into Equation (4) the quantity  $\tau_o$ , which represents the point of intersection of the line on the shear stress axis.

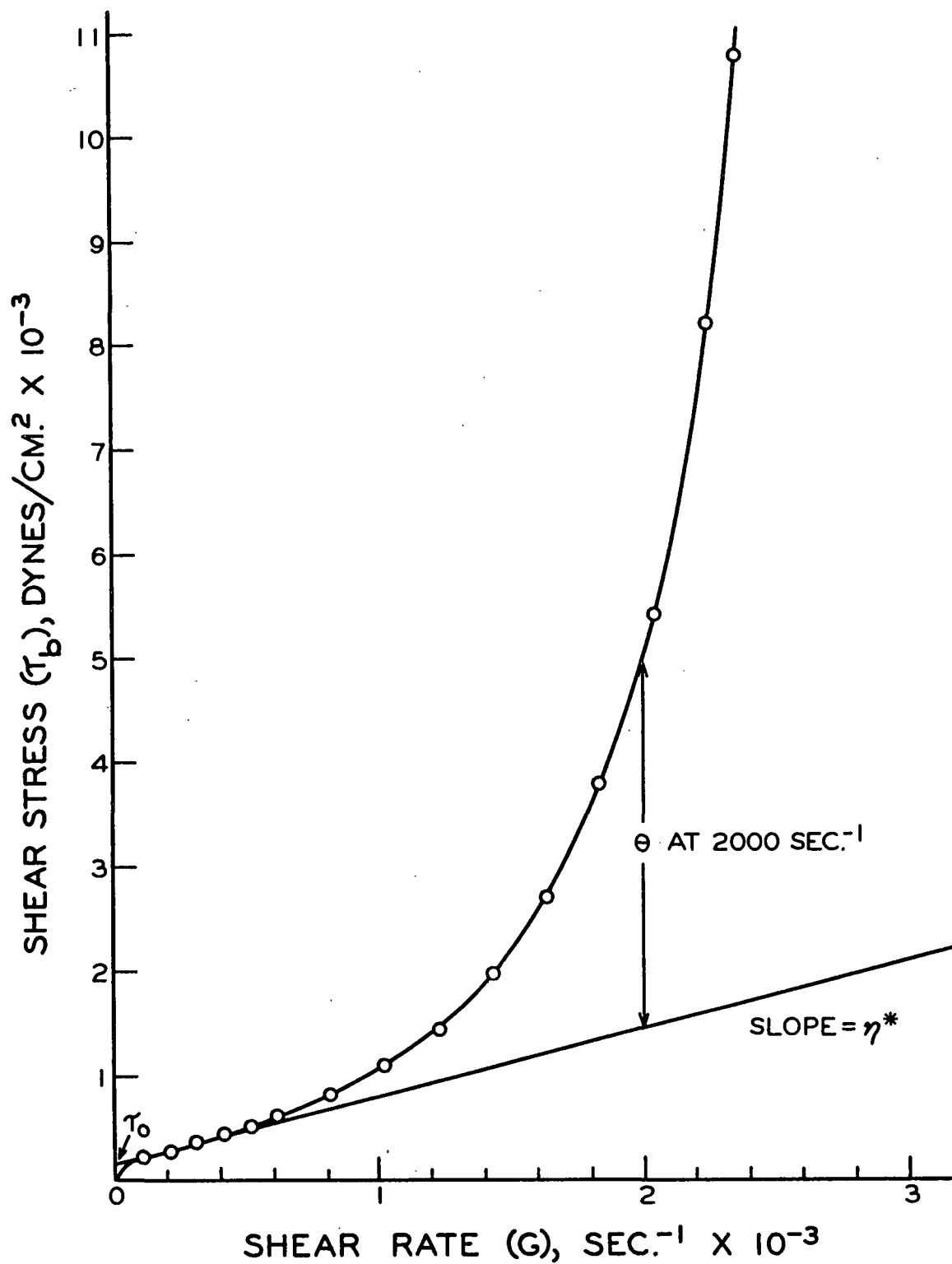


Figure 13. Determination of Newtonian Viscosity and Dilatant Shear Stress. (Suspension 151)

In this study, values of  $\theta$ , obtained at a common rate of shear, were used as indices to compare the extent of dilatancy of different suspensions. The shear stress-shear rate relationships obtained at each level of adsorbed charge are tabulated in Appendix III.

#### Presentation of Data

In Fig. 14, the dilatant components of shear stress,  $\theta$ , are plotted as a function of pH at two different levels of shear rate. For purposes of comparison, the surface charge is shown in the upper curve. These curves show that the extent of dilatancy decreases as the charge on the pigment increases. Note that the dilatant component of shear stress is a minimum at the pH where the adsorbed charge is a maximum.

The results shown in Fig. 14 are of central significance to this thesis. As previously discussed, if the Brownian motion hypothesis were valid, the extent of dilatancy would be expected to increase with increasing colloidal stability. Since just the opposite relationship is observed in Fig. 14, it must be concluded that the extent of rheological dilatancy is not controlled by the level of Brownian motion of the particles. Rather, the data support the hypothesis that rheological dilatancy results from a shear-induced flocculation mechanism. This interpretation will be discussed in greater detail in a later section.

### THE RELATIONSHIP BETWEEN RHEOLOGICAL BEHAVIOR AND PIGMENT VOLUME CONCENTRATION

#### EXTENT OF DILATANCY AS A FUNCTION OF PIGMENT VOLUME CONCENTRATION

Shear stress-shear rate measurements were obtained as a function of PVC at two different levels of adsorbed charge. At each level of charge, the PVC was varied between 47 and 40%. As discussed in the experimental section, the PVC was varied in such a manner that the adsorbed charge remained essentially constant.

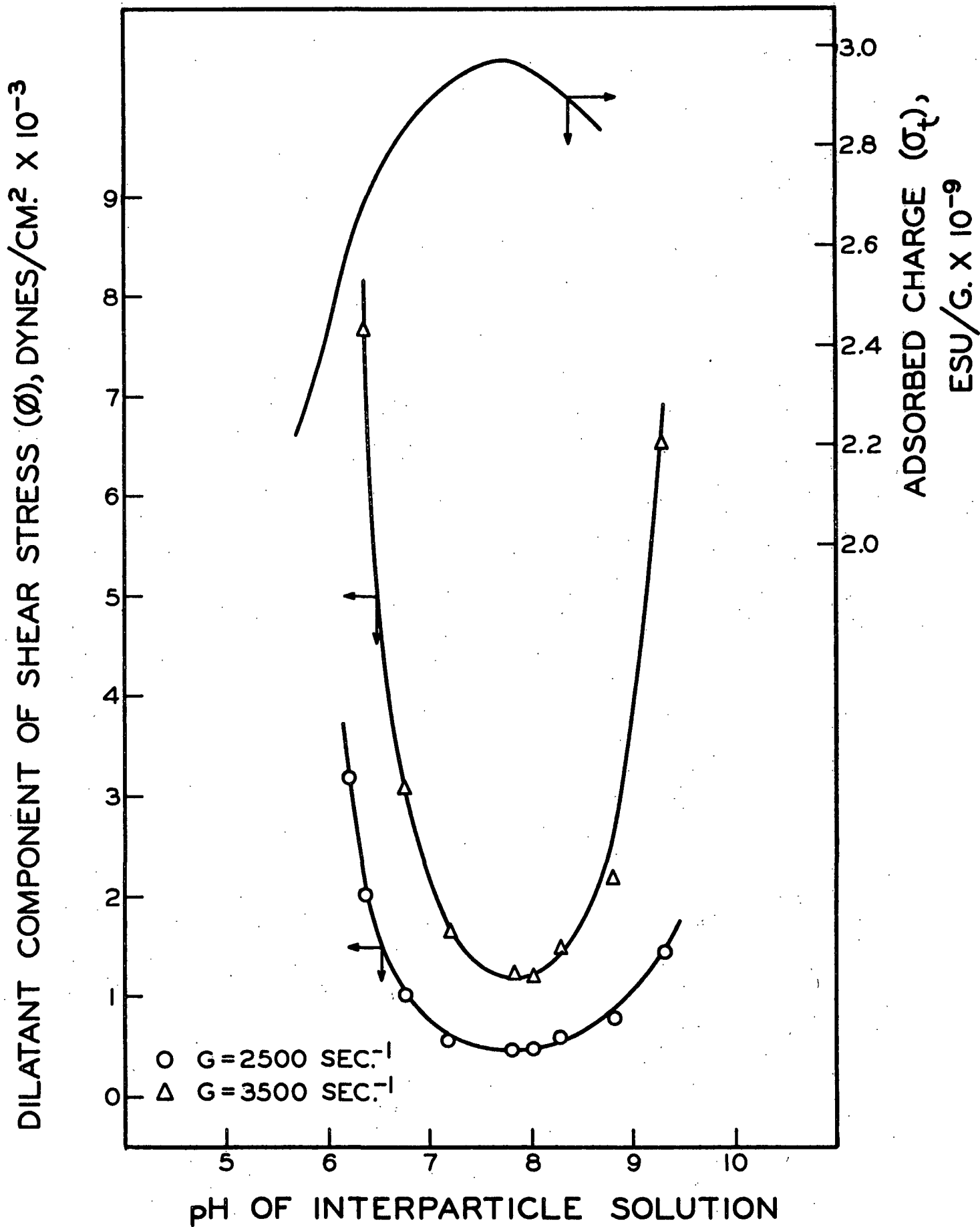


Figure 14. Dilatant Component of Shear Stress and Adsorbed Charge as a Function of pH - PVC = 45%

For each of the two series of suspensions, adsorption measurements were obtained and these are presented in Appendix III along with the tabulated shear stress-shear rate measurements.

The experiments showed that the extent of dilatancy is highly dependent upon the pigment volume concentration. The data in Fig. 15 ( $\sigma_H + \sigma_P = 2.8 \times 10^9$  esu/g.) show the relationships obtained between shear stress and shear rate at four different concentrations of pigment.

In Fig. 16 ( $\sigma_H + \sigma_P = 2.8 \times 10^9$  esu/g.) and Fig. 17 ( $\sigma_H + \sigma_P = 2.62 \times 10^9$  esu/g.) the logarithm of the dilatant shear stress,  $\theta$ , is plotted as a function of PVC at two levels of shear rate. The data appear to show a linear relationship when plotted in this manner which indicates that the extent of dilatancy is exponentially dependent upon the concentration of pigment. Within the limits of the experimental error, the slopes of the lines appear to be independent of the rate of shear. Note, however, that the slopes of the lines in Fig. 16 are not the same as those in Fig. 17. Evidently, the rate of change of  $\theta$  with PVC becomes more pronounced as the surface charge is decreased.

#### NEWTONIAN VISCOSITY AS A FUNCTION OF PIGMENT VOLUME CONCENTRATION

A number of theoretically based equations have been developed which relate the viscosity of monodisperse, Newtonian suspensions to particle concentration and viscosity of the suspending fluid (7, 8). In particular, an equation derived by Happel (43) has been shown to give good agreement with experimental data in the range of PVC investigated in this study. Happel used a "free surface" model to obtain a solution to the Navier-Stokes equations. In this model, the disturbance due to each sphere is assumed to be confined to a frictionless envelope surrounding it.

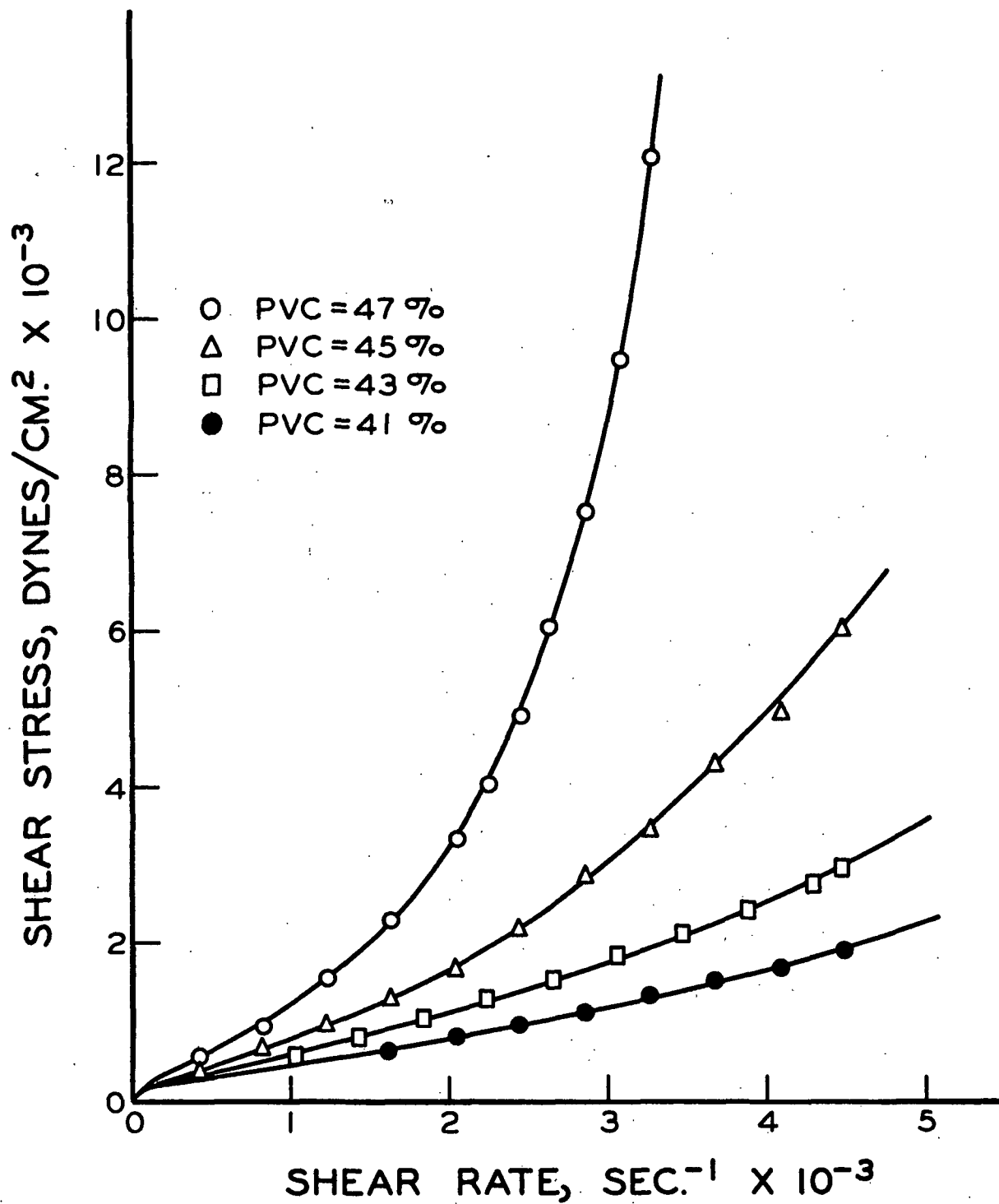


Figure 15. The Effect of Pigment Volume Concentration on the Extent of Dilatancy

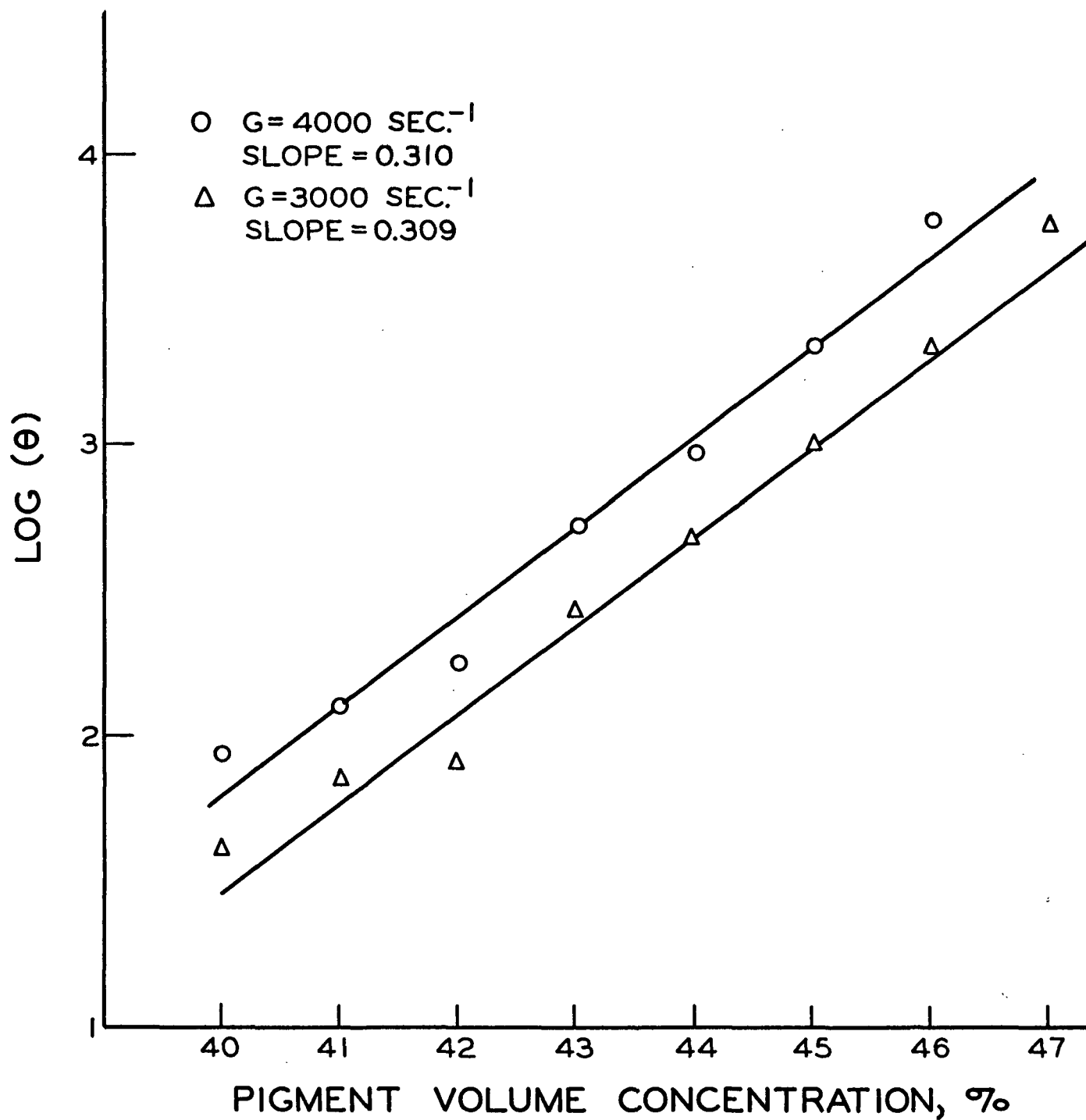


Figure 16. Logarithm of Dilatant Shear Stress as a Function of Pigment Volume Concentration - Suspensions 163 to 170, ( $\sigma_{\underline{p}} + \sigma_{\underline{H}} = 2.8 \times 10^9 \text{ esu/g.}$ )

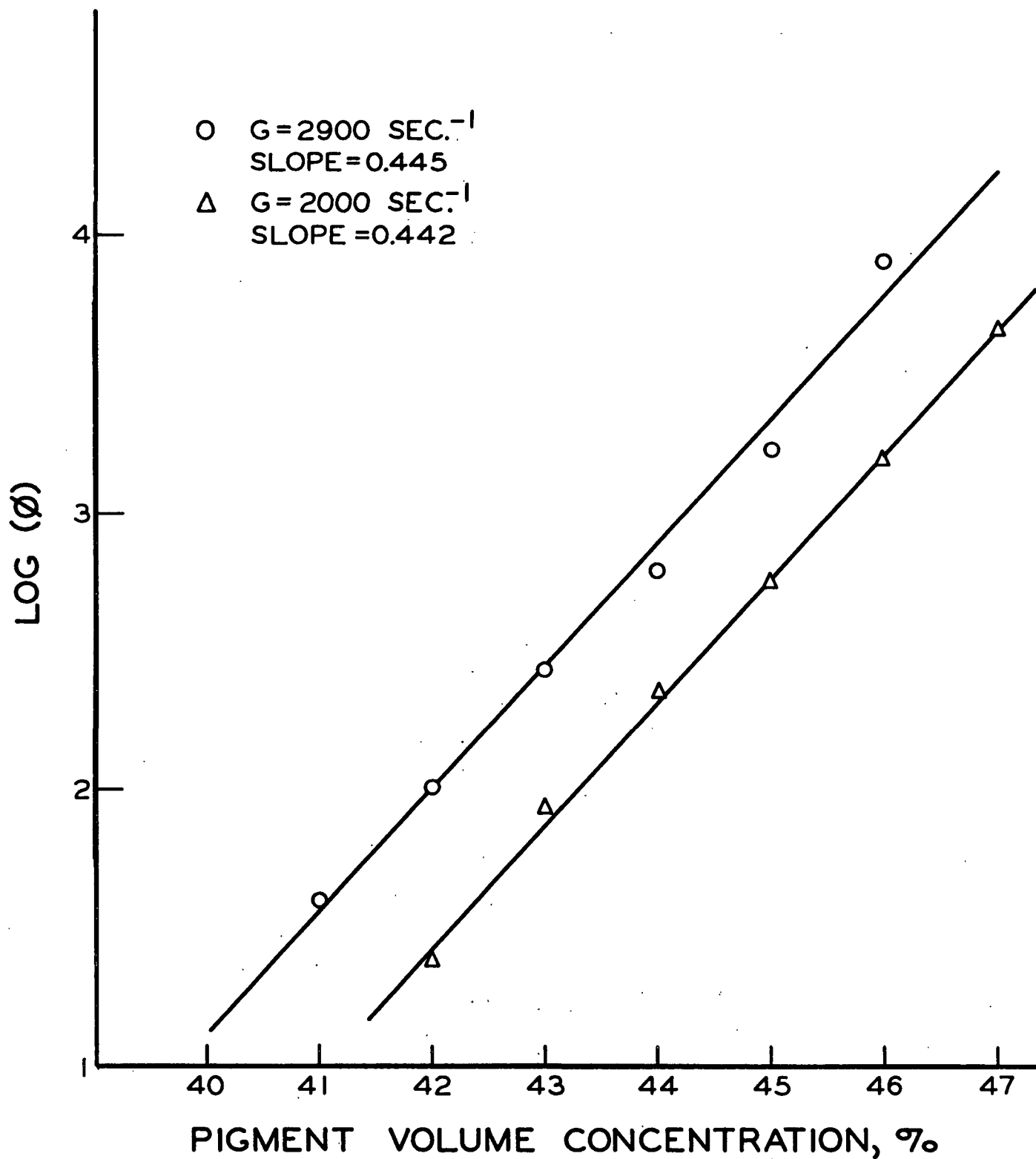


Figure 17. Logarithm of Dilatant Shear Stress as a Function of Pigment Volume Concentration - Suspensions 171 to 177, ( $\sigma_p + \sigma_H = 2.62 \times 10^9 \text{ esu/g.}$ )

It is instructive to compare the relationship between  $\eta^*$  and PVC obtained in this study with that predicted by Happel's equation. This comparison is shown in Fig. 18 where the relative viscosity,  $\eta^*/\eta_0$ , is plotted as a function of PVC. The quantity  $\eta_0$  refers to the viscosity of the suspending fluid and was determined at each level of charge using a Hoesppler falling ball viscometer. Curve A represents data obtained at  $\sigma_{\underline{H}} + \sigma_{\underline{P}} = 2.62 \times 10^9$  esu/g. while Curve B represents data obtained at  $\sigma_{\underline{H}} + \sigma_{\underline{P}} = 2.9 \times 10^9$  esu/g.

It is recalled that the values of  $\eta^*$  were obtained in a range of shear intermediate between pseudoplasticity and dilatancy. Thus, the data shown in Fig. 18 represent the minimum viscosities of the suspensions and therefore correspond to the minimum levels of particle aggregation. However, the viscosities of the suspensions are seen to be much greater than those predicted by Happel's equation for monodisperse suspensions. This result indicates that, at the point where pseudoplasticity is no longer observed, the particles are still in a state of partial flocculation. Furthermore, as indicated by the difference between Curves A and B, the level of the minimum state of flocculation is a function of the surface charge.

#### SEIZURE AND FRACTURE OF DILATANT SUSPENSIONS

During the preliminary stages of this study, suspensions were prepared using iron oxide pigments of slightly smaller particle size (Chas. Pfizer Co.-R6098 and R7098). Measurements of the colloidal variables were not obtained but two unusual flow phenomena were observed which deserve mention. These are shown in Fig. 19 in which the flow data are expressed in terms of torque and rate of rotation of the bob. The PVC of these suspensions was 45%.

With the smallest sized pigment, R6098, the flow was typically dilatant up to a bob speed of 830 r.p.m. At this point, an abrupt increase in torque was observed. In essence, the suspension appeared to seize and behave as a solid.

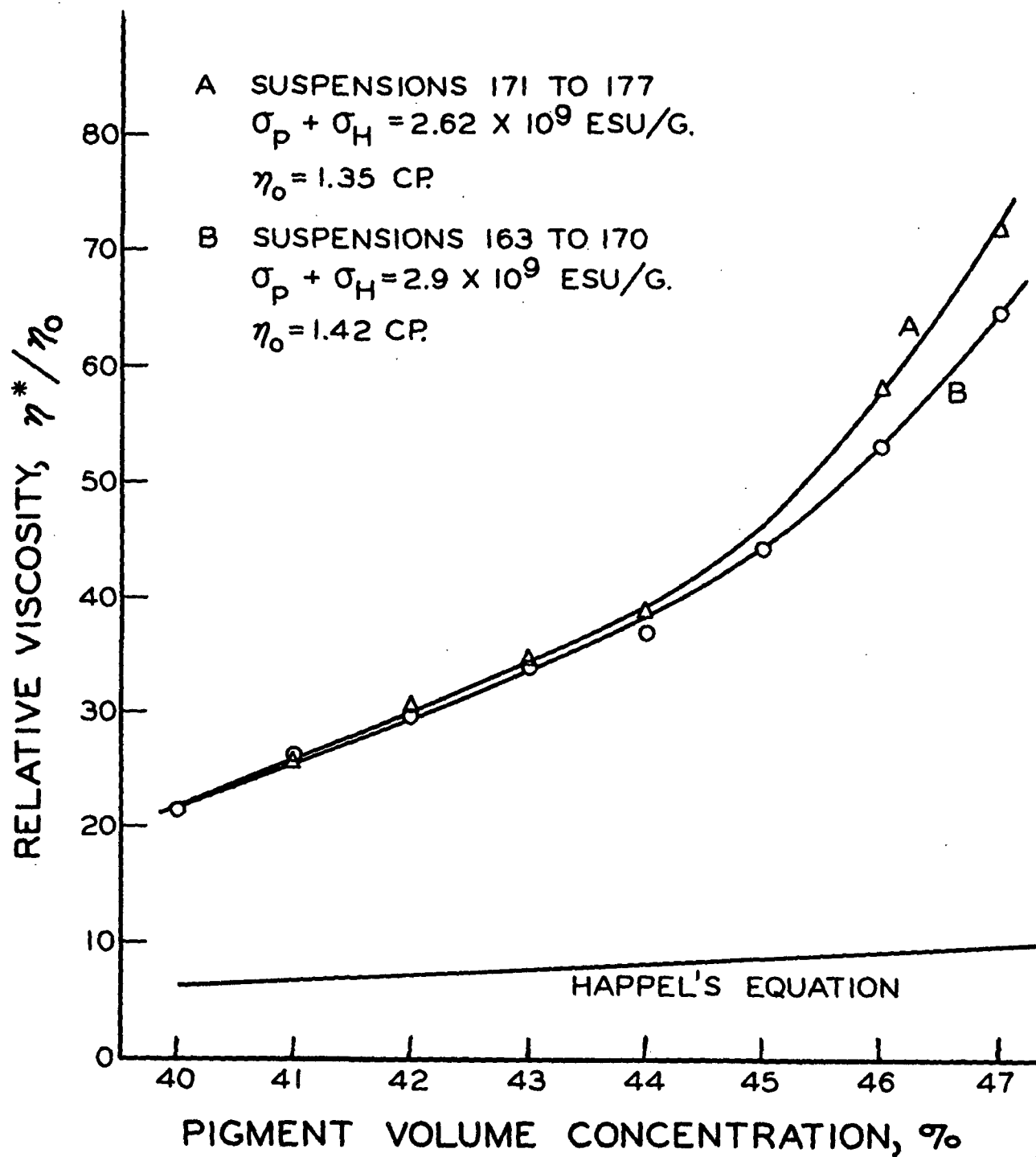


Figure 18. Relative Viscosities of Suspensions as Compared With Happel's Equation

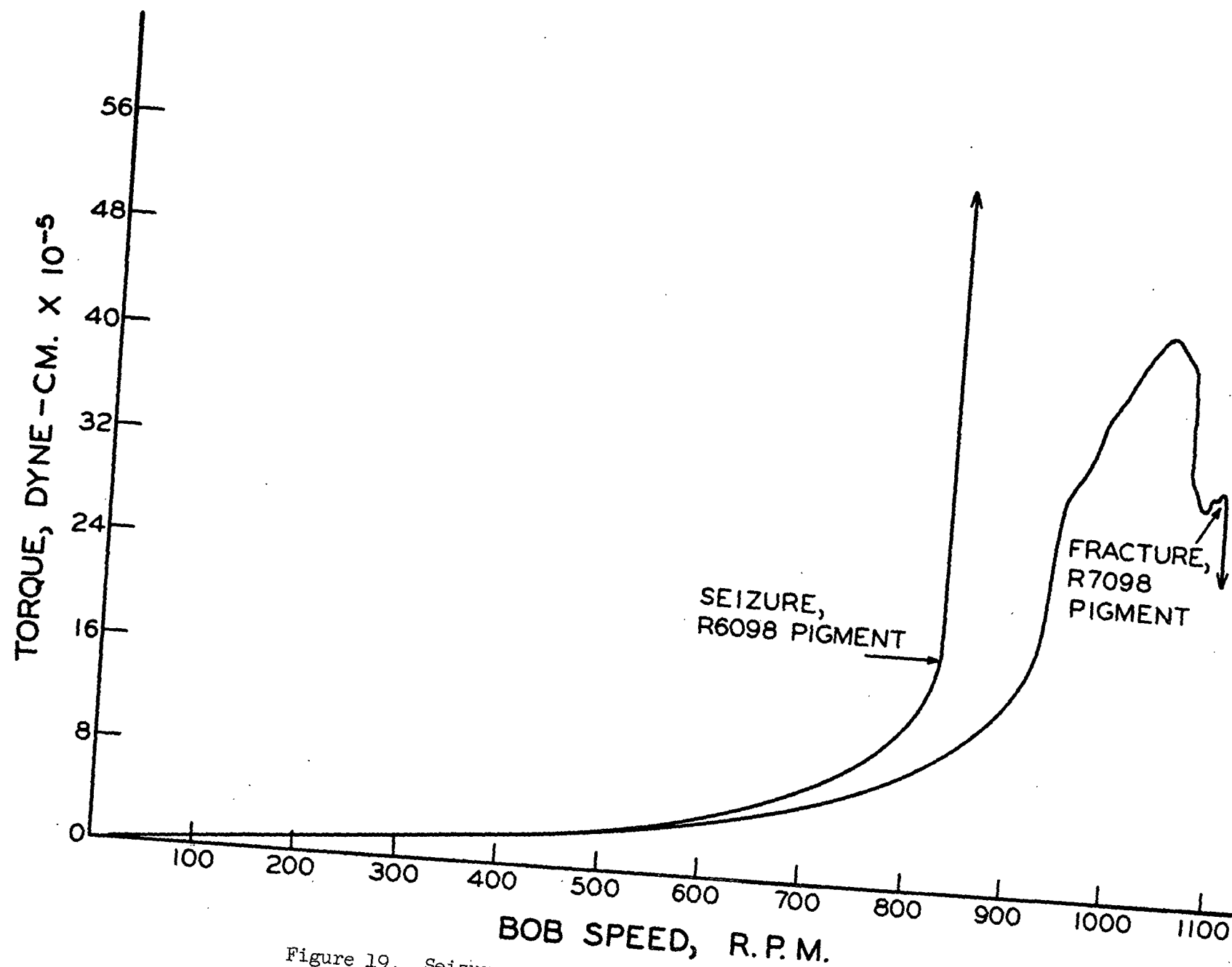


Figure 19. Seizure and Fracture of Dilatant Suspensions

As seen in Fig. 19, a somewhat different phenomenon was observed with a suspension of the R7098 pigment. At a bob speed of approximately 970 r.p.m., the flow became unstable and the torque reading was highly erratic. When the rate of shear was further increased, a loud cracking noise emanated from the region of shear and an abrupt decrease in torque was noted. That is, the suspension appeared to fracture. Metzner and Whitlock (24) and Metzner (62) reported a similar observation with suspensions of  $\text{TiO}_2$  and with suspensions of cornstarch. In their experiments, the fracture was audible in both a rotational and capillary viscometer and the critical value of the shear stress was the same in both instruments.

It seems reasonable that the seizure and fracture phenomenon are related. In both cases, it is hypothesized that the extent of the shear-induced flocculation becomes so great that relative motion between aggregates is no longer possible and the suspension then has the properties of a solid. If the force transmitted to the suspension is insufficient to overcome the internal strength of the flocs, then seizure results. However, if the energy input is large enough, the floc fractures in a manner analogous to the rupture of a solid.

## DISCUSSION

### MECHANISMS OF COLLOIDAL STABILIZATION

Because of the importance which has been attached to the relationship between dilatancy and colloidal stability, it is appropriate to consider more carefully the mechanisms responsible for colloidal stability in the system. It is recalled that the Brookfield viscosity data showed that the adsorbed charge is a valid index of the degree of colloidal stability of the suspensions. This evidence suggests that the stability is primarily a function of the magnitude of the electrostatic forces between the particles. However, although electrostatic repulsion is no doubt a significant factor, there is reason to believe that other mechanisms are also of considerable importance.

### STERIC HINDRANCE OR ENTROPIC STABILIZATION

Based on the polymer adsorption data and assuming a molecular weight of 4000, calculations were made to estimate the average number of polymethacrylate molecules adsorbed per particle of pigment. Depending upon the pH, the number of molecules per particle varied between 1400 and 5000. It seems likely, therefore, that the interaction between adsorbed molecules on adjacent particles must be a factor which contributes to the colloidal stability. At a pigment volume concentration of 45% and an average particle diameter of 0.20  $\mu\text{m}$ ., the average distance between the particles is about 0.01  $\mu\text{m}$ . According to an equation derived by Hamaker (44), this corresponds approximately to the distance at which the London-van der Waals attractive forces become significant. Based on a molecular weight of 4000, the total length of a molecule of polymethacrylic acid is about 0.015  $\mu\text{m}$ . Depending upon the configuration of the adsorbed polymer and upon the number of contact points with the surface, the distance that the molecules extend away from the

surface is probably somewhat less than the total extended length of the chains. Nevertheless, it is apparent that the molecular weight of the polymer is such that steric interactions will be significant at distances of separation where the attractive forces begin to be of importance.

Experimental verification of the mechanism of stearic stabilization has been reported by Heller and Pugh (45, 46), Mathai and Ottewill (47), and Van der Waarden (48). In general, the extent of stabilization has been found to increase with both the amount of adsorbed polymer and the molecular weight. Theoretical equations describing this type of stabilization have been reported by Makkor (49, 50) and by Clayfield and Lumb (51). Estimates of the energy of repulsion were obtained by considering the reduction in entropy of adsorbed molecules due to interactions with molecules adsorbed on adjacent particles. Clayfield and Lumb concluded that the energy of repulsion due to entropic stabilization could be as high as  $100 \text{ KT}$  — a value which is comparable to the magnitude of the attractive energy at a distance of separation of  $0.002 \text{ }\mu\text{m}$ .

#### HYDRATION OF THE PIGMENT SURFACE

Heller and Pugh (45) have pointed out that the chemical nature of the adsorbed polymer is of considerable importance. Hydrophilic groups, such as carboxyls, increase the extent of stabilization because the pigment-polymer interface becomes more hydrated. That is, the presence of hydrophilic groups increases the energy of attraction between the particle and the suspending fluid and thus decreases the effectiveness of the interparticle attractive forces. Since the polymer used in this study contained carboxyl groups, it is reasonable to assume that part of the stabilization resulted from this type of mechanism.

## RELATIONSHIP BETWEEN CHARGE AND COLLOIDAL STABILITY

Because the carboxyl groups on the adsorbed polymer are partially ionized, it is clear that electrostatic repulsion must contribute to the colloidal stability. The magnitude of the electrostatic repulsive force is also a function of the level of adsorption or desorption of the smaller ions such as hydroxyl, sulfate, and chloride. In the case of dilute, lyophobic sols in which the surface potential results from the adsorption of small ions, the Verwey-Overbeek theory (52) accounts satisfactorily for the stability requirements of the system. But the assumptions of this theory are such that it cannot be expected to apply in the case of concentrated suspensions which are stabilized by polyelectrolyte adsorption. For example, one of the assumptions of the Verwey-Overbeek theory is that the adsorbed charge is uniformly distributed over the plane of the particle surface. This assumption is clearly not valid in the case of polyanion adsorption since the polymer molecules extend an appreciable distance away from the surface. Furthermore, the distance of this extension probably depends on the extent of the interaction between adjacent particles.

Perhaps more important than the electrostatic repulsion between particles is the extent to which the configuration and stiffness of the adsorbed polymer vary with the degree of dissociation. It is well established that polyelectrolyte molecules expand considerably with increasing charge. In the case of polymethacrylic acid, Tanford (35) has shown that the equivalent radius of the molecule in water increases by as much as 200% when the degree of dissociation is increased from zero to 0.7. The configuration of the polymer is of considerable significance with regard to the extent of entropic stabilization. As the degree of dissociation increases, it is reasonable to expect that the adsorbed molecules become more rigid and extend further away from the surface. This in turn would be expected to increase the extent of steric interaction and stabilization.

Based on the considerations discussed above, it is possible to give a more complete explanation for the relationship observed between adsorbed charge and stability as measured by Brookfield viscosity (see Fig. 12). As the degree of dissociation increases, the level of entropic and electrostatic repulsion due to a given amount of adsorbed polymer increases. At the same time, however, the amount of polymer adsorbed decreases. It is the balance between these opposing mechanisms which is thought to account for the minima observed in the plots of pH versus Brookfield viscosity and extent of dilatancy.

#### THE MECHANISM OF RHEOLOGICAL DILATANCY

##### QUALITATIVE CONSIDERATIONS

Earlier in this dissertation it was concluded that the extent of Brownian motion would increase with increasing colloidal stability providing the initial level of flocculation were appreciable. It is felt that the data shown in Fig. 18 justify this conclusion. The data show that the minimum apparent viscosity is much greater than that expected for a monodisperse suspension. Note also that the minimum apparent viscosity decreases with increasing adsorbed charge. Based on these considerations, it is felt that the increase in Brownian motion due to the decrease in flocculation is considerably more significant than any decrease in Brownian motion which might result from the increased energy of repulsion between adjacent particles. Since the extent of dilatancy does not increase with increasing colloidal stability it is concluded that the Brownian motion hypothesis is incorrect.

The experimental results obtained in this study have shown that the extent of dilatancy increases with decreasing colloidal stability. As discussed in the beginning of this thesis, this finding suggests that rheological dilatancy is caused by a shear-induced flocculation process. When the rate of shear is increased,

there is an increase in both the particle collision frequency and the force with which the collisions occur. Since the particles are better able to overcome the repulsive energy barriers responsible for stability, there is a progressive increase in the extent of flocculation, and therefore the viscosity of the suspension. If the magnitude of the repulsive barrier is increased, it follows that a suspension will be less dilatant since a greater level of stress will be required to reach a given level of flocculation.

#### DILATANCY AND PSEUDOPLASTICITY CONSIDERED AS COMPETITIVE RATE PROCESSES

At first thought, the concept of shear-induced flocculation seems to be in conflict with the more traditional idea that the application of shear causes a disruption in floc structure. The pseudoplastic behavior observed at very low rates of shear is explained on the basis of floc disruption; whereas, the dilatant behavior at high shear rates is explained on the basis of floc formation. This apparent anomaly can be resolved by considering pseudoplasticity and dilatancy as competitive rate processes.

The equations to follow were used by Joly (54) to describe the kinetics of flocculation in a colloidal suspension. Joly's analysis is similar to that proposed by Blatz and Tobolsky (53) to describe the kinetics of a linear polymer system manifesting simultaneous polymerization and depolymerization. Of interest is the manner in which the number of aggregates per unit volume containing  $s$  particles,  $N_s$ , changes with time. It is assumed that aggregates of this type can be created or destroyed by two processes; (1) bimolecular collisions between two aggregates to give a larger aggregate, and (2) unimolecular disruption into smaller aggregates due to the shear stresses within the suspension. The simultaneous collision of more than two aggregates is assumed to be negligible.

According to Joly (54), the rate of change of  $\underline{N}_s$  with time due to collision and disruption is given by:

$$dN_s/dt = 1/2 \sum_{i=1}^{i=s-1} A_{i,s-1} N_i N_{s-1} - N_s \sum_{i=1}^{i=\lambda} A_{i,s} N_i + 2 \sum_{i=s+1}^{i=\lambda} B_i N_i - B_s (s-1) N_s \quad (5)$$

where

$\underline{A}_{\underline{l},\underline{m}}$  = rate constant for the bimolecular collision of an aggregate containing  $\underline{l}$  particles with one containing  $\underline{m}$  particles,  $\text{cm}^3/\text{sec}.$ ;

$\underline{B}_{\underline{q}}$  = rate constant for unimolecular disruption of an aggregate containing  $\underline{q}$  particles,  $\text{sec}^{-1}$ ;

$\lambda$  = the upper limit of the number of particles per aggregate.

In this equation, the quantity  $\underline{A}_{\underline{l},\underline{m}} \underline{N}_{\underline{l}} \underline{N}_{\underline{m}}$  represents the number of collisions per second per  $\text{cm}^3$  between aggregates  $\underline{l}$  and  $\underline{m}$  which produce an aggregate containing  $\underline{l}+\underline{m}$  particles. Terms of the type  $\underline{B}_{\underline{q}} \underline{N}_{\underline{q}}$  represent the number of aggregates containing  $\underline{q}$  particles which disrupt per second per  $\text{cm}^3$ .

In Equation (5), the first term accounts for the formation of  $\underline{N}_s$  by collisions between aggregates containing less than  $\underline{s}$  particles. The disappearance of aggregates containing  $\underline{s}$  particles due to collision and addition with other aggregates is given by the second term. The third term accounts for the formation of  $\underline{N}_s$  due to disruption of larger aggregates while the last term accounts for the disruption of  $\underline{N}_s$ .

The average aggregate size at time  $\underline{t}$  is defined as

$$X_t = \frac{\sum_{s=1}^{\lambda} s N_s}{\sum_{s=1}^{\lambda} N_s} \quad (6).$$

By assuming that the rate constants,  $\underline{A}$  and  $\underline{B}$  were independent of aggregate size, Joly (54) was able to solve Equation (5) for  $\underline{X}_t$ . For the special case where the

particles are linked together in a linear manner, this assumption is not unreasonable. However, for more complex and realistic floc geometries, the rate constants will actually depend to some extent on the aggregate sizes. Nevertheless, Joly's solution is of interest because it indicates the functional dependence of  $\underline{X}_t$  on both  $\underline{A}$  and  $\underline{B}$ . The solution is

$$\underline{X}_t = \frac{1 + (2B/N_o A)^{1/2} \coth [(N_o AB/2)^{1/2} t]}{(2B/N_o A)^{1/2} \coth [(N_o AB/2)^{1/2} t]} \quad (7)$$

where  $\underline{N}_o$  is the total number of primary particles per cm.<sup>3</sup>. At equilibrium ( $\underline{t}$  large), the equation reduces to

$$\underline{X} \approx (N_o A/2B)^{1/2} \quad (8).$$

Thus, the average aggregate size depends upon the ratio of the rate constants for collision and disruption as well as upon the total particle concentration.

To understand the relationship between dilatancy and pseudoplasticity, it is necessary to consider the functional relationship between the rate constants and the rate of shear. Figure 20 illustrates the manner in which the rate constants must vary with shear rate so that both pseudoplasticity and dilatancy will be exhibited in the same suspension.

In Fig. 20, the relative magnitude of the two rate constants is entirely arbitrary. The important point is the manner in which each constant varies with shear. At low rates of shear, the rate of change of  $\underline{B}$  with shear is greater than that for  $\underline{A}$ . Therefore, the ratio of  $\underline{A}$  to  $\underline{B}$  must decrease. As required by Equation (8) the average aggregate size must decrease which will result in a decrease in viscosity. Therefore, in this region of shear, the flow will be pseudoplastic. Note however, that as the shear is increased, a point is reached where the rate of

change of A with shear exceeds that for B. At this point, the ratio of A to B begins to increase and consequently the average aggregate size must increase. Therefore, at the higher levels of shear, the flow becomes dilatant.

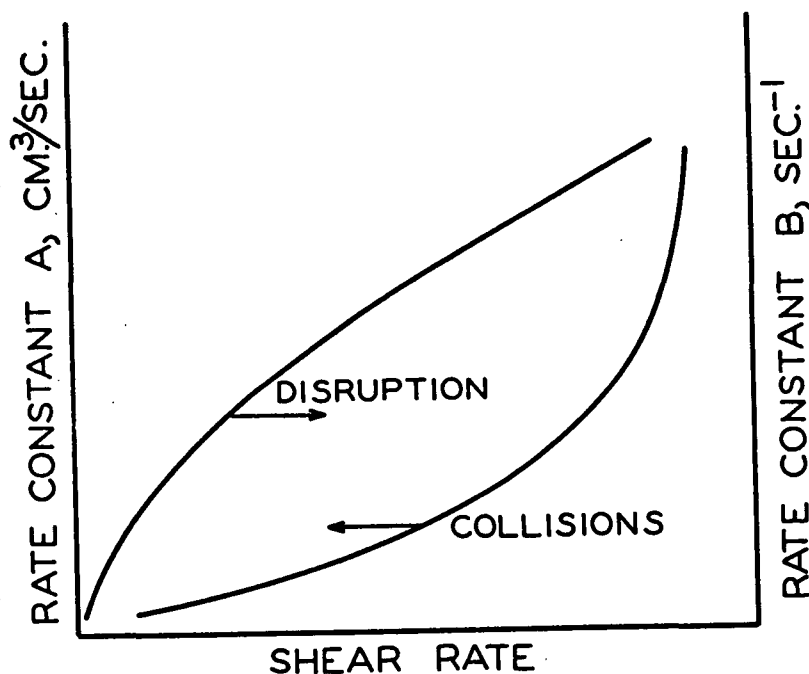


Figure 20. Variations of Rate Constants with Shear Rate

With regard to Fig. 20, it is reasonable to expect that the rate constant for the collision process will be much more highly dependent on the repulsive energy of interaction than will the rate constant for disruption. The energy required for collision and flocculation is primarily dependent upon the height of the repulsive energy barrier between the particles or aggregates. However, once this barrier is overcome and the particles are flocculated, the energy required for disruption is primarily dependent upon the short-range adhesive forces. These forces are not highly dependent upon the height of the repulsive barrier and are controlled principally by molecular interactions. Therefore, the effect of decreasing the level of colloidal stability is primarily to increase both the height and extent of curvature of Curve A in Fig. 20.

In Fig. 20, the rate constant descriptive of the collision process was arbitrarily drawn as an exponential function of shear rate. An analysis developed by de Vries (55) lends support to this idea. de Vries derived an expression for the collision frequency between monodisperse particles which are stabilized by a repulsive energy barrier. His analysis takes into account the effects of both shear and Brownian motion. The rate constant which he obtained for the bimolecular collision process is

$$A^1 = \frac{4\pi D \exp (GR_{ij}^3 / 3\pi D r_m)}{P \exp (V_m / KT)} \quad (9)$$

where

$\underline{D}$  = diffusion coefficient of the particles;

$\underline{R}_{ij}$  = the distance between particle centers at the moment of collision;

$\underline{V}_m$  = the height of the potential energy barrier;

$\underline{r}_m$  = the distance between the particles corresponding to the maximum in the potential energy function;

$\underline{K}$  = Boltzmann's constant;

$\underline{T}$  = absolute temperature.

The equation shows that the rate constant for association varies exponentially with the rate of shear. Furthermore, it is seen that the rate constant decreases exponentially with the maximum repulsive energy between the particles. Thus, de Vries' analysis gives credence to the mechanism which has been postulated to explain dilatancy. It is to be emphasized however, that Equation (9) was derived for the case of monodisperse particles. In the case of collisions between aggregates of varying size, the corresponding equation would probably be more complex.

Unfortunately, there appears to be little work reported in the literature concerning the dependence of the rate constant for disruption on shear rate.

Gillespie (56, 57) developed a structural model for pseudoplastic flow in which the rate constant for disruption was assumed to be a linear function of the shear rate. Although Gillespie reports a satisfactory fit with experimental data, his equation is such that it is not possible to verify this assumption.

#### THE EFFECT OF PIGMENT VOLUME CONCENTRATION

Qualitatively, the importance of particle concentration can be realized by referring to Equation (5). The collision frequency is proportional to the product of two concentration terms; whereas, the frequency of disruption is only first order with respect to particle concentration. Therefore, an increase in particle concentration increases the number of aggregates per unit volume which, under conditions of constant charge and shear, will increase the average size of the aggregates. Stated in another way, by increasing the particle concentration, a given level of floc size is reached at a lower level of shear rate. Accordingly, the suspensions become more dilatant with increasing PVC.

The experimental results showed that the dilatant component of shear stress,  $\theta$ , varied exponentially with PVC. This finding cannot be fully explained without the aid of a quantitative theory for the description of dilatant flow. As previously mentioned, the rate constants for collision and disruption are undoubtedly dependent upon the size of the aggregates in question. It seems reasonable that the probability for collision between two aggregates will increase in proportion to their size. Thus, an increase in the particle concentration may have a multiple effect in that the increase in floc size causes a further increase in the collision frequency. Such a mechanism could account for the exponential dependence of the dilatant shear stress on PVC.

In addition to a knowledge of the relationships between the rate constants and floc size, a quantitative analysis of the data would also require a model to

relate the energy required for flow to both the number and size of the aggregates. The exponential dependence of the extent of dilatancy on  $\text{PVC}$  may be due to the fact that the energy required at a given rate of shear is a nonlinear function of the aggregate size and/or the number of aggregates.

When the logarithm of the dilatant component of shear stress,  $\log \theta$ , was plotted as a function of  $\text{PVC}$ , the slopes of the straight lines obtained increased with decreasing adsorbed charge. This can be seen by referring again to Fig. 16 and 17. A possible explanation for this effect is that the energy of interaction between the particles depends upon the particle concentration. At very low levels of  $\text{PVC}$ , the equilibrium distance between the particles is considerably greater than the distance corresponding to the point of maximum repulsive energy. However, in highly concentrated suspensions, the average distance of separation is of the same order of magnitude as the distance of the repulsive barrier. Therefore, the energy of interaction between particles will vary with  $\text{PVC}$ . On this basis it is reasonable to expect that the rate of change of the dilatant shear stress with  $\text{PVC}$  will be a function of the magnitude of the potential energy barrier.

A somewhat similar explanation concerns the way in which the energy of repulsion between two particles is influenced by the proximity of the surrounding particles. de Vries (58) has considered this problem and concluded that, due to relativistic effects, the repulsive energy between two particles at a fixed distance of separation is decreased as the number of surrounding particles is increased.

#### THE EFFECT OF PARTICLE SIZE ON DILATANCY

In the preceding discussion, a careful distinction was not made between  $\text{PVC}$  and the number of particles per unit volume,  $N_0$ . With regard to the frequency of

collision and disruption, however, it is the number of particles which is of interest rather than the  $\underline{PVC}$ . Assuming the particles to be monodisperse and spherical, the relationship between  $\underline{N}_0$ ,  $\underline{PVC}$  and the particle radius,  $\underline{a}$ , is given by,

$$N_0 = 0.03 \text{ PVC} / 4\pi a^3 \quad (10).$$

This equation shows that the number of particles per unit volume is inversely proportional to the cube of the particle radius. As previously discussed, the aggregate size, and therefore the extent of dilatancy, is believed to increase with increasing particle concentration. On this basis, it seems reasonable to expect that the extent of dilatancy will increase with decreasing particle size. However, there is another factor which must also be considered. At a constant  $\underline{PVC}$ , the distance of separation between the particles decreases linearly with decreasing particle size. This means that, as the particle size is decreased, the particles will eventually be so close to one another that, regardless of the magnitude of the repulsive forces, the attractive forces will predominate and the particles will flocculate. Thus, it is hypothesized that the extent of dilatancy will increase with decreasing particle size until the extent of flocculation becomes so great that the flow is pseudoplastic over the range of shear of interest.

In colloidal suspensions of the type investigated in this thesis, the relationship between particle size and colloidal stability is very complex. In the case where the particles are stabilized solely by electrostatic repulsion, the degree of colloidal stability usually decreases with decreasing particle size. To quantitatively determine the relationship between particle size and dilatancy it would be necessary to adjust the colloidal variables in such a way that the energy of interaction as a function of the distance between particles was the same regardless of size. From an experimental point of view, this would be most difficult

since a quantitative understanding of the mechanism of stabilization in concentrated suspensions is lacking.

The results of this thesis provide an explanation why Metzner and Whitlock (24) were not able to observe rheological dilatancy in suspensions containing particles with diameters of 29  $\mu\text{m.}$  or larger. With particles of this size, the colloidal forces are relatively insignificant in comparison to the hydrodynamic forces acting on the particles. Since flocculation is no longer a significant factor, the flow is Newtonian rather than dilatant. It is concluded therefore that rheological dilatancy is restricted to suspensions containing colloidal sized particles and that within this size range the extent of dilatancy is expected to increase with decreasing size.

## CONCLUSIONS

For the pigment suspensions investigated in this thesis, the colloidal variables were found to exert a pronounced influence on the extent of rheological dilatancy. To provide an explanation for this effect, a study was made to determine the mechanisms responsible for colloidal stability in the system. It was found that the stability was primarily controlled by the extent of adsorption and degree of dissociation of the carboxylated polymer which was used as the dispersant. The stability is believed to be due to two interrelated mechanisms: (1) electrostatic repulsion due to the ionized carboxyl groups on the adsorbed polymer and the adsorption of hydroxyl groups onto the pigment surface, and (2) steric hindrance between the adsorbed polymer molecules on adjacent particles. The total adsorbed charge was found to correlate well with the stability of the suspensions as measured with a Brookfield viscometer.

High-shear rheological measurements showed that the extent of dilatancy increased as the degree of colloidal stability decreased. Based on this finding, it was concluded that rheological dilatancy is caused by a progressive build up of floc structure within the suspension due to shear. The data showed that the suspensions were pseudoplastic at very low rates of shear and dilatant at high levels of shear. This reversal in flow behavior is explained by considering the manner in which the frequency of both the disruption and collisions of flocs varies with the rate of shear. In the range of pseudoplasticity, the rate constant for disruption is believed to increase more rapidly with shear than does the rate constant for collisions. This causes the floc size and the viscosity to decrease. At higher shear rates, the rate constant for the collision process is thought to increase more rapidly than the rate constant for disruption. As a result, the average floc size is increased and the flow becomes dilatant.

Under conditions in which the adsorbed charge was maintained essentially constant, the effect of pigment volume concentration was determined over the range of 40 to 47%. A marked increase in the extent of dilatancy was noted as the particle concentration was increased. This effect is consistent with the concept that dilatancy results from a shear-induced flocculation mechanism. An increase in particle concentration is believed to increase the frequency of collisions between aggregates to a greater extent than it increases the frequency of disruption. Therefore, the average aggregate size increases. Thus, as the particle concentration increases, a given state of flocculation can be reached at progressively lower rates of shear.

There was no indication in this study that a critical particle concentration is required in order that a suspension exhibit dilatancy. At any particle concentration, the extent to which the flow is dilatant depends upon the colloidal forces between the particles and the range of shear rate in which the shear stress is measured. It is felt that dilatancy could be observed at much lower particle concentration provided sufficiently high rates of shear could be attained.

Based on the mechanism which has been advanced to explain rheological dilatancy, it is reasonable to expect that this type of flow is restricted to suspensions in which the particles are of colloidal size. Within the colloidal size range, it is hypothesized that the extent of dilatancy will increase with decreasing particle size providing the colloidal stability of the particles remains unchanged.

## SUGGESTIONS FOR FUTURE WORK

With regard to the iron oxide suspensions used in this study, it would be helpful to obtain electrophoretic mobility measurements as a function of the level of adsorbed charge. Measurements of this type would provide a check on the adsorption measurements which were used in this study to determine changes in surface charge. Also, electrophoretic mobility measurements might provide information concerning the relative importance of electrostatic stabilization as compared to entropic stabilization. It is expected that the measurement of mobilities in concentrated suspensions would present a number of experimental difficulties. However, an electrophoretic mass transport cell has recently been marketed by the Numinco Co. which may be suitable for this type of application (64).

An extension of this study to other types of pigment suspensions is recommended. In particular, rheological dilatancy should be studied in a system in which the particles can be stabilized solely by electrostatic forces. Suspensions of  $\text{TiO}_2$  stabilized by polyphosphate addition offer one possibility. The shape of  $\text{TiO}_2$  particles is similar to the iron oxide particles used in this study. It would be helpful to use a pigment which is more nearly spherical in shape. In this regard, Robinson (59) has described a method for the preparation of spherical silica particles which are of colloidal size.

Particle size is another variable which warrants additional study. However, such a study might be somewhat difficult to interpret since the relationship between size and colloidal stability is complex.

Most important of all, this study has demonstrated the need for a theoretically based analysis of dilatant flow. As a starting point, quantitative relationships are needed to relate the average aggregate size to shear rate, particle concentration,

and the appropriate colloidal variables. It would then be necessary to develop a flow model such that the energy required for flow could be related to the extent of flocculation of the suspensions.

# NOMENCLATURE

<u>a</u>	= average particle radius, cm.
<u>A</u>	= rate constant for aggregate collisions, cm. <sup>3</sup> /sec.
<u>A'</u>	= rate constant for aggregate collisions as defined by Equation (9)
<u>b</u>	= $\frac{R_c}{R_b}$
<u>B</u>	= rate constant for aggregate disruption, sec. <sup>-1</sup>
<u>C</u>	= concentration of HCl or NaOH in polymer solution
<u>D</u>	= diffusion coefficient of particle in suspending fluid
<u>f</u>	= activity coefficient
<u>g</u>	= acceleration of gravity, cm./sec. <sup>2</sup>
<u>G</u>	= rate of shear at the bob, sec. <sup>-1</sup>
<u>h</u>	= calculated bob length, cm.
<u>K</u>	= Boltzmann's constant
<u>N<sub>a</sub></u>	= Avogadro's number
<u>N<sub>O</sub></u>	= total number of primary particles per cm. <sup>3</sup>
<u>N<sub>s</sub></u>	= number of aggregates per cm. <sup>3</sup> containing <u>s</u> particles
<u>pK<sub>int</sub></u>	= intrinsic dissociation constant
<u>PVC</u>	= pigment volume concentration, %
<u>r<sub>m</sub></u>	= distance between particles corresponding to the point of maximum repulsive energy, cm.
<u>R<sub>b</sub></u>	= radius of viscometer bob, cm.
<u>R<sub>c</sub></u>	= radius of viscometer cup, cm.
<u>R<sub>i,j</sub></u>	= distance between centers of particles during collisions, cm.
<u>s</u>	= number of particles per aggregate
<u>t</u>	= time, sec.
<u>T</u>	= absolute temperature
<u>T<sub>b</sub></u>	= torque on viscometer cup, dyne-cm./cm.

$\underline{V_m}$	= maximum height of repulsive energy barrier, ergs
$\underline{w}$	= electrostatic interaction factor defined in Equation (14) Appendix I
$\underline{X}$	= average number of particles per aggregate at equilibrium
$\underline{X_t}$	= average number of particles per aggregate at time $\underline{t}$
$\underline{Y}$	= meq. carboxyl per liter; Equations (12) and (13)
$\underline{Z}$	= total charge on polymer molecule
$\underline{\alpha_f}$	= degree of dissociation of carboxyl groups on the polymer in the inter-particle solution
$\alpha_o$	= degree of dissociation of polymer solution before pigment addition
$\underline{\Gamma_c}$	= meq. of adsorbed carboxyl per gram pigment
$\underline{\Gamma_{Cl}}$	= meq. of adsorbed chloride per gram pigment
$\underline{\Gamma_{SO_4}}$	= meq. of adsorbed sulfate per gram pigment
$\epsilon$	= charge on an electron, $4.8 \times 10^{-10}$ esu
$\eta^*$	= Newtonian viscosity
$\eta_o$	= viscosity of suspending fluid, cp.
$\theta$	= dilatant component of shear stress, dynes/cm. <sup>2</sup>
$\lambda$	= upper limit of number of particles per aggregate
$\underline{\sigma_p}$	= charge due to polymer adsorption, esu/g.
$\underline{\sigma_H}$	= charge due to hydrogen ion desorption, esu/g.
$\underline{\sigma_{Cl}}$	= charge due to chloride ion adsorption, esu/g.
$\underline{\sigma_{SO_4}}$	= charge due to sulfate adsorption, esu/g.
$\underline{\sigma_t}$	= total adsorbed charge, esu/g.
$\underline{\tau_b}$	= shear stress at the bob, dynes/cm. <sup>2</sup>
$\tau_o$	= shear stress component as defined by Equation (4)
$\omega$	= angular velocity of viscometer bob, radians/sec.

#### ACKNOWLEDGMENTS

Space does not permit the acknowledgment of all of the people whose assistance was of value to this study. To these people, I extend my sincere appreciation.

I would like especially to acknowledge the guidance and contributions of the members of my thesis advisory committee: Mr. H. Meyer, Dr. C. Garey, Dr. G. Richards, and Dr. S. Kurath. Their assistance was of great value during the course of this study.

The valuable assistance of the following people is also acknowledged:

Miss Olga Smith for her help in the preparation of electron micrographs;

Dr. D. Williams and Mr. J. Swanson for their helpful discussions regarding the colloidal aspects of this study;

Mr. M. Filz for his assistance in the design and construction of equipment and apparatus.

Finally, I wish to thank my wife Judy, for typing the original manuscript of this dissertation and for her encouragement during this work.

LITERATURE CITED

1. Kruyt, H. R. Colloid science. Vol. 1. London, Elsevier, 1952. 389 p.
2. Fischer, E. K. Colloidal dispersions. New York, John Wiley and Sons, 1950. 387 p.
3. Thomas, D. G., Ind. Eng. Chem. 55, no. 11:18-29(1963).
4. Michaels, A. S., and Bolger, J. C., Ind. Eng. Chem. Fund. 1, no. 3:153-62 (1962).
5. Casson, N. In Mill's Rheology of disperse systems. p. 84-104. New York, Pergamon Press, 1959.
6. Krieger, I. M., and Dougherty, T. J., Trans. Soc. Rheology. III:137-52(1959).
7. Chong, J. S. The rheology of concentrated suspensions. Doctor's Dissertation. University of Utah, 1964. 184 p.
8. Rutgers, R., Rheol. Acta. 2, no. 4:305-48(1962).
9. Reynolds, O., Phil. Mag. 20, no. 5:469-81(1885); Reiner, M. Deformation and flow. p. 317-20. London, H. K. Lewis and Co., 1949.
10. Williamson, R. V., J. Phys. Chem. 35:354-9(1931).
11. Freundlich, H., and Jones, A. D., J. Phys. Chem. 40:1217-39(1936).
12. Daniel, F. K., India Rubber World 101, no. 4:33-7(1939).
13. Pryce-Jones, J., Proc. Univ. Durham Phil. Soc. Series A. 10:427-67(1948).
14. Daugherty, T. H., J. Chem. Educ. 25:482-8(1948).
15. Green, H. Industrial rheology and rheological structures. p. 214-16. New York, John Wiley and Sons, 1949.
16. Jobling, A., and Roberts, J. E. In Mill's Rheology of disperse systems. p. 127-38. New York, Pergamon Press, 1959.
17. Williamson, R. V., and Heckert, W. W., Ind. Eng. Chem. 23, no. 6:667-70 (1931).
18. Freundlich, H., and Roder, H. L., Trans. Faraday Soc. 34:308-16(1938).
19. Gallay, W., and Puddington, I. E., Can. J. Research, 218:179-85(1943).
20. Verwey, E. J., and de Boer, J. H., Recueil Des Travaux Chimiques Des Pays-Bas 57:383-9(1938).
21. Sheets, G. H., Tech. Assoc. Papers. 25:528-36(1942).

22. Fischer, E. K. Colloidal dispersions. p. 194-205. New York, John Wiley and Sons, 1950.
23. Roberts, A. S., J. Chem. Eng. Data. 8, no. 3:440-4(1963).
24. Metzner, A. B., and Whitlock, M., Trans. Soc. Rheol. II:239-54(1958).
25. Parks, G. A., and de Bruyn, P. L., J. Phys. Chem. 66, no. 5:967-73(1962).
26. Atkinson, R. J., Posner, A. M., and Quirk, J. P., J. Phys. Chem. 71, no. 3: 550-8(1967).
27. Johansen, P. G., and Buchanan, A. S., Australian J. Chem. 10, no. 10:392-403 (1957).
28. Princen, L. H., Official Digest 37:766-81(1965).
29. Healey, F. H., Chessick, J. J., and Fraioli, A. V., J. Phys. Chem. 60:1001-4 (1956).
30. Jurinak, J. J., J. Colloid. Sci. 19, no. 5:477-86(1964).
31. Shimoizaka, J., Yusa, M., and Matsuoka, I., J. Mining Met. Inst. Japan. 77:253 (1961), Chem. Abstr. 56:10947b.
32. Kling, W., and Lange, H., Kolloid-Z. 127:19-27(1952).
33. Strange, H. O., and Hazel, J. F., J. Phys. Chem. 61:1281-3(1957).
34. Glusker, D. L. Personal communication. 1966.
35. Tanford, C. Physical chemistry of macromolecules. 2nd ed. p. 526-86. New York, John Wiley and Sons, 1963.
36. Krieger, I. M., and Elron, H., J. Appl. Phys. 24, no. 2:134-6(1953).
37. Kenchington, A. W. Analytical information from titration curves. In Alexander and Block's A laboratory manual of analytical methods of protein chemistry. p. 358-88. New York, Pergamon Press, 1960.
38. Tanford, C. Hydrogen ion titration curves of proteins. In Shedlovsky's Electrochemistry in biology and medicine. p. 248-65. New York, John Wiley and Sons, 1955.
39. Fritz, J. S., and Yamamura, S. S., Anal. Chem. 27, no. 9:1461-4(1955).
40. Kolthoff, I. M., and Sandell, E. B. Textbook of quantitative inorganic analysis. 3rd ed. p. 545. New York, The Macmillan Co., 1952.
41. Michaels, A. S., and Morelos, O., Ind. Eng. Chem. 47, no. 9:1801-9(1955).
42. Goodeve, C. F., Trans. Faraday Soc. 35:358(1939).
43. Happel, J., J. Appl. Phys. 28, no. 11:1288-92(1957).
44. Hamaker, H. C., Physica 4:1058(1937); see also reference (1).

45. Heller, W., and Pugh, T. L., J. Polymer Sci. 47:203-17(1960).
46. Pugh, T. L., and Heller, W., J. Polymer Sci. 47:219-27(1960).
47. Mathai, K. G., and Ottewill, R. H., Trans. Faraday Soc. 62, no. 519:751-69 (1966).
48. Van der Waarden, M., J. Colloid Sci. 5:317(1950).
49. Mackor, E. L., J. Colloid Sci. 6:492-5(1951).
50. Mackor, E. L., J. Colloid Sci. 7:535-50(1952).
51. Clayfield, E. J., and Lumb, E. C., J. Colloid and Interface Sci. 22:269-84 (1966).
52. Verwey, E. J. W., and Overbeck, J. Th. G. Theory of the stability of lyophobic colloids. New York, Elsevier, 1948. 205 p.
53. Blatz, P. J., and Tobolsky, A. V., J. Phys. Chem. 49:77-80(1945).
54. Joly, M., Rheol. Acta. 1, no. 2-3:180-5(1958).
55. de Vries, A. J. Effect of particle aggregation on the rheological behavior of disperse systems. In Sherman's Rheology of emulsions. p. 43-58. New York, Pergamon Press 1963.
56. Gillespie, T., J. Colloid Sci. 15:219-31(1960).
57. Gillespie, T., J. Colloid and Interface Sci. 22:554-62(1966).
58. de Vries, A. J., Rheol. Acta. 1, no. 2-3:180-5(1958).
59. Robinson, J. V., J. Phys. and Colloid Chem. 53:1042-56(1949).
60. Stanley, H. Chas. Pfizer Co. Research Dept., Easton, Pa. Personal communication, 1965.
61. Young, D. S. Calgon Corp., Paper Chemicals Dept., Pittsburg, Pa. Personal communication, 1965.
62. Metzner, A. B., Ind. Eng. Chem. 50, no. 10:1577-9(1958).
63. Smith, J. W., and Applegate, P. D., Tech. Assoc. Papers 31:208-14(1948).
64. Sennett, P., and Olivier, J. P., Ind. Eng. Chem. 57, no. 8:32-50(1965).

## APPENDIX I

### EXPERIMENTAL PROCEDURES AND APPARATUS

#### PREPARATION OF ELECTRON MICROGRAPHS

Electron micrographs of the pigment were prepared according to a procedure recommended by a representative of the Chas. F. Pfizer Co. (60). The pigment was first dispersed in water with Tamol 850 in the usual manner and then a drop of the concentrated suspension was diluted to approximately 500 ml. with n-propyl alcohol. This suspension was dispersed ultrasonically for five minutes at 300 kilocycles per second using a General Electric ultrasonic generator (G.E. 1-29578C). A drop of the suspension was then placed on an electron microscope grid, allowed to dry, and photographs were obtained using a RCA electron microscope (Model F3).

Two measurements were made on each of the particles on the micrographs: the maximum dimension and the minimum dimension. The average minimum diameter was 0.18  $\mu$ m. while the average maximum diameter was 0.23  $\mu$ m.

#### REMOVAL OF SOLUBLE SALTS

The soluble salts were removed from the pigment using a batch leaching process. One-hundred pounds of pigment were placed in a large stainless steel tank and sufficient distilled water was added to give a slurry concentration of 5% by weight. The slurry was agitated with two Lightnin' Mixers for eight hours and allowed to sediment overnight. A syphon was then used to remove the supernatant above the sediment. The sediment was rediluted to 5% and the leaching procedure repeated. Each batch of pigment was washed a total of five times in this manner. After the last leaching cycle, the sediment was removed from the tank and dewatered using a large Buchner funnel and number 42 Whatman filter paper. The remaining

water in the filter cake was removed by drying in an oven at 110°C. A total of 200 pounds of washed pigment was prepared in this manner.

#### EVALUATION OF DISPERSING AGENTS

Preliminary experiments indicated that addition of a dispersing agent was necessary in order to obtain fluid suspensions at the high pigment concentrations of interest. It was not possible to adequately disperse the pigment by addition of NaOH. The following dispersing agents were evaluated:

1. sodium hexametaphosphate
2. sodium tetrphosphate
3. Tamol 731 - Rohm and Haas Co.
4. Tamol 850 - Rohm and Haas Co.
5. sodium triphosphate
6. Daxad 23 - W. R. Grace Co.
7. Triton CF-10 - Rohm and Haas Co.
8. Triton X-102 - Rohm and Haas Co.
9. Nopcosant L - Nopco Chemical Co.

The effectiveness of these dispersants was determined over the range of addition of 0.2 to 2% based on the weight of pigment. It was found that fluid suspensions of PVC greater than 40% could be obtained only with the first four dispersants listed above.

Both sodium hexametaphosphate and sodium tetrphosphate resulted in high initial levels of dispersion. However, concentrated suspensions dispersed with these compounds were not stable with respect to aging. This behavior is believed to be due to the slow formation of soluble ferric metaphosphate (61).

A very high level of dispersion was obtained using Tamol 731. However, when suspensions dispersed with this product were subjected to mechanical dispersion, a stable foam was created which could not be broken under vacuum. This problem was not encountered with Tamol 850 and accordingly this product was selected for use in this study.

## ACID-BASE TITRATION OF TAMOL 850

### Experimental Method

The procedures used for the titrations were similar to those recommended by Kenchington (37) and Tanford (38). A standard Beckman reference electrode was used in conjunction with a Beckman E-2 glass electrode. Measurements of pH were made with a Beckman Model G meter. National Bureau of Standards buffers were used to standardize the meter and the accuracy of the measurements were within  $\pm 0.015$  pH units. During the titrations, nitrogen was bubbled through the samples to purge the solutions of dissolved carbon dioxide. All of the titrations were made at  $25.0^{\circ}\text{C}$ .

### Calculations

The degree of dissociation was calculated from the titration data according to a procedure proposed by Kenchington (37). Assume that the polymer is added to a solution of HCl having a concentration  $\underline{C}_1$  moles per liter. The initial concentration of hydrogen ion is also  $\underline{C}_1$  and the pH of the solution is given by  $\text{pH}_1 = -\log \underline{f}_1 \underline{C}_1$ , where  $\underline{f}_1$  is the activity coefficient. After addition of  $\underline{Y}$  meq. carboxyl per liter, the hydrogen ion concentration will be  $\underline{C}_2$  since  $(\underline{C}_1 - \underline{C}_2)/\underline{Y}$  moles of hydrogen ion will have combined with the carboxyl groups. The pH will then be  $\text{pH}_2 = -\log \underline{f}_2 \underline{C}_2$ .

Combining the expressions for  $\text{pH}_1$  and  $\text{pH}_2$  gives,

$$\log(\underline{C}_2/\underline{C}_1) = \text{pH}_1 - \text{pH}_2 + \log(\underline{f}_1/\underline{f}_2) \quad (11).$$

The assumption is made that the activity coefficient of the two solutions are the same so that the last term in Equation (11) is zero. The equations can then be rearranged to give the ratio of the moles of bound protons to the total moles of carboxyl present,

$$\frac{C_1 - C_2}{Y} = \frac{C_1}{Y} [1 - \exp_{10} (pH_1 - pH_2)] \quad (12).$$

In like manner, if the sample is titrated with  $C_1$  moles per liter NaOH, the fraction of bound hydroxyl ions (or negatively bound protons) is given by

$$\frac{C_1 - C_2}{Y} = \frac{C_1}{Y} [1 - \exp_{10} (pH_2 - pH_1)] \quad (13).$$

When the fraction of bound protons was plotted as a function of pH, the zero point on the bound proton scale necessarily occurred at the pH of the solution before acid or base were added. Therefore, it was necessary to shift the ordinate in such a way that the zero point corresponded to the pH at which the carboxyl groups were completely ionized. This pH was determined by means of a conductometric titration. Finally, the degree of dissociation was calculated by subtracting the values of the fraction of carboxyl groups in the acid form from unity. The raw titration data are tabulated in Appendix III.

#### Analysis of Titration Data to Obtain the Intrinsic Dissociation Constant

Tanford (35) has shown that the ionization of a polyelectrolyte, which contains a number of identical dissociable sites, can be described by the equation

$$pH = pK_{int} + \log(\alpha/1-\alpha) - 0.868wZ \quad (14)$$

where

$pK_{int}$  = intrinsic dissociation constant which all individual groups of that type would have if present in a monofunctional compound;

$w$  = an electrostatic factor;

$Z$  = net charge on polymer.

When  $Z$  equals zero, the equation reduces to the standard form used to describe the ionization of an independent group. The last term accounts for the electrostatic interaction between the ionizable group and the rest of the charged polymer.

When the degree of dissociation is zero, the net charge,  $\underline{Z}$ , is zero. Therefore a plot of  $\text{pH} - \log(\alpha/1-\alpha)$  versus  $\alpha$  should have an intercept equal to the  $\text{pK}_{\text{int}}$  of the individual ionizable group. This plot is shown in Fig. 21 and the intercept gives a  $\text{pK}$  value of approximately 4.9. This is a very reasonable value for the  $\text{pK}$  of a carboxyl group (e.g. the  $\text{pK}$  of acetic acid is 4.76). Tanford obtained a value of 4.85 using polymethacrylic acid.

#### OXIDATION OF POLYMER IN SUSPENDING FLUIDS PRIOR TO CHLORIDE AND SULFATE ANALYSES

For the chloride analyses, a sample of the suspending fluid was neutralized with excess NaOH and then evaporated to dryness. A carefully weighed aliquot of the residue was then placed in a Schoniger combustion flask containing 10 ml.  $\text{H}_2\text{O}$ , 1 ml. 2N KOH, and three drops of 30%  $\text{H}_2\text{O}_2$ . The flask was then filled with oxygen and ignited. After standing for 30 minutes, the solution was boiled to remove peroxide. Chloride concentration was then determined as discussed in the body of this thesis. The oxidation procedure used for the sulfate analyses was essentially the same except that KOH was not added to the flask.

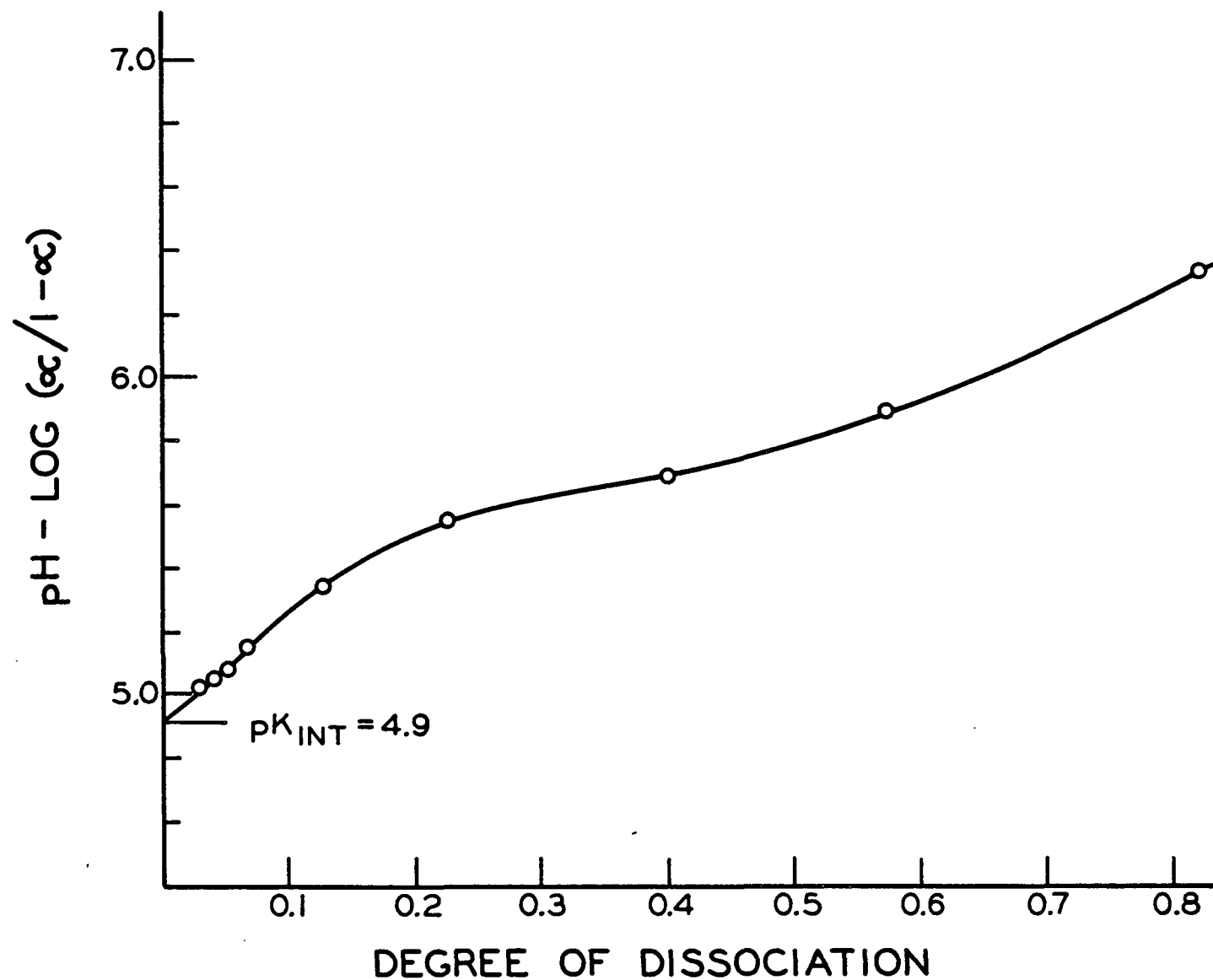


Figure 21. Determination of Intrinsic Dissociation Constant Titration  
Curve No. 1

## APPENDIX II

### DETERMINATION OF SHEAR STRESS AND SHEAR RATE WITH THE HERCULES VISCOMETER

#### CUP AND BOB GEOMETRY

The viscometer was equipped with five bobs of different sizes. For this work, all of the flow curves were obtained using Bob A, the dimensions of which are shown in Table IV. The calculated bob length was determined by calibration with a silicone oil of accurately known viscosity.

TABLE IV  
DIMENSIONS OF CUP AND BOB A

Actual bob length, cm.	5.0
Calculated bob length, cm.	5.17
Radius of bob, $\underline{R_b}$ , cm.	1.95
Radius of cup, $\underline{R_c}$ , cm.	2.00

#### MEASUREMENT OF BOB SPEED AND TORQUE

The design of the viscometer is such that the rate of revolution of the bob in r.p.m. and the torque transmitted to the cup are plotted directly onto the ordinate and abscissa of a piece of graph paper. Both the gear ratios and spring constants were such that the readings were even multiples of the distance along each axis (measured in centimeters). The load-elongation behavior of the springs was determined using an Instron load-elongation tester. It was found that the extension of the springs was a linear function of the applied force, and the spring constants obtained were in excellent agreement with those reported by the manufacturer of the viscometer.

Using Equations (1) and (2) given in the experimental section, and the values reported in Table IV, the shear rate and shear stress were calculated as follows:

$$G, \text{ sec.}^{-1} = 4.08 \text{ r.p.m.} \quad (15)$$

$$\tau_b, \text{ dynes/cm.}^2 = \text{Torque, dynes-cm./123.8} \quad (16).$$

#### RIGOROUS CALCULATION OF THE RATE OF SHEAR AT THE BOB

For non-Newtonian fluids, the rate of shear at the bob can be rigorously calculated using an equation derived by Krieger and Elron (36);

$$G = \frac{\omega}{\ln b} \left[ 1 + (\ln b) \frac{d(\ln \omega)}{d(\ln T_b)} + \frac{(\ln b)^2}{3\omega} \frac{d^2(\ln \omega)}{d(\ln T_b)^2} - \frac{(\ln b)^4}{45\omega} \frac{d^4(\ln \omega)}{d(\ln T_b)^4} + \dots \right], \quad (17)$$

where  $\underline{b} = \underline{R_c}/\underline{R_b}$ .

The derivatives in this equation are determined graphically from a plot of  $\ln \omega$  vs.  $\ln \underline{T_b}$ . For the cup and bob arrangement used in this study, all of the terms containing derivatives of order greater than one can be neglected with negligible error.

As discussed in the experimental section, the difference in the shear rates calculated by Equations (15) and (17) was less than 2%. This was due to the fact that the gap thickness was quite small. For larger gap thicknesses, however, the error introduced by using Equation (16) will become increasingly significant.

# APPENDIX III

## EXPERIMENTAL DATA

### TITRATION DATA

Data obtained from the acid-base titrations of Tamol 850 are summarized in Table V. At each level of carboxyl concentration, separate titrations were made; one with HCl and one with NaOH. In all of the titrations, the initial volume of solution was 100 ml. Titration number one was made using a starting carboxyl concentration of 16.5 meq. per 100 ml. of solution, while titration number two was made using a starting carboxyl concentration of 12.4 meq. per 100 ml.

The symbols in Table V have the following meanings:

$\underline{F}_a$  = ml. of 1.0020N HCl added;

$\underline{F}_b$  = ml. of 0.9960N NaOH added;

$\underline{pH}_b$  = pH of blank solution of distilled water, initial volume = 100 ml.;

$\alpha$  = degree of dissociation after adjustment of the zero point (see Appendix I).

### ADSORPTION DATA

All of the adsorption data are summarized in Table VI. The data shown for Suspension 163 also apply for Suspensions 164 to 170, while the data reported for Suspension 171 apply to Suspensions 172 to 177. Values with negative signs indicate that desorption occurred. As discussed in the experimental section, to determine the adsorbed charge it was necessary to multiply by Avogadro's number and the charge on an electron.

TABLE V

ACID-BASE TITRATIONS OF TAMOL 850<sup>a</sup>

TITRATION WITH NaOH

Titration No. 1				Titration No. 2			
$\frac{F}{b}$	pH	pH <sub>b</sub>	$\alpha$	$\frac{F}{b}$	pH	pH <sub>b</sub>	$\alpha$
0	8.84	--	--	0	8.94	--	--
0.1	9.62	11.02	0.996	0.1	9.59	11.02	0.997
0.2	10.23	11.31	1.000	0.2	10.54	11.31	1.000
0.3	10.85	11.47	--	0.3	11.06	11.47	--
0.4	11.14	11.58	--	0.4	11.24	11.58	--
0.6	11.42	11.74	--	0.6	11.46	11.74	--
1.0	11.71	11.94	--	1.0	11.75	11.94	--
2.0	12.04	12.20	--	2.0	12.05	12.20	--
4.0	12.36	12.46	--	4.0	12.39	12.47	--

TITRATION WITH HCl

Titration No. 1				Titration No. 2			
$\frac{F}{a}$	pH	pH <sub>b</sub>	$\alpha$	$\frac{F}{a}$	pH	pH <sub>b</sub>	$\alpha$
0	8.84	--	--	0	8.93	--	--
0.1	8.53	--	0.984	0.1	8.51	--	0.992
0.2	8.28	--	0.978	0.2	8.33	--	0.984
0.4	8.08	--	0.966	0.4	8.02	--	0.968
0.6	7.88	--	0.954	0.6	7.85	--	0.951
1.0	7.62	--	0.929	1.0	7.60	--	0.919
2.0	7.23	--	0.869	2.0	7.14	--	0.838
4.0	6.68	--	0.748	3.0	6.77	--	0.757
6.0	6.21	--	0.627	5.0	6.18	--	0.594
9.1	5.60	--	0.439	7.0	5.62	--	0.432
11.0	5.34	--	0.324	10.0	4.90	3.81	0.189
12.0	5.18	--	0.263	11.0	4.38	3.32	0.108
13.0	4.92	--	0.203	11.5	4.01	2.97	0.068
14.0	4.61	3.64	0.142	11.8	3.77	2.74	0.044
14.5	4.31	3.36	0.112	12.0	3.51	2.49	0.029
15.0	4.15	3.21	0.082	12.2	3.23	2.21	0.016
15.5	3.88	2.95	0.052	12.4	2.92	1.91	0.006
15.8	3.61	2.68	0.035	12.6	2.65	1.65	0.002
16.0	3.43	2.51	0.024	13.0	2.31	1.32	--
16.2	3.23	2.31	0.014	14.0	1.90	0.93	--
16.4	2.99	2.08	0.005				
16.6	2.73	1.83	--				
16.8	2.55	1.65	--				
17.0	2.39	1.49	--				
18.0	1.95	1.08	--				
19.0	1.74	0.89	--				
20.0	1.60	0.76	--				

<sup>a</sup>Values of pH and  $\alpha$  plotted in Fig. 6.

TABLE VI

ADSORPTION MEASUREMENTS

Suspension	$\text{pH}_{\text{H}_2\text{O}}^a$	$\text{pH}_{\text{f}}^b$	$\alpha_{\text{f}}$	Carboxyl Adsorption, $3 \times 10^3$ meq./g. x $10^3$	Hydrogen Ion Adsorption, $3 \times 10^3$ meq./g. x $10^3$	Chloride Desorption, $3 \times 10^3$ meq./g. x $10^3$	Sulfate Desorption, $3 \times 10^3$ meq./g. x $10^3$
153	5.62	5.69	0.445	19.20	0.71	2.820	3.54
151	5.86	5.92	0.520	16.10	0.47	2.110	2.96
152	6.20	6.22	0.606	14.70	0.17	1.210	3.42
156	6.35	6.37	0.645	14.20	0.17	0.900	--
157	6.76	6.76	0.743	12.10	0.00	0.545	--
149	7.22	7.20	0.845	11.40	-0.12	--	--
154	8.88	7.83	0.933	9.60	-1.54	0.145	--
148 & 155	8.94	7.83	0.933	9.50	-1.54	--	4.10
159	11.05	8.03	0.953	8.82	-1.90	--	4.42
160	11.59	8.29	0.972	8.07	-2.18	--	--
158	11.87	8.82	0.995	6.76	-3.32	--	3.84
161	12.10	9.31	0.998	4.39	-5.22	--	4.76
163	6.72	6.72	0.735	13.15	0.00	--	--
171	6.31	6.32	0.627	14.70	0.15	--	--

<sup>a</sup>  $\text{pH}_{\text{H}_2\text{O}}$  refers to the  $\text{pH}$  of the suspending fluid prior to pigment addition.

<sup>b</sup>  $\text{pH}_{\text{f}}$  refers to the  $\text{pH}$  of the interparticle solution.

# BROOKFIELD VISCOSITY DATA

The Brookfield viscosity data was obtained at 60 r.p.m. using spindle number three. These data are summarized in Table VII and are shown graphically in Fig. 12.

TABLE VII

BROOKFIELD VISCOSITY		
Suspension	pH <sub>f</sub>	Brookfield Viscosity, poise
153	5.69	10.5
151	5.92	10.4
152	6.22	10.9
156	6.37	10.7
157	6.76	9.60
149	7.20	8.36
148	7.83	7.84
155	7.83	8.67
159	8.03	8.86
160	8.29	9.38
158	8.82	10.1
161	9.31	10.2

# SHEAR STRESS-SHEAR RATE DATA

As obtained directly from the Hercules viscometer, the flow curves were defined in terms of r.p.m. and torque. For each of the flow curves, a smooth line was drawn through the experimental points and values of shear stress and shear rate were calculated at regular intervals of r.p.m. The calculated values of shear stress and shear rate, as well as the actual values of r.p.m. and torque taken from the smoothed curves, are summarized in Table VIII.

Table IX contains the values of  $\eta^*$  and  $\theta$  which were obtained from plots of shear stress and shear rate. These are the data which were used in Fig. 13 to 18 in the presentation of the experimental results section.

TABLE VIII

## SUMMARY OF FLOW CURVES

Suspension 153 PVC = 45%, $\bar{p}H_f = 5.69$				Suspension 151 PVC = 45%, $\bar{p}H_f = 5.92$			
r.p.m.	Torque, dyne-cm. $\times 10^{-5}$	$\tau_b$ , dynes/cm. <sup>2</sup>	$\bar{G}$ , sec. <sup>-1</sup>	r.p.m.	Torque, dyne-cm. $\times 10^{-5}$	$\tau_b$ , dynes/cm. <sup>2</sup>	$\bar{G}$ , sec. <sup>-1</sup>
25	0.35	283	102	25	0.28	226	102
50	0.35	283	204	50	0.35	283	204
75	0.41	331	306	75	0.45	364	306
100	0.54	436	408	100	0.54	437	408
125	0.62	501	510	125	0.62	501	510
150	0.80	646	612				
175	0.99	800	714	150	0.75	606	612
				175	0.89	719	714
200	1.20	969	816	200	1.00	808	816
250	1.92	1551	1020	250	1.35	1090	1020
300	3.27	2641	1225	300	1.80	1454	1225
350	5.61	4531	1430				
375	7.51	6066	1530	350	2.45	1980	1430
400	10.63	8586	1631	400	3.35	2710	1631
				450	4.69	3790	1835
				500	6.70	5420	2040
				550	10.15	8200	2240
				575	13.30	10,750	2345

TABLE VIII (Continued)

## SUMMARY OF FLOW CURVES

Suspension 152 PVC = 45%, $\text{pH}_f = 6.22$				Suspension 156 PVC = 45%, $\text{pH}_f = 6.37$			
r.p.m.	Torque, dyne-cm. $\times 10^{-5}$	$\tau_b$ , dynes/cm. <sup>2</sup>	$\dot{G}$ , sec. <sup>-1</sup>	r.p.m.	Torque, dyne-cm. $\times 10^{-5}$	$\tau_b$ , dynes/cm. <sup>2</sup>	$\dot{G}$ , sec. <sup>-1</sup>
25	0.28	226	102	25	0.25	202	102
50	0.40	323	204	50	0.36	291	204
75	0.49	396	306	75	0.45	363	306
100	0.55	444	408	100	0.52	420	408
125	0.62	501	510	125	0.60	485	510
				150	0.71	573	612
150	0.73	590	612				
175	0.84	679	714	175	0.80	646	714
200	0.98	792	816	200	0.91	735	816
250	1.21	977	1020	250	1.18	953	1020
300	1.54	1244	1225	300	1.43	1155	1225
				350	1.79	1446	1430
350	1.92	1551	1430	400	2.16	1745	1631
400	2.38	1922	1631				
450	2.90	2342	1835	450	2.61	2108	1835
500	3.55	2867	2040	500	3.13	2528	2040
550	4.45	3595	2240	550	3.75	3029	2244
				600	4.49	3626	2448
600	5.68	4588	2448	650	5.42	4378	2652
650	7.35	5937	2652	700	6.60	5331	2855
700	9.54	7706	2855				
750	12.51	10,105	3060	750	8.00	6461	3060
800	16.7	13,490	3264	800	9.72	7851	3264
				850	12.05	9733	3468
				900	15.10	12,196	3672

TABLE VIII (Continued)

## SUMMARY OF FLOW CURVES

Suspension 157 PVC = 45%, $\text{pH}_f = 6.76$				Suspension 154 PVC = 45%, $\text{pH}_f = 7.83$			
r.p.m.	Torque, dyne-cm. $\times 10^{-5}$	$\tau_b$ , dynes/cm. <sup>2</sup>	$\underline{G}$ , sec. <sup>-1</sup>	r.p.m.	Torque, dyne-cm. $\times 10^{-5}$	$\tau_b$ , dynes/cm. <sup>2</sup>	$\underline{G}$ , sec. <sup>-1</sup>
25	0.21	170	102	25	0.26	210	102
50	0.33	266	204	50	0.39	315	204
75	0.41	331	306	75	0.50	404	306
100	0.50	404	408	100	0.60	485	408
125	0.60	485	510	125	0.69	557	510
150	0.70	565	612	150	0.80	646	612
175	0.80	646	714	175	0.91	735	714
200	0.90	727	816	200	1.04	840	816
250	1.12	905	1020	250	1.29	1042	1020
300	1.39	1123	1225	300	1.52	1228	1225
350	1.68	1357	1430	350	1.80	1454	1430
400	1.98	1599	1631	400	2.10	1696	1631
450	2.30	1858	1835	450	2.40	1939	1835
500	2.67	2157	2040	500	2.70	2181	2040
550	3.09	2496	2244	550	3.08	2488	2244
600	3.51	2835	2448	600	3.46	2795	2448
650	4.01	3239	2652	650	3.85	3110	2652
700	4.60	3716	2855	700	4.25	3433	2855
750	5.27	4257	3060	750	4.66	3764	3060
800	6.01	4855	3264	800	5.10	4119	3264
850	6.89	5565	3468	850	5.58	4507	3468
900	7.90	6381	3672	900	6.08	4911	3672
950	9.05	7310	3876	950	6.62	5347	3876
1000	10.35	8360	4080	1000	7.21	5824	4080
1050	11.75	9490	4284	1050	7.85	6341	4284
1100	13.29	10,734	4488	1100	8.51	6874	4488

TABLE VIII (Continued)

## SUMMARY OF FLOW CURVES

Suspension 149 PVC = 45%, $\text{pH}_f = 7.20$				Suspension 155 PVC = 45%, $\text{pH}_f = 7.83$			
r.p.m.	Torque, dyne-cm. $\times 10^{-5}$	$\tau_b$ , dynes/cm. <sup>2</sup>	$\underline{G}$ , sec. <sup>-1</sup>	r.p.m.	Torque, dyne-cm. $\times 10^{-5}$	$\tau_b$ , dyne/cm. <sup>2</sup>	$\underline{G}$ , sec. <sup>-1</sup>
25	0.23	185.8	102	25	0.26	210	102
50	0.32	258.5	204	50	0.40	323	204
75	0.45	363.5	306	75	0.50	404	306
100	0.55	444.3	408	100	0.60	485	408
125	0.65	525	510	125	0.70	565	510
150	0.72	581.6	612	150	0.80	646	612
175	--	--	714	175	0.90	727	714
200	0.97	783.5	816	200	1.00	808	816
250	1.20	969.3	1020	250	1.25	1010	1020
300	1.43	155.1	1225	300	1.50	1212	1225
350	1.70	1373.2	1430	350	1.75	1414	1430
400	2.00	1615.5	1631	400	2.02	1632	1631
450	2.30	1857.8	1835	450	2.32	1874	1835
500	2.60	2100.2	2040	500	2.65	2141	2040
550	2.97	2399.0	2240	550	2.98	2407	2244
600	3.32	2681.7	2448	600	3.30	2665	2448
650	3.73	3012.9	2652	650	3.65	2948	2652
700	4.19	3384.5	2855	700	4.02	3247	2855
750	--	--	3060	750	4.46	3602	3060
800	5.12	3135.7	3264	800	4.91	3966	3264
850	--	--	3468	850	5.40	4362	3468
900	6.29	5080.8	3672	900	5.91	4774	3672
950	--	--	3876	950	6.45	5210	3876
1000	7.75	6260.1	4080	1000	7.01	5662	4080
1050	--	--	4284	1050	7.60	6139	4284
1100	9.45	7633.3	4488	1100	8.20	6623	4488

TABLE VIII (Continued)

## SUMMARY OF FLOW CURVES

Suspension 148 PVC = 45%, $\text{pH}_f = 7.83$				Suspension 159 PVC = 45%, $\text{pH}_f = 8.03$			
r.p.m.	Torque, dyne-cm. $\times 10^{-5}$	$\tau_b$ , dynes/cm. <sup>2</sup>	G, sec. <sup>-1</sup>	r.p.m.	Torque, dyne-cm. $\times 10^{-5}$	$\tau_b$ , dynes/cm. <sup>2</sup>	G, sec. <sup>-1</sup>
25	0.25	202	102	25	0.28	226	102
50	0.38	307	204	50	0.39	315	204
75	--	--	306	75	0.48	388	306
100	0.59	477	408	100	0.56	452	408
125	--	--	510	125	0.65	525	510
150	0.80	647	612	150	0.74	598	612
175	1.00	--	714	175	0.85	686	714
200	1.00	808	816	200	0.92	743	816
250	1.23	995	1020	250	1.15	929	1020
300	1.50	1212	1225	300	1.37	1107	1225
350	1.75	1413	1430	350	1.60	1292	1430
400	2.02	1631	1631	400	1.82	1470	1631
450	--	--	1835	450	2.10	1696	1835
500	2.59	2090	2040	500	2.32	1874	2040
550	--	--	2240	550	2.60	2100	2244
600	3.16	2550	2448	600	2.89	2334	2448
650	--	--	2652	650	3.19	2577	2652
700	3.85	3110	2855	700	3.50	2827	2855
750	--	--	3060	750	3.85	3110	3060
800	4.69	3790	3264	800	4.21	3401	3264
850	--	--	3468	850	4.60	3716	3468
900	5.61	4530	3672	900	5.0	4039	3672
950	--	--	3876	950	5.40	4362	3876
1000	6.62	5350	4080	1000	5.80	4685	4080
1050	--	--	4284	1050	6.20	5008	4284
1100	7.67	6200	4488	1100	6.62	5347	4488

TABLE VIII (Continued)

## SUMMARY OF FLOW CURVES

Suspension 160 PVC = 45%, $\text{pH}_f = 8.29$				Suspension 158 PVC = 45%, $\text{pH}_f = 8.82$			
r.p.m.	Torque, dyne-cm. $\times 10^{-5}$	$\tau_b$ , dynes/cm. <sup>2</sup>	$\dot{G}$ , sec. <sup>-1</sup>	r.p.m.	Torque, dyne-cm. $\times 10^{-5}$	$\tau_b$ , dynes/cm. <sup>2</sup>	$\dot{G}$ , sec. <sup>-1</sup>
25	0.30	242	102	25	0.32	259	102
50	0.40	323	204	50	0.45	364	204
75	0.50	404	306	75	0.55	444	306
100	0.61	492	408	100	0.69	557	408
125	0.72	577	510	125	0.78	630	510
				150	0.90	727	612
150	0.81	654	612				
175	0.92	743	714	175	1.00	808	714
200	1.05	848	816	200	1.11	897	816
250	1.28	1034	1020	250	1.37	1107	1020
300	1.51	1220	1225	300	1.62	1308	1225
350	1.79	1446	1430	350	1.91	1542	1430
				400	2.25	1817	1631
400	2.02	1632	1631	450	2.60	2100	1835
450	2.31	1866	1835				
500	2.61	2108	2040	500	2.97	2399	2040
550	2.92	2359	2244	550	3.35	2706	2244
600	3.29	2658	2448	600	3.78	3053	2448
650	3.61	2916	2652	650	4.20	3392	2652
700	4.01	3239	2855	700	4.70	3796	2855
				750	5.23	4224	3060
750	4.43	3578	3060	800	5.85	4725	3264
800	4.89	3950	3264				
850	5.37	4338	3468	850	6.55	5291	3468
900	5.88	4750	3672	900	7.34	5929	3672
950	6.42	5186	3876	950	8.25	6664	3876
1000	7.01	5662	4080	1000	9.25	7472	4080
1050	7.60	6139	4284	1050	10.23	8263	4284
1100	8.20	6624	4488	1100	11.50	9289	4488

TABLE VIII (Continued)

## SUMMARY OF FLOW CURVES

Suspension 161 PVC = 45%, $\text{pH}_f = 9.31$				Suspension 163 PVC = 47%, $\text{pH}_f = 6.72$			
r.p.m.	Torque, dyne-cm. $\times 10^{-5}$	$\tau_b$ , dynes/cm. <sup>2</sup>	$G$ , sec. <sup>-1</sup>	r.p.m.	Torque, dyne-cm. $\times 10^{-5}$	$\tau_b$ , dynes/cm. <sup>2</sup>	$G$ , sec. <sup>-1</sup>
25	0.33	267	102	25	0.32	259	102
50	0.45	363	204	50	0.45	364	204
75	0.59	476	306	75	0.56	452	306
100	0.70	565	408	100	0.69	557	408
125	0.85	686	510	125	0.81	654	510
150	0.95	767	612	150	0.93	751	612
175	1.07	864	714	175	1.09	881	714
200	1.20	969	816	200	1.22	985	816
250	1.45	1171	1020	250	1.58	1276	1020
300	1.80	1454	1225	300	1.95	1575	1225
350	2.15	1736	1430	350	2.39	1930	1430
400	2.50	2019	1631	400	2.89	2334	1631
450	2.95	2383	1835	450	3.47	2803	1835
500	3.45	2787	2040	500	4.12	3328	2040
550	4.00	3231	2244	550	5.02	4055	2240
600	4.77	3853	2448	600	6.11	4935	2448
650	5.70	4604	2652	650	7.49	6050	2652
700	6.90	5573	2855	700	9.30	7512	2855
750	8.35	6744	3060	750	11.72	9467	3060
800	10.10	8158	3264	800	14.95	12,076	3264
850	12.19	9846	3468				

TABLE VIII (Continued).

## SUMMARY OF FLOW CURVES

Suspension 165 PVC = 46%, $\text{pH}_f = 6.72$				Suspension 166 PVC = 45%, $\text{pH}_f = 6.72$			
r.p.m.	Torque, dyne-cm. $\times 10^{-5}$	$\tau_b$ , dynes/cm. <sup>2</sup>	$G$ , sec. <sup>-1</sup>	r.p.m.	Torque, dyne-cm. $\times 10^{-5}$	$\tau_b$ , dynes/cm. <sup>2</sup>	$G$ , sec. <sup>-1</sup>
25	0.28	226	102	25	0.20	162	102
50	0.39	315	204	50	0.29	234	204
75	0.49	396	306	75	0.39	315	306
100	0.57	460	408	100	0.46	372	408
125	0.66	533	510	125	0.55	444	510
150	0.78	630	612	150	0.61	493	612
175	0.88	711	714	200	0.80	646	816
200	1.00	808	816	250	1.00	808	1020
250	1.25	1010	1020	300	1.20	969	1225
300	1.51	1220	1225	400	1.61	1300	1631
350	1.80	1454	1430	500	2.10	1696	2040
400	2.12	1712	1631	600	2.72	2197	2448
450	2.50	2019	1835	700	3.47	2803	2855
500	2.91	2351	2040	800	4.28	3457	3264
550	3.36	2714	2240	900	5.13	4144	3672
600	3.85	3110	2448	950	5.61	4531	3876
650	4.40	3554	2652	1000	6.14	4960	4080
700	5.02	4055	2855	1050	6.74	5444	4284
750	5.78	4669	3060	1100	7.45	6018	4488
800	6.60	5331	3264				
850	7.60	6139	3468	175	0.71	574	714
900	8.72	7044	672				
950	10.07	9134	3876				
1000	11.69	9442	4080				
1050	13.63	11,010	4284				
1100							

TABLE VIII (Continued)

## SUMMARY OF FLOW CURVES

Suspension 167 PVC = 44%, $\text{pH}_f = 6.72$				Suspension 168 PVC = 43%, $\text{pH}_f = 6.72$			
r.p.m.	Torque, dyne-cm. $\times 10^{-5}$	$\tau_b$ , dynes/cm. <sup>2</sup>	$\dot{G}$ , sec. <sup>-1</sup>	r.p.m.	Torque, dyne-cm. $\times 10^{-5}$	$\tau_b$ , dynes/cm. <sup>2</sup>	$\dot{G}$ , sec. <sup>-1</sup>
25	0.20	162	102	25	0.17	137	102
50	0.27	218	204	50	0.24	194	204
75	0.34	275	306	75	0.29	234	306
100	0.40	323	408	100	0.35	283	408
125	0.48	384	510	125	0.41	327	510
150	0.54	436	612	150	0.47	380	612
175	0.62	501	714	175	0.53	428	714
200	0.69	557	816	200	0.60	485	816
250	0.84	679	1020	250	0.72	582	1020
300	1.00	808	1225	300	0.86	695	1225
350	1.16	937	1430	350	1.00	808	1430
400	1.33	1074	1631	400	1.16	937	1631
450	1.55	1252	1835	450	1.30	1050	1835
500	1.72	1389	2040	500	1.46	1179	2040
550	1.91	1543	2240	550	1.62	1309	2240
600	2.11	1704	2448	600	1.77	1430	2448
650	2.31	1866	2652	650	1.95	1575	2652
700	2.52	2036	2855	700	2.12	1712	2855
750	2.74	2213	3060	750	2.29	1850	3060
800	2.95	2383	3264	800	2.46	1987	3264
850	3.19	2577	3468	850	2.65	2141	3468
900	3.44	2779	3672	900	2.83	2286	3672
950	3.72	3005	3876	950	3.02	2439	3876
1000	4.00	3231	4080	1000	3.23	2609	4080
1050	4.33	3498	4284	1050	3.45	2787	4284
1100	4.72	3812	4484	1100	3.69	2981	4484

TABLE VIII (Continued).

## SUMMARY OF FLOW CURVES.

Suspension 169 PVC = 42%, $\text{pH}_f = 6.72$				Suspension 170 PVC = 41%, $\text{pH}_f = 6.72$			
r.p.m.	Torque, dyne-cm. $\times 10^{-5}$	$\tau_b$ , dynes/cm. <sup>2</sup>	$G$ , sec. <sup>-1</sup>	r.p.m.	Torque, dyne-cm. $\times 10^{-5}$	$\tau_b$ , dynes/cm. <sup>2</sup>	$G$ , sec. <sup>-1</sup>
25	0.14	113	102	50	0.15	121	204
50	0.19	154	204	100	0.25	202	408
75	0.24	194	306	125	0.30	242	510
100	0.30	242	408	150	0.35	283	612
125	0.35	283	510	175	0.39	315	714
150	0.41	331	612	200	0.44	355	816
175	0.46	372	714				
				250	0.54	436	1020
200	0.52	420	816	300	0.64	513	1225
250	0.62	501	1020	350	0.73	590	1429
300	0.73	590	1225	400	0.83	670	1631
400	0.95	767	1631	500	1.03	828	2040
500	1.19	961	2040	600	1.23	994	2448
600	1.43	1155	2448				
				700	1.44	1163	2855
700	1.67	1349	2855	800	1.67	1349	3264
800	1.92	1551	3264	900	1.89	1527	3672
900	2.20	1773	3672	1000	2.13	1721	4080
1000	2.48	2003	4080	1050	2.26	1825	4284
1050	2.63	2124	4284	1100	2.40	1939	4484
1100	2.80	2262	4484				

TABLE VIII (Continued) (continued)

## SUMMARY OF FLOW CURVES

Suspension 164 PVC = 40%, $\text{pH}_f = 6.72$				Suspension 171 PVC = 47%, $\text{pH}_f = 6.32$			
r.p.m.	Torque, dyne-cm. $\times 10^{-5}$	$\tau_b$ , dynes/cm. <sup>2</sup>	$G$ , sec. <sup>-1</sup>	r.p.m.	Torque, dyne-cm. $\times 10^{-5}$	$\tau_b$ , dynes/cm. <sup>2</sup>	$G$ , sec. <sup>-1</sup>
50	0.12	97	204	25	0.39	315	102
100	0.19	154	408	50	0.50	404	204
125	0.23	182	510	75	0.63	509	306
150	0.27	218	612	100	0.78	630	408
175	0.30	242	714				
200	0.34	275	816	125	0.90	727	510
				150	1.05	848	612
250	0.42	339	1020	175	1.20	969	714
300	0.50	404	1225	200	1.40	1131	816
350	0.59	473	1429				
400	0.67	541	1631	250	1.89	1527	1020
500	0.84	679	2040	300	2.50	2019	1225
600	1.02	820	2448	350	3.30	2665	1430
				400	4.40	3554	1631
700	1.19	961	2855				
800	1.38	1116	3264	450	6.06	4895	1835
900	1.58	1276	3672	500	9.16	7399	2040
1000	1.78	1434	4080	525	12.15	9814	2140
1050	1.88	1518	4284	550	15.95	12,884	2248
1100	1.98	1599	4484				

TABLE VIII (Continued).

## SUMMARY OF FLOW CURVES

Suspension 172 PVC = 46%, $\text{pH}_f = 6.32$				Suspension 173 PVC = 45%, $\text{pH}_f = 6.32$			
r.p.m.	Torque, dyne-cm. $\times 10^{-5}$	$\tau_b$ , dynes/cm. <sup>2</sup>	$\dot{G}$ , sec. <sup>-1</sup>	r.p.m.	Torque, dyne-cm. $\times 10^{-5}$	$\tau_b$ , dynes/cm. <sup>2</sup>	$\dot{G}$ , sec. <sup>-1</sup>
25	0.25	202	102	25	0.20	162	102
50	0.35	283	204	50	0.30	242	204
75	0.45	364	306	75	0.37	299	306
100	0.56	452	408	100	0.46	372	408
125	0.68	549	510	125	0.52	420	510
150	0.80	646	612	150	0.61	493	612
175	0.92	743	714	175	0.71	574	714
200	1.07	864	816	200	0.80	646	816
250	1.38	1115	1020	250	1.01	816	1020
300	1.72	1389	1225	300	1.23	994	1225
350	2.16	1745	1430	350	1.49	1204	1430
400	2.68	2165	1631	400	1.75	1413	1631
450	3.32	2682	1835	450	2.05	1656	1835
500	4.11	3320	2040	500	2.40	1938	2040
550	5.19	4192	2244	550	2.79	2254	2244
600	6.70	5412	2448	600	3.21	2593	2448
650	8.85	7149	2652	650	3.69	2981	2652
700	12.10	9774	2855	700	4.21	3401	2855
725	14.37	11,607	2940	750	4.85	3918	3060
				800	5.58	4507	3264
				850	6.40	5170	3468
				900	7.35	5937	3672
				950	8.50	6866	3876
				1000	9.85	7956	4080
				1050	11.39	9200	4284
				1100	13.09	10,573	4488

TABLE VIII (Continued)

## SUMMARY OF FLOW CURVES

Suspension 174 PVC = 44%, $\text{pH}_f = 6.32$				Suspension 175 PVC = 43%, $\text{pH}_f = 6.32$			
r.p.m.	Torque, dyne-cm. $\times 10^{-5}$	$\tau_b$ , dynes/cm. <sup>2</sup>	G, sec. <sup>-1</sup>	r.p.m.	Torque, dyne-cm. $\times 10^{-5}$	$\tau_b$ , dynes/cm. <sup>2</sup>	G, sec. <sup>-1</sup>
25	0.16	129	102	25	0.13	105	102
50	0.25	202	204	50	0.20	162	204
75	0.30	242	306	75	0.28	226	306
100	0.38	307	408	100	0.31	250	408
125	0.44	355	510	125	0.38	307	510
150	0.50	404	612	150	0.42	339	612
175	0.58	469	714	175	0.50	404	714
200	0.64	517	816	200	0.54	436	816
250	0.80	646	1020	250	0.69	557	1020
300	0.98	792	1225	300	0.80	646	1225
350	1.15	929	1430	350	0.95	767	1430
400	1.33	1074	1631	400	1.10	889	1631
450	1.54	1244	1835	450	1.22	986	1835
500	1.74	1405	2040	500	1.39	1123	2040
550	1.95	1575	2244	550	1.54	1244	2244
600	2.19	1769	2448	600	1.70	1373	2448
650	2.42	1955	2652	650	1.89	1527	2652
700	2.70	2181	2855	700	2.05	1656	2855
750	3.00	2423	3060	750	2.24	1809	3060
800	3.32	2682	3264	800	2.43	1963	3264
850	3.66	2956	3468	850	2.65	2140	3468
900	4.02	3247	3672	900	2.86	2310	3672
950	4.44	3586	3876	950	3.10	2504	3876
1000	4.89	3950	4080	1000	3.35	2706	4080
1050	5.36	4329	4284	1050	3.63	2932	4284
1100	5.85	4725	4488	1100	3.95	3190	4488

TABLE VIII (Continued)

## SUMMARY OF FLOW CURVES

Suspension 176 PVC = 42%, $\text{pH}_f = 6.32$				Suspension 177 PVC = 41%, $\text{pH}_f = 6.32$			
r.p.m.	Torque, dyne-cm. $\times 10^{-5}$	$\tau_b$ , dynes/cm. <sup>2</sup>	$\underline{G}$ , sec. <sup>-1</sup>	r.p.m.	Torque, dyne-cm. $\times 10^{-5}$	$\tau_b$ , dynes/cm. <sup>2</sup>	$\underline{G}$ , sec. <sup>-1</sup>
25	0.12	97	102	25	0.08	60	102
50	0.17	137	204	50	0.14	111	204
75	0.23	186	306	75	0.20	158	306
100	0.29	234	408	100	0.25	202	408
125	0.33	267	510	125	0.30	242	510
150	0.39	315	612	150	0.34	275	612
175	0.43	347	714	175	0.38	307	714
200	0.49	396	816	200	0.43	347	816
250	0.60	485	1020	250	0.53	424	1020
300	0.71	574	1225	300	0.62	501	1225
350	0.81	654	1430	350	0.70	565	1430
400	0.93	751	1631	400	0.79	638	1631
450	1.05	848	1835	450	0.87	703	1835
500	1.16	937	2040	500	0.98	792	2040
550	1.28	1034	2244	550	1.08	868	2244
600	1.41	1135	2448	600	1.18	949	2448
650	1.53	1236	2652	650	1.28	1030	2652
700	1.66	1341	2855	700	1.38	1111	2855
750	1.79	1446	3060	750	1.48	1191	3060
800	1.82	1470	3264	800	1.58	1272	3264
850	2.06	1664	3468	850	1.68	1357	3468
900	2.20	1777	3672	900	1.80	1454	3672
950	2.35	1898	3876	950	1.92	1551	3876
1000	2.52	2035	4080	1000	2.05	1652	4080
1050	2.70	2181	4284	1050	2.18	1761	4284
1100	2.91	2351	4488	1100	2.33	1882	4488

TABLE IX

NEWTONIAN VISCOSITIES AND DILATANT COMPONENTS  
OF SHEAR STRESS

Suspension	PVC, %	pH <sub>f</sub>	$\eta^*$ , poise	$\theta$ , dynes/cm. <sup>2</sup> at	
				$\underline{G} = 2500 \text{ sec.}^{-1}$	$\underline{G} = 3500 \text{ sec.}^{-1}$
153	45	5.69	0.723	off scale	off scale
151	45	5.92	0.650	off scale	off scale
152	45	6.22	0.583	3200	off scale
156	45	6.37	0.672	2010	7680
157	45	6.76	0.727	1010	3070
149	45	7.20	0.841	570	1640
154	45	7.83	0.788	470	1240
148	45	7.83	0.809	620	1520
155	45	7.83	0.777	730	1660
159	45	8.03	0.694	480	1175
160	45	8.29	0.791	570	1460
158	45	8.82	0.873	770	2160
161	45	9.31	0.980	1430	6520

				$\theta$ , dynes/cm. <sup>2</sup> at	
				$\underline{G} = 3000 \text{ sec.}^{-1}$	$\underline{G} = 4000 \text{ sec.}^{-1}$
163	47	6.72	0.974	5730	off scale
165	46	6.72	0.755	2080	5720
166	45	6.72	0.632	1000	2135
167	44	6.72	0.523	480	940
168	43	6.72	0.485	270	520
169	42	6.72	0.424	80	175
170	41	6.72	0.370	71	120
164	40	6.72	0.307	40	90

				$\theta$ , dynes/cm. <sup>2</sup> at	
				$\underline{G} = 2000 \text{ sec.}^{-1}$	$\underline{G} = 2900 \text{ sec.}^{-1}$
171	47	6.32	0.972	4520	--
172	46	6.32	0.772	1500	8280
173	45	6.32	0.604	560	1680
174	44	6.32	0.523	225	625
175	43	6.32	0.470	90	270
176	42	6.32	0.417	25	104
177	41	6.32	0.343	--	40